Production Performance Analysis of Horizontal Infill Wells in a Mature Field

Master Thesis

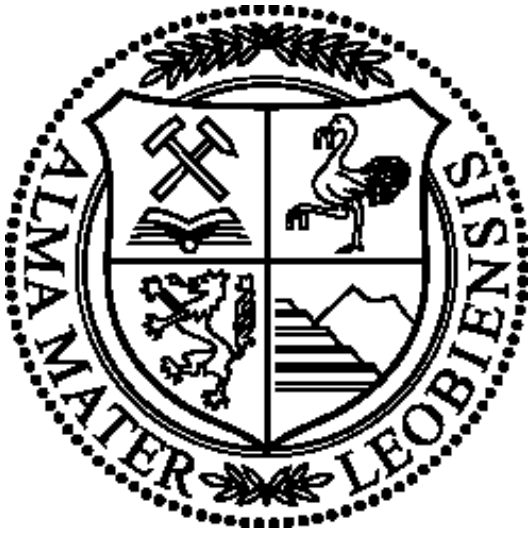

The energy for a better life.

OMV

Written by:
Hans Thomas Maier, BSc
m01035234

Advisor:
Univ.-Prof. Dipl.-Ing. Dr.mont. Herbert Hofstätter
Dipl.-Ing. Ilhami Giden (OMV Austria E&P)

Leoben, 13. August 2018

EIDESSTATTLICHE ERKLÄRUNG

Ich erkläre an Eides statt, dass ich die vorliegende Diplomarbeit selbständig und ohne fremde Hilfe verfasst, andere als die angegebenen Quellen und Hilfsmittel nicht benutzt und die den benutzten Quellen wörtlich und inhaltlich entnommenen Stellen als solche erkenntlich gemacht habe.

09.08.2018
Datum

Unterschrift

AFFIDAVIT

I hereby declare that the content of this work is my own composition and has not been submitted previously for any higher degree. All extracts have been distinguished using quoted references and all information sources have been acknowledged.

09.08.2018
.....
Date

.....
Signature

Acknowledgement

I would like to express my great appreciation to Dipl. Ing. Ilhami Giden. He gave me the chance to prove myself by creating this master thesis for OMV Austria E&P GmbH. His patient guidance and valuable pieces of advice were of inestimable value for me. In addition, I would like to thank all people of OMV Gänserndorf, for answering my sheer infinite number of questions.

Special thanks should also be given to my academic supervisor Univ.-Prof. Dipl.-Ing. Dr.mont. Herbert Hofstätter for his professional assistance and constructive advices.

Finally I would like to thank my family and friends who supported me all the way.

Kurzfassung

Im Zuge des Neuentwicklungsprojektes, das sich auf den 16. Torton bezieht, wurden drei horizontale Ölsonden in eine schon erschlossene Lagerstätte abgeteuft. Ziel war es das vorhandene Öl, welches sich am Top der Struktur angesammelt hat abzufördern. Daraus entstand die Idee, die Produktion von bestehenden vertikalen Ölsonden mit den neugebohrten horizontalen Sonden zu vergleichen.

Im westlichen Teil des 16.Tortons (Bockfließ) wurden die Horiztonalbohrungen abgeteuft. Die drei Bohrungen wurden auf verschiedene Weise komplettiert und die Komplettierungen wurden in Abhängigkeit von geologischen Gegebenheiten und möglichen Gasvorkommen gewählt. Bockfließ 204 und Bockfließ 208 wiesen kein Gasvorkommen auf und wurden ohne Produktionskolonne komplettiert. BO 204 komplettierte man mit geschlitzten Produktionsrohren und BO 208 mit Produktionsrohren, die mit autonom funktionierenden Zuflussregeleinheiten (AICDs) ausgestattet wurden. Bei Bockfließ 205 wurde die Produktionskolonne zementiert um mögliches Gas unter Kontrolle zu behalten. Aus dieser Diplomarbeit wurden Informationen generiert, die Aufschluss über den Produktionsunterschied zwischen horizontalen und vertikalen Bohrungen geben. Zusätzlich wurden, die erstmals verwendeten AICDs, auf ihre Effizient untersucht. Damit all diese Daten verarbeitet werden konnten, beinhaltet diese Arbeit einen generellen Überblick über die theoretischen Hintergrundinformationen bezüglich des Erdölreservoir, Komplettierungsarten, Fördersysteme und Zuflussregeleinheiten. Außerdem wurden verschiedene mathematische Modelle zur Ermittlung der Produktionsperformance von vertikalen und horizontalen Bohrungen besprochen. Diese Berechnungen wurden mittels einer Erdölsoftware namens NETool™ und MS Excel® durchgeführt.

Analysiert wurden drei horizontale und sechs vertikale Ölsonden unter Verwendung von Produktionsdaten der letzten 30 Monate. Die kumulative Ölproduktion der horizontalen Sonden überstieg die Produktion der besten vertikalen Sonde um den Faktor 2,2. Außerdem waren die Ergebnisse der BO 208-Analyse herausstechend. Die Funktion der AICDs bei BO 208 zeichnete sich deutlich durch eine stark abgeflachte Verwässerungskurve ab. Mithilfe der verwendeten Daten und Modellen wurde festgestellt, dass ein statisches NETool™-Modell keine eindeutigen Informationen über das Produktionsverhalten der Horizontalbohrungen liefert. Die Analyse der kumulativen Ölproduktion zeigte, dass Horizontalsonden deutlich mehr Öl zu Tage fördern als vertikale Sonden. Die Anwendung von AICDs zeigten eine deutliche Abflachung des ansteigenden Wasser-Öl Trends, was für zukünftige Bohrungen in Österreich von entscheidendem Vorteil sein wird.

Abstract

In the course of the redevelopment project of the 16th Torton Horizon, three horizontal infill wells were drilled. These wells targeted the attic oil in the top region of the reservoir and, as result, increased the oil production for this production unit. Out of this redevelopment project, the idea was born to compare the production performance of these oil wells.

The western part of the 16th Torton is called Bockfliess and is the main target of the infill wells. It was the first time that OMV Austria drilled horizontal wells in this reservoir region; therefore, it was decided to vary the type of completion depending on the geological setting and the presence of a gas cap. In the case of Bockfliess 204 and Bockfliess 208, no significant amount of gas presence was given, therefore well BO 204 was completed with a slotted liner while the other one (BO 208) was completed with a combination of blank pipes and autonomous inflow control devices (AICDs). Bockfliess 205 showed the presence of a gas cap, and therefore a standard cemented cased hole completion was implemented. This thesis generates information about the production performance difference between horizontal and vertical wells and in addition how efficient the newly introduced AICD completion works. In order to reprocess all the necessary data, this thesis overviews the theoretical information about the reservoir, completion types, and artificial lift systems, including inflow control devices. In addition, it also discusses the mathematical methods used to estimate the production performance of horizontal and vertical wells. All necessary analyses were performed with applications such as NETool™ and MS Excel®.

The analysis covers three horizontal and six vertical wells and uses the production data of each well from the last 30 months. With this data it was observed that the cumulative oil production rate of the horizontal wells was approximately 2.2 times higher compared to the neighbouring vertical well. The results from the BO 208 analysis were notable. The AICDs, which were mounted at the horizontal section, choked the production fluid in such a way that the water cut trend maintained a constant rate compared to all other wells, where the water cut constantly increased. Through the different analytical methods of the production data and the investigation of the completion types, it was determined that a static NETool™ model does not provide clear information about the production behaviour of the horizontal wells. A study of the cumulative oil production showed that the application of horizontal wells is more efficient than vertical ones. Several completion types were examined, and the use of AICDs in horizontal sections showed the ability to flatten the increasing water cut trend, which will be even more useful for future wells in Austria.

List of Tables

List of Figures

Abbreviations

AL	Artificial Lift
ALS	Artificial Lift System
AOF	Absolute Open Flow
BEP	Best Efficiency Point
BP	Blank Pipe
CH	Cased Hole
cP	Centipoise
ECP	External Casing Packer
ESP	Electrical Submersible Pump
ESR	Effective Stress Ratio
FCD	Flow Control Device
FIT	Formation Integrity Test
GDB	Gewinnungsdatenbank – "Production Data Base"
GMS	Geomechanic Study
GOC	Gas Oil Contact
GP	Gravel Pack
HSSE	Health, Safety, Security and Environment
ICD	Inflow Control Device
ICV	Inflow Control Valve
IGIP	Initial Gas In Place
KH	Horizontal Permeability
KV	Vertical Permeability
LOT	Leak Off Test
MD	Measured Depth
MD	Mud Weight
OFU	Oil Field Unit
OH	Open Hole
OHSAS	Occupational Health and Safety Assessment System
OOIP	Original Oil In Place
Pa	Pascal
PDL	Pre-Drilled Liners
PL	Pre-Perforated Liner
Por	Porosity
PPP	Petroleum Production and Processing
rad	Radians

RCP	Rate Controlled Production
SEP	Swellable Elastomer Packer
SG	Specific Gravity
SL	Slotted Liner
SRP	Sucker Rod Pump
SS	Steady State
SW	Water Saturation
TH	Torton Horizon
TVD	Total Vertical Depth
TVDSS	Total Vertical Depth Sub Sea
UCS	Uniaxial Compressive Strength
WO	Workover
ZI	Zonal Isolation

Table of content

Page

1 Introduction

In a non-natural flowing reservoir, an artificial lift system (ALS) in combination with various recovery mechanisms is the only possibility for producing hydrocarbons from depths of several thousand metres to the surface. In addition to the ALS configuration, the type of completion that regulates the inflow from the reservoir to the wellbore is critical. In 2011, a redevelopment project began in the Bockfliess area in which three horizontal infill wells were drilled. The main aim of these infill wells was to produce so-called 'attic oil'; therefore, each horizontal well was completed in a different manner with respect to the geological position and reservoir state at its location. The objectives of this thesis are to investigate the inflow performance of each horizontal well with respect to the wellbore completion as well as provide answers for the differences in efficiency between the horizontal wells and performance differences between horizontal and vertical wells.

The Bockfliess area, southwest of the Matzen oil field (approximately 23 km northeast of Vienna), has been producing oil since 1950. As of today, the production in this area is through 75 sucker rod pumps, 34 gas lift systems, and 39 electrical submersible pumps (including newly installed ones from the redevelopment programme). The major goal of the redevelopment project was to increase the oil production by doubling the gross production rate; to achieve this goal, measures were used such as exchanging SRPs for ESPs, converting existing producers to injector wells, and drilling horizontal infill wells to maximise reservoir contact.

The process of creating a structured thesis began by defining the wells to be observed and gathering the geological and reservoir information about the area of interest. This was followed by describing theoretical information about a petroleum production system, the various types of production performance parameters, and a summary of available completion types. Subsequently, a detailed examination of inflow control devices was performed.

Using the gathered data of the examined wells, several analytical calculations were performed, which included various simulations using NETool™.

Finally, the results of the production data analysis were used to gather and highlight the most critical figures and provide OMV Austria with recommendations for future wells.

2 Literature Review

In this chapter, an overview is provided of the geology and reservoir parameters of OMV's oil reserves in Austria; in addition, necessary background information about general oil production systems combined with common and advanced completion techniques is described.

2.1 Austrian Mature Oil Field

The Matzen Field is located between 30 and 40 km northeast of Austria's capital city Vienna. More precisely, it is located in the north-central part of the Neogene Vienna Basin, and it is the largest multi-pool oil province in onshore Central and Western Europe. This huge reservoir was discovered in 1949, and until 1992, approximately 1340 wells have been drilled. The field covers an area of 26.1 km^2 and is divided into 25 crucial oil and gas bearing horizons, which are at depths between 500–6000 m [1]. The main productive oil zone is the 16th Torton Horizon (TH), which is also the main focus area of this thesis. Figure 1 presents a relief map of Austria that includes the location of the Matzen Field.

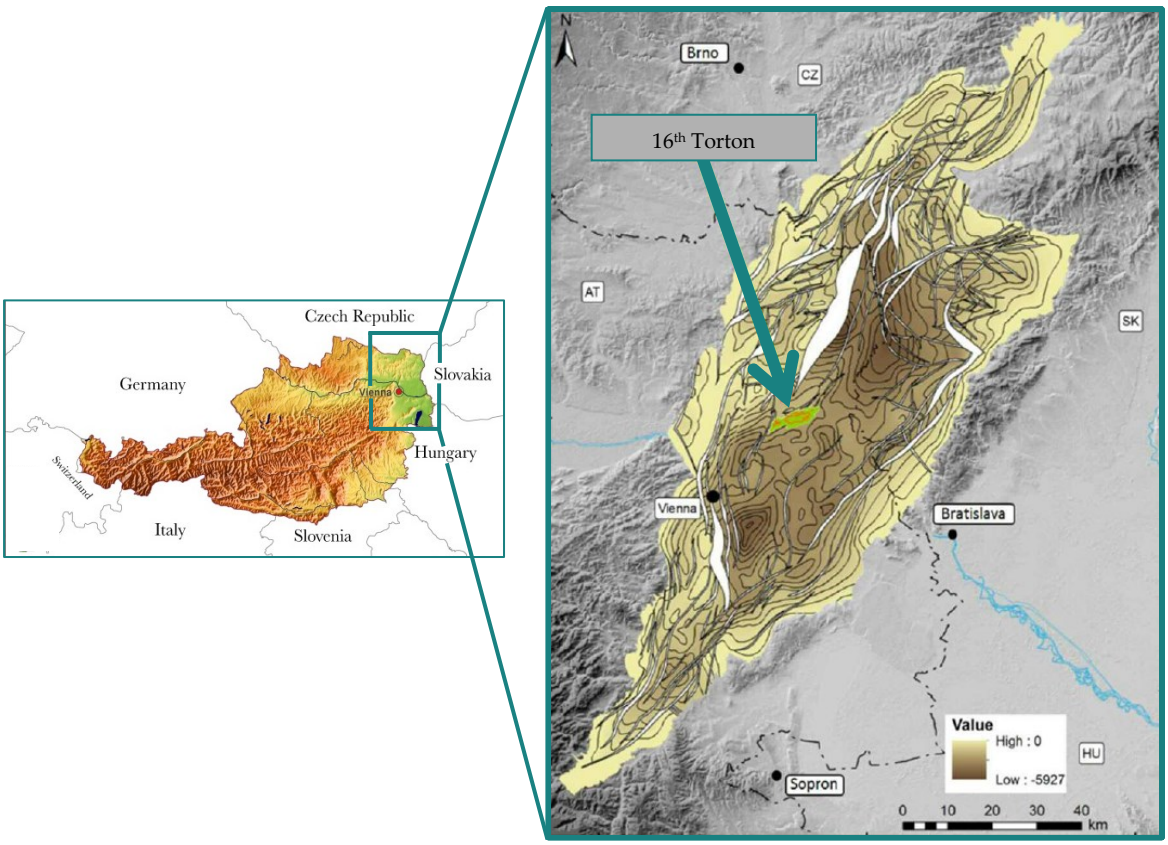

Figure 1: Relief map and depth structure map of the 16th Torton Horizon located in the Vienna Basin, Austria; modified after [1]

The Matzen Sand is divided into eight main layers, which are subdivided into fifteen sublayers for reasonable lithofacies- and log-mapping. The thickness of the Matzen Sand varies greatly (from 1 m to 70 m), and out of the thickness distribution, three main depositional axes have been identified (Eastern, Central, and Western Depression).
Sediments from a northern to north-west directed sedimentary area (the Molasse Zone) have been deposited in a marine environment, which can more accurately be described as a shallow marine transgressive milieu. A key indicator for the 16th TH and transgressive setting is that the main layers and sublayers of the reservoir comprise reworked, sand-prone delta front sediments. These sediments are the fundamental reason for the excellent reservoir properties of the Matzen Sand. Between the sand layers, nonconformities in the form of so-called "Harte Lagen" are present. These layers were identified from microlog data and their thicknesses differ from 10 cm to 1 m. According to an investigating on rock properties, they are thick, calcitic layers with very low permeability, which can form vertical barriers for the migration of oil and gas [1; 2].

The Matzen Field covers a productive region of 26.1 km^2 that includes original oil in place (OOIP) of 94.56 million m^3 and initial gas in place of 17.64 million m^3. Based on core analysis, an average permeability of 1190 mD (original values between 17.8 to 20,400 mD were measured) and porosity between 17% and 42% were found, which results in an average porosity of approximately 27%. The oil found under initial conditions was already in a saturated phase, which means that the bubble point pressure of the oil equalled the initial reservoir pressure. Therefore, all individual oil zones had an initial gas cap. The oil from the 16th TH has a API-gravity of 24.85° (specific gravity of 0.905 kg/m^3) and an oil viscosity in an initial phase from 5.8 cP [2].

In its initial state, the reservoir had a pressure of 165 bar at the oil water contact below -1490 m and a standardised initial reservoir pressure in the centre of the reservoir volume at -1468m estimated to be 163.6 bar. From the beginning of production in Austria, the reservoir pressure permanently declined until 1971 because of a recalculation of the overall mass balance of the reservoir. The following readjustments of the injectors have led to a near constant reservoir pressure of approximately 120 bar for several years. The reservoir temperature is approximately 60°C. Furthermore, the main drive mechanism of the Matzen Sand is the water drive effect, which was investigated and proven in 1957. In addition to the water drive mechanism, which covers approximately 80% of the reservoir drive mechanism, 10% is covered by solution gas drive and 10% by gas cap drive [2]. Today, because of the long production by water drive for the last 69 years, the average water cut now usually exceeds 96%.

Nowadays, OMV Austria Exploration & Production GmbH operates nearly 1,100 wells in the whole area of Gänserndorf, and from this, approximately 13% (only producer wells) operate in the 16th TH, which can be subdivided into two main regions (see Figure 2). Specifically, this thesis focuses on the westernmost part of the 16th TH—the so-called Bockfliess area—and covers nearly 12 km². It is operated with 77 units; 62 are producer wells and 15 wells perform as injectors [3].

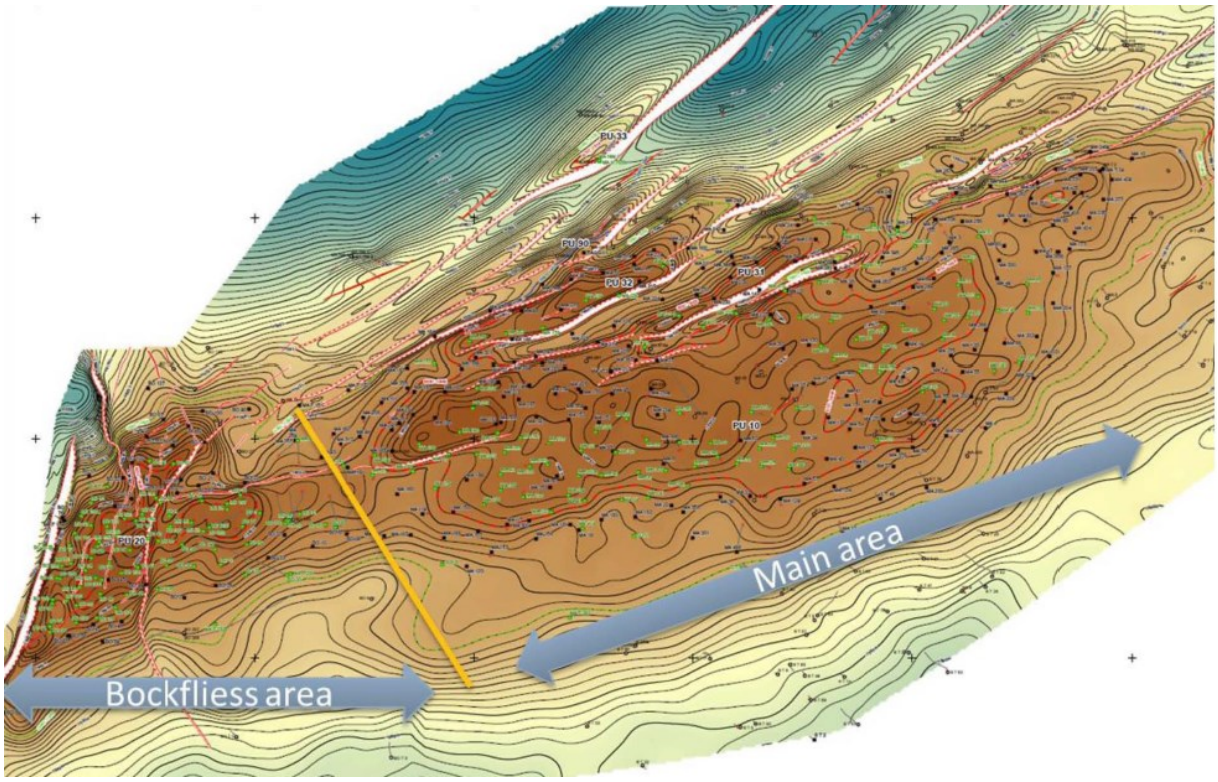

Figure 2: Structural Map of the top structure of the 16th Torton Horizon [3]

In 2013, because of high water production, OMV Austria began redevelopment of the Bockfliess area and started drilling horizontal wells. This thesis concentrates on the wells BO 204, BO 205, and BO 208, which are horizontal wells with various types of completion. The technique of horizontal well completion is explained in detail in subsequent chapters.

2.2 Reservoir Properties

Table provides the reservoir properties of the investigated area. The table contains data that were taken on the 17th of February, 2016, and also data from one of the latest PVT reports, to show if any changes occurred in the reservoir parameters. The representative data are taken as reference values. By meaning "Initial Reservoir Conditions", these values are related to the time when the first samples were taken from well Matzen H 703 in 2000.

		Standard Conditions	Initial Reservoir Conditions	Current Reservoir Conditions	
		p_{std}	p_i	p_{res}	
Pressure	p	1.01325	139.0	120.0	bar
Temperature	T	15.6	60.0	60.0	°C
Viscosity oil	μ_o	90.230	3.842	4.747	mPa.s
Formation volume factor oil (DLE)	B_{od}	1.000	1.151	1.134	-
Formation volume factor oil (Flash)	B_{of}	1.000	1.149	1.132	-
Inverse formation volume factor gas	b_g	1.002	-	-	-
Gas oil ratio (DLE)	R_{sd}	0.0	49.47	46.66	Sm^3/Sm^3
Gas oil ratio (Flash)	R_{sf}	0.0	46.50	43.69	Sm^3/Sm^3
Compressibility oil	C_o	1.233E-04	1.073E-04	4.413E-04	1/bar
Compressibility factor gas	Z	0.9977	-	-	
Density oil	ρ_o	906.16	821.1	832.1	kg/m^3
Density gas	ρ_g	0.786	-	-	kg/m^3
Thermal expansion oil (T_{res})	C_T	5.455E-04	-	-	1/C

Table 1: PVT data; initial vs. present of Matzen H 703 [4]

A critical aspect of oil production is the change in viscosity of the fluid. Because viscosity does not change linearly, it is important to observe the temperature of the reservoir. A small decrease in temperature can have a large impact on the viscosity, and therefore on the production performance of a petroleum system. In the following diagram, the kinematic and dynamic viscosity curve is measured with a temperature range from 60°C (as the initial temperature) to 15°C. The measurement of the viscosity was performed with stock tank oil produced by a single stage flash to the atmosphere of the separator oil. In the diagram, the viscosity at 60°C is higher than in Table 1, which is because the measurement was conducted as a Dead/Stock Tank Oil measurement at atmospheric pressure. This means that all solved gases were already flashed, which led to a higher viscosity than under reservoir conditions.

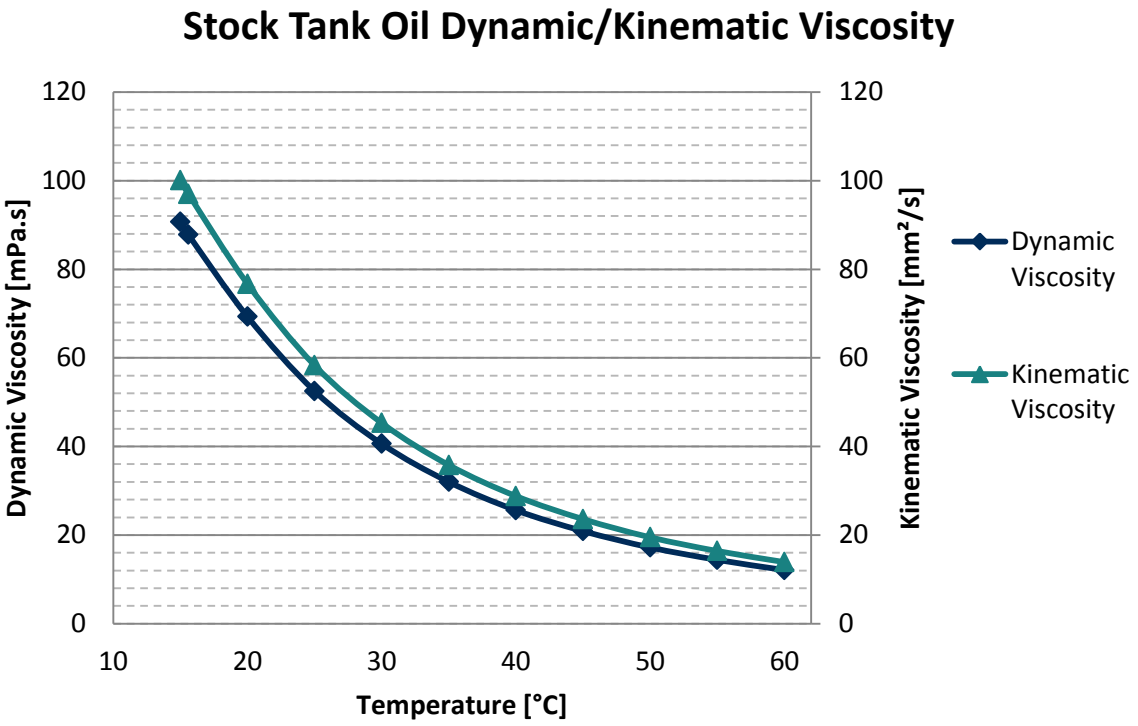

Figure 3: Viscosity vs. temperature behaviour; modified from [4]

The results from the 2016 PVT report indicated that no significant change occurred in the reservoir temperature, as well as that a difference of approximately 0.905 mPa.s (or 0.905 cP) is referred to as the pressure change over the last decades.

2.3 Production System

In the oil and gas industry, the consistent performance of a well over its whole lifetime is one of the most crucial goals. The transport of oil and gas from the reservoir zone to the surface facilities requires much energy, and therefore, the complete system should be designed to be as efficient as possible. Analyses to estimate all occurring losses from the bottom to the top are based on reservoir properties such as permeability, porosity, temperature, and pressure; on fluid properties such as viscosity and density; and also on the design parameters of the pipe system.

In general, every part of a production system causes an energy or pressure loss during the production of the fluid (see Figure 4). This thesis concentrates on the pressures indicated in the figure by $p_e, \bar{p}_r, p_{wfs}$ until p_{wf}, which are of utmost importance. The resulting pressure drop of the system is calculated by subtracting the final fluid pressure from the initial fluid pressure (see Equation **2.3.1**)

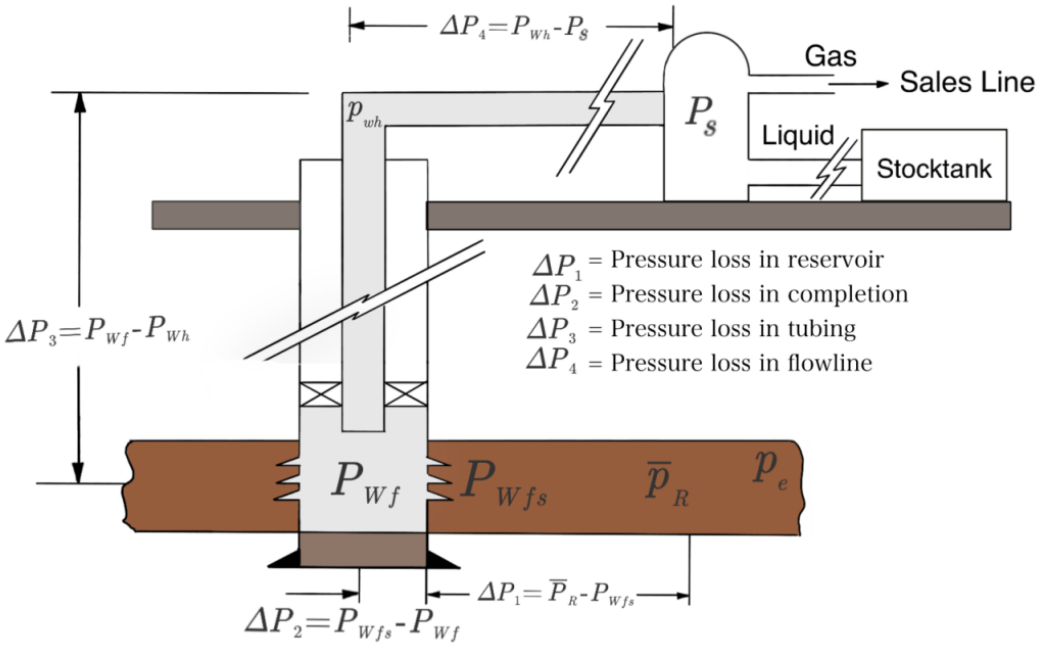

Figure 4: Pressure losses in a production system; modified from [5]

$$\Delta p = p_r - p_{wfs} - p_{wf} - p_{wh} - p_s \ldots\ldots \textit{Total Pressure Loss of System} \qquad \textbf{2.3.1}$$

Where

p_s	Inlet of separator pressure on surface [Bar]
p_e	External boundary pressure [Bar]
$\bar{p}_r$	Pressure, reservoir average [Bar]
p_{wfs}	Bottom-hole pressure, sandface [Bar]
p_{wf}	Bottom-hole pressure, flowing [Bar]
p_{wh}	Tubing pressure, flowing [Bar]

The pressure drop of the system defines the production ability of a system, and therefore, the combination of all components must be designed carefully. Because I examined the performance of horizontal wells, I mainly observed the pressure losses that occurred in the porous media and took effect until the horizontal or vertical wellbore.

2.4 Well Performance

The first pressure drop that appears in a system is the pressure drawdown from the reservoir to the well itself. To describe the motion of fluid and the included energy losses, a mathematical approach had to be found. The impact of friction forces and viscous shear forces in a porous medium was first explained by Henry Darcy in 1856 [5]. Not only did he develop the fundamental law of fluid motion for a horizontal linear system, but later on also developed the same for a radial system. The general Darcy law (**2.4.1**) only applies if the following aspects are fulfilled [6]:

- Laminar (viscous) fluid flow
- Steady-state fluid flow
- Incompressible fluids
- Homogeneous formation
- Constant temperature
- Newtonian fluid
- Nonreactive rock/medium

$$v = \frac{q}{A} = -\frac{k}{\mu}\frac{dp}{dx} \qquad Linear\ System \qquad \textbf{2.4.1}$$

$$v = \frac{q_r}{A_r} = -\frac{k}{\mu}\left(\frac{\partial p}{\partial r}\right)_r \qquad \text{Radial System} \qquad \textbf{2.4.2}$$

If higher velocities exist, which lead to turbulent flow, the equation must be modified [6]. If all requirements for Darcy flow are fulfilled, the final expression for the flow rate after Darcy (**2.4.3**) is as follows:

$$q = \frac{kA(p_1 - p_2)}{\mu L} \qquad \textbf{2.4.3}$$

Where

q	Flow rate [m³/s]
k	Absolute permeability [m²]
p_1, p_2	Pressure [Pa]
μ	Viscosity [mPa.s]
L	Distance [m]
A	Cross-sectional area [m²]

To include the drainage area of a well into Darcy's law, the radial form of Equation **2.4.3** is integrated, which results in two formulas, one for the steady state and laminar flow (**2.4.4**) of a reservoir and one for the pseudo-steady state or stabilised flow ($\bar{p}_r - p_{wf} = const.$, **2.4.5**) [6]

$$q_o = \frac{k_o h(p_e - p_{wf})}{\mu_o B_o \left[\ln \frac{r_e}{r_w}\right]} \qquad \textbf{2.4.4}$$

$$q_o = \frac{k_o h(\bar{p}_r - p_{wf})}{\mu_o B_o \left[\ln \frac{r_e}{r_w} - 0.75 + s\right]} \qquad \textbf{2.4.5}$$

Where

r_e	Radius to no-flow boundary [m]
r_w	Wellbore radius [m]
k_o	Effective permeability oil [m²]
s	Skin factor [-]
h	Thickness [m]
μ_o	Oil viscosity [mPa.s]
B_o	Oil Formation Volume Factor [-]

2.4.1 Productivity Index

To evaluate the productivity of a well, a specific performance property was introduced. The productivity index (PI) is the well's ability to produce hydrocarbons. It is defined by the symbol J, and is the ratio of the total liquid flowrate to the pressure difference of the drainage area pressure minus the bottom-hole flowing pressure. In the case of water free oil production, 2.4.6 shows the PI:

$$J = \frac{Q_o}{\bar{p}_r - p_{wf}} = \frac{Q_o}{\Delta p} \qquad \textbf{2.4.6}$$

Where

Q_o	Oil flow rate [m³/day]
J	Productivity index [m³/day/bar]
$\bar{p}_r$	Reservoir pressure (static pressure) [bar]
p_{wf}	Bottom-hole flowing pressure [bar]
Δp	Drawdown [bar]

PI is commonly evaluated during a production test. During the test, the well is shut-in until the wellbore reaches the static reservoir pressure. Subsequently, the well is adjusted to produce with a constant flow rate Q and stabilised bottom-hole flow pressure. The p_{wf} (bottom-hole flow pressure) should be recorded continuously to ensure accurate deliverables [6].

During the buildup of pressure in the wellbore, a change from a transient to pseudosteady-state region is recognised. After the pseudosteady-state flow is reached, the pressure drawdown stays the same and the PI becomes constant (see Figure 5).

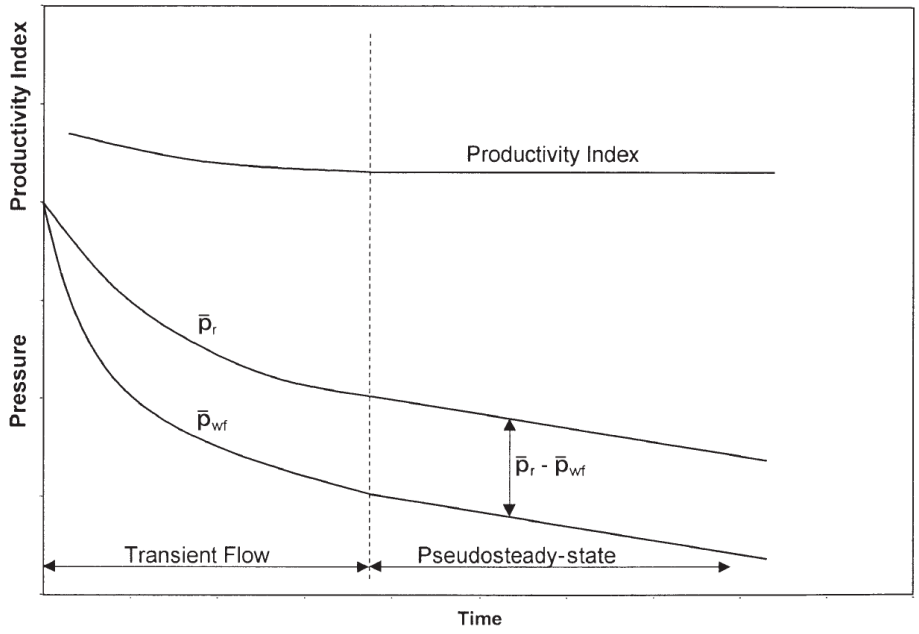

Figure 5: Productivity index changes over time [6]

Equation 2.4.6 for the PI and pseudosteady-state flow equation for slightly compressible fluids (Equation **2.4.7**) are combined into

$$Q_o = \frac{k_o h(\bar{p}_r - p_{wf})}{\mu_o B_o \left[\ln\frac{r_e}{r_w} - 0.75 + s\right]} \qquad \textbf{2.4.7}$$

This results in the PI, which is dependent on the fluid, rock, and wellbore parameters with Equation **2.4.8**:

$$\mathrm{J} = \frac{Q_o}{\bar{p}_r - p_{wf}} = \frac{k_o h}{\mu_o B_o \left[\ln\frac{r_e}{r_w} - 0.75 + s\right]} \qquad \textbf{2.4.8}$$

Because nearly all wells are situated in a steady-state flow regime condition during their lifetime, the PI calculation is not only effective for present performance evaluation, but it is also valid for determining future production data and also whether any deviations occur from the predicted production because of damage to the completion or reservoir itself. Due to the fact that perforation intervals and thicknesses of the reservoir can vary, it is necessary to normalise the PI to make it comparable. As result of this normalisation, the specific productivity index J_s was defined [6].

$$J_s = \frac{J}{h} = \frac{Q_o}{h * (\bar{p}_r - p_{wf})} \qquad \textbf{2.4.9}$$

The already known formulation of J can be rearranged as a straight line equation of the bottom-hole pressure and the flow rate. The resulting expression is as follows:

$$p_{wf} = \bar{p}_r - \left(\frac{1}{J}\right) Q_o \qquad \textbf{2.4.10}$$

As a result out of the equation of the PI and the rearrangement to the flow rate and bottom-hole pressure, we arrive at a graphical interpretation known as an inflow performance relationship (IPR) curve.

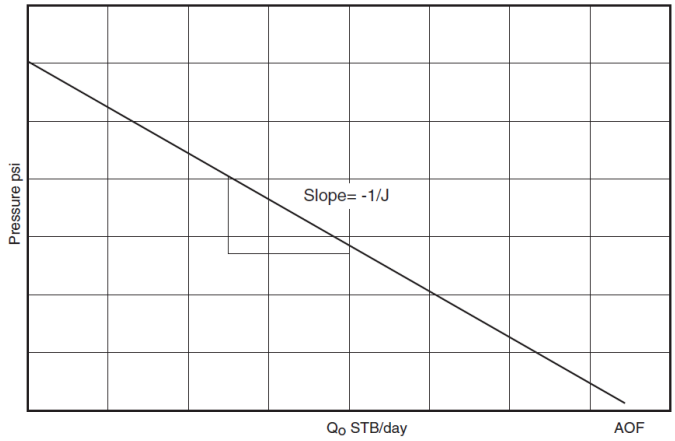

Figure 6: Inflow performance relationship [6]

Referring to Equation **2.4.10**, on the left side of Figure 6, where $p_{wf} = \bar{p}_r$, the flow rate Q_o is zero because of the mathematical definition. However, if $p_{wf} = 0$, the flow rate of the systems maximises, which is described as absolute open flow (AOF; see **2.4.11**).

$$\mathrm{AOF} = \mathrm{J}\bar{p}_r \qquad \textbf{2.4.11}$$

This definition of the inflow performance relation is valid when the system pressure is over the bubble point pressure. There, the inflow into the wellbore is directly proportional to the pressure drawdown. In the 1940s and 1960s, scientists (Muskat & Evinger 1941; Vogel 1968) observed that if the pressure drops below the bubble point pressure of the fluid, the straight line changes, as seen in Figure 7.

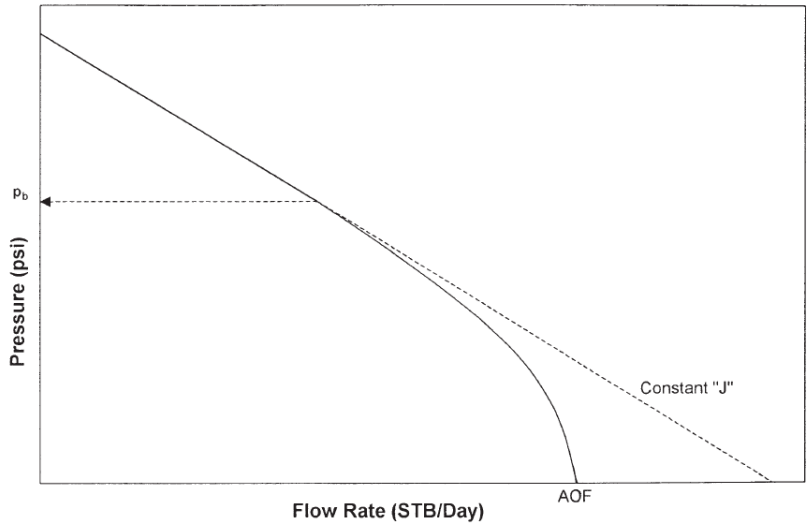

Figure 7: Inflow performance relationship changes at bubble point pressure [6]

To introduce the fluid properties into the PI equation, the oil relative permeability or pressure function was implemented into Equation **2.4.8** to give:

$$\mathrm{J} = \frac{hk}{\left[\ln\frac{r_e}{r_w} - 0.75 + s\right]}\frac{k_{ro}}{\mu_o B_o} \qquad \textbf{2.4.12}$$

Because we define the first part of the equation as being constant (Equation **2.4.13**),

$$\mathrm{c} = \frac{hk}{\left[\ln\frac{r_e}{r_w} - 0.75 + s\right]} \qquad \textbf{2.4.13}$$

it is seen that the PI (Equation **2.4.12**) is only dependent on oil viscosity, oil formation volume factor, and the relative permeability to oil. These three parameters and their dependence on the pressure are presented in Figure 8.

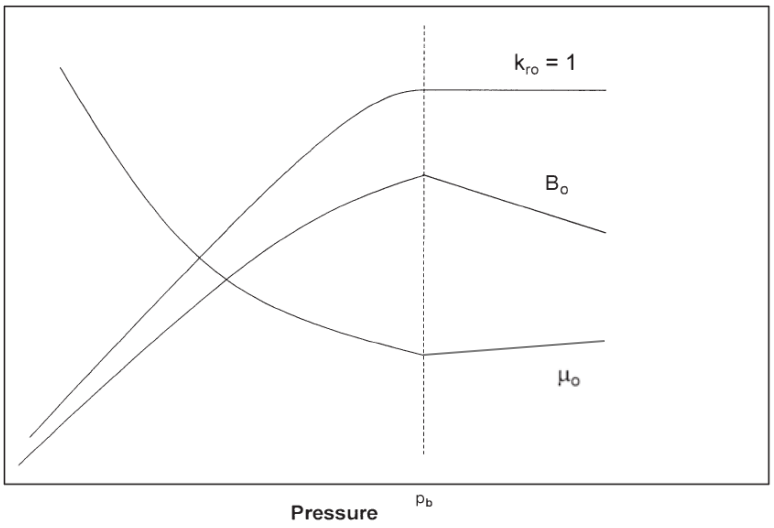

Figure 8: Pressure dependence of μ_o, B_o, and k_{ro}; modified after[6]

Pressure decreases because of reservoir depletion and if the initial reservoir pressure is reduced and due this reduction, the oil formation volume factor increases due to the expansion of the oil and will increase further on until bubble point pressure is reached. With ongoing decreasing of the reservoir pressure below the bubble point pressure, gas stored in the solution will be released and B_o starts to decrease until the oil formation volume factor equal one. The relative oil permeability stays constant until the pressure reaches the bubble point pressure. Below the bubble point pressure, the released gas increases the gas saturation and due to this the relative oil permeability is being lowered.

The oil viscosity decreases almost linearly until the bubble point pressure is reached. This decrease of μ_o until p_b, is a result of the oil compressibility. By lowering the reservoir pressure to p_b, decrease of μ_o is almost linear. By lowering the pressure below p_b, the lighter gas components will go out of the fluid, which results in an increase in viscosity due to the fact that only the heavy components remain in the fluid.

Understanding the phase behaviour of oil in a reservoir caused by pressure change is critical. Phase diagrams display the behaviour of a reservoir fluid when pressure or temperature change. The process begins with a saturated reservoir. Significant for a saturated oil reservoir is a well-developed separation between the gas cap and oil. Gas and saturated oil are in equilibrium and remain in this condition until the pressure of the reservoir changes. When the black line (Black Oil) in Figure 9 is followed from point A, the so-called bubble point line is reached. When the pressure falls below the bubble point pressure, gas is freed from the oil and the value for k_{ro} decreases. This behaviour shows that if production proceeds at a pressure that lowers p_{wf} below p_b, then the PI will decrease.

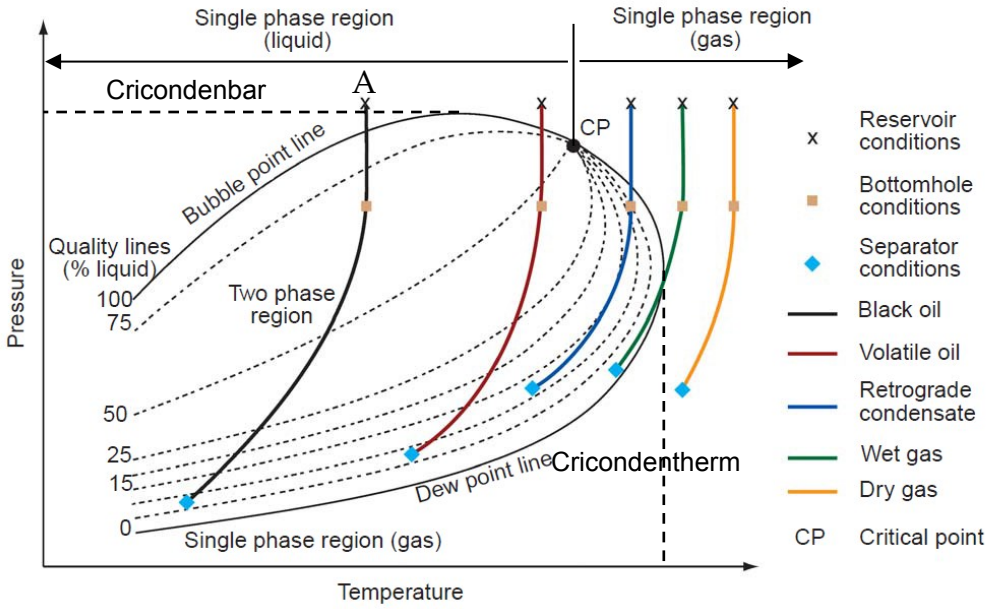

Figure 9: Phase diagram of a general multicomponent reservoir; modified after [7]

To observe the phase behaviour of the specific oil produced from the 16th TH in Upper Austria, an additional phase diagram is shown. The PVT study was conducted within a Research and Development project with the title "Changes in PVT properties over a lifetime of an oilfield" (Matzen). Accordingly, nearly up-to-date data are available for the observed area [4].

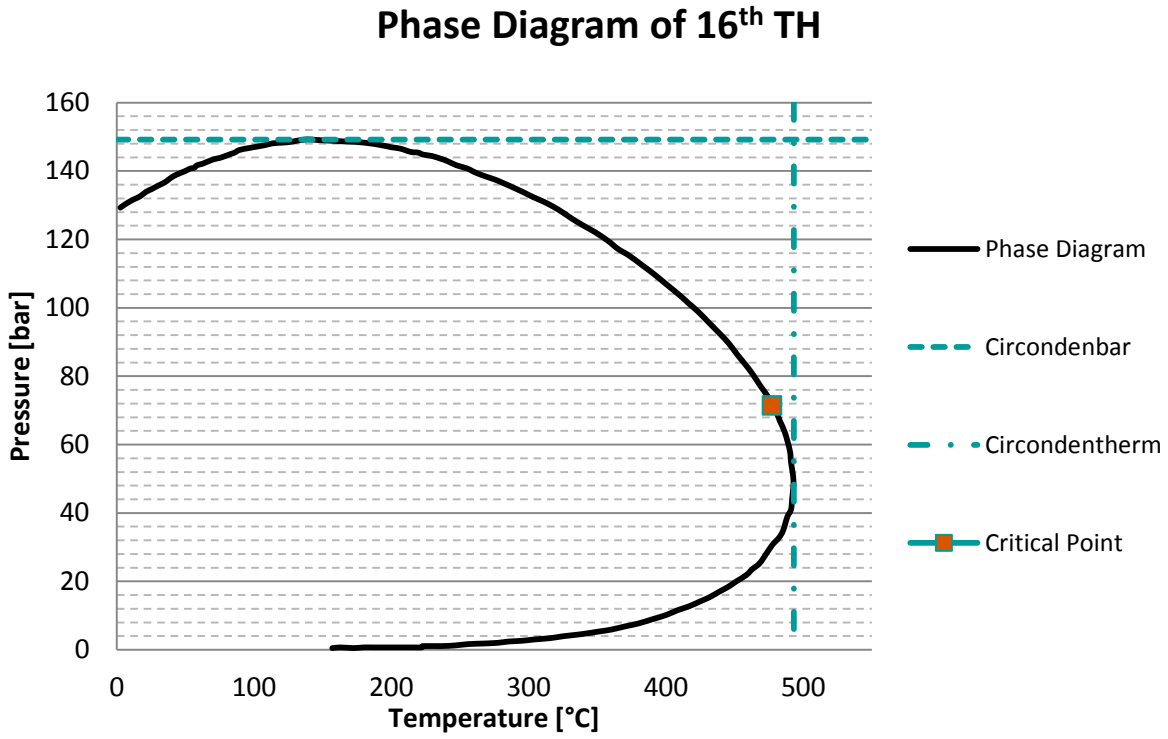

Figure 10: Phase diagram from the 16th TH; modified after [4]

Another effect occurring simultaneously to the creation of free gas is the reduction of the liquid's ability to flow in the porous media. The newly generated gas occupies more space in the pores, and therefore limits the effective flow area. The relative permeability is the ratio between the effective permeability of one fluid to the absolute permeability of the porous reservoir rock (see Equation **2.4.14**)

$$\mathrm{k}_{ro} = k_o/k \qquad \textbf{2.4.14}$$

Where

k_{ro}	Relative oil permeability [mD]
k_o	Effective oil permeability [mD]
k	Absolute permeability [mD]

The absolute permeability of a completely saturated reservoir rock is independent of the fluid until it behaves as a Newtonian fluid [5].

Another parameter that influences the PI is the oil viscosity. The viscosity of saturated oil will increase once the pressure falls below p_b. The growth is seen in Figure 8 and is explained by the solubility of the different C-components of the oil. The lighter components become gas, and the heavier elements with higher viscosities remain concentrated in the oil.

Also seen in Figure 8, the oil formation volume factor (B_o or FVF) is explained as an affecting factor of J. In the following equation, B_o is defined as follows:

$$B_o = \frac{(V_o)_{p,T}}{(V_o)_{ST}} \qquad \textbf{2.4.15}$$

Where

B_o	Oil formation volume factor [-]
$(V_o)_{p,T}$	Volume of oil under reservoir conditions [m³]
$(V_o)_{ST}$	Volume of oil under standard/stock tank conditions [m³]

When the bubble point pressure is reached, gas is freed, which forces the oil to shrink.

The following productivity graph (Figure 11) shows different curves of a reservoir when the pressure is alternated.

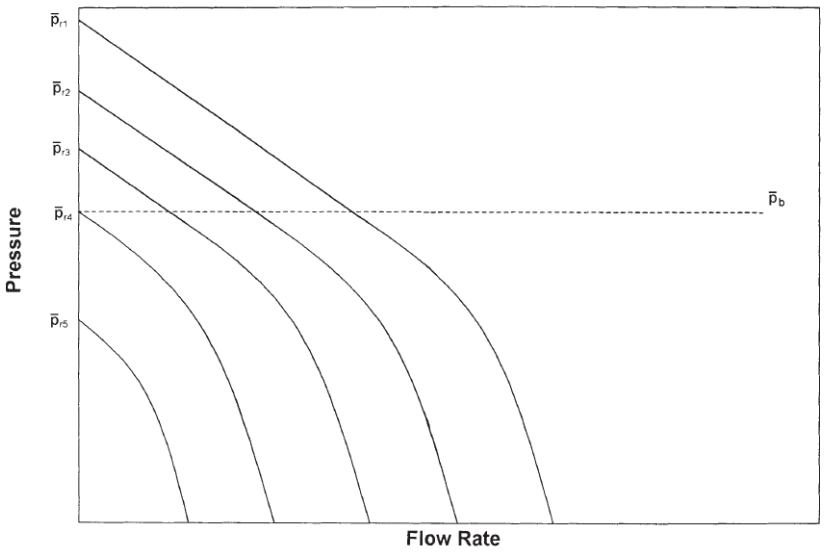

Figure 11: Effect of variable reservoir pressure on inflow performance ratio curves [6]

Over recent decades, numerous methods have been estimated to predict the nonlinearity behaviour of the IPR for reservoirs where solution gas drive occurs. Although a wide variety of methods exist, all of them include two basic computational steps:

- IPR curve construction at present average reservoir pressure (stabilised flow test).
- Prediction of future IPRs as function of average reservoir pressure.

A summary of the most crucial principal factors that affect IPR are listed as follows [5].

- As gas saturation increases (p_{wf} below p_b), k_{ro} decreases.
- Oil viscosity increases due to pressure decreases and freed gas.
- Oil shrinkage occurs because of pressure decreases and freed gas.
- Formation damage impinges on the skin factor.

2.4.2 Vertical Well Production

For vertical wells, various analytical and empirical methods exist to estimate the IPR, which were developed over the years. The most common methods are those by Vogel (1968), Wiggins (1993), Fetkovich (1973), and Standing (1970). As mentioned in the PI section of this thesis, the IPR exists for saturated and undersaturated oil reservoirs. In this thesis, the main focus is within saturated equations because the reservoir pressure of the 16th TH is already below the bubble point pressure.

Vogel's method (1968) is applicable for a multitude of reservoir conditions and requires the bubble point pressure p_b, stabilised wellbore pressure and rate (p_{wf}, Q_o), and the average reservoir pressure $\bar{p}_r$. Its mathematical origin is out of 21 reservoir data sets, which were used to develop the following IPR equation [8]. The basic Vogel equation for saturated oil reservoirs ($\bar{p}_r \leq p_b$) is presented in Equation **2.4.16**.

$$Q_o = (Q_o)_{max}\left[1 - 0.2\left(\frac{p_{wf}}{\bar{p}_r}\right) - 0.8\left(\frac{p_{wf}}{\bar{p}_r}\right)^2\right] \qquad \textbf{2.4.16}$$

Where

Q_o	Oil rate at p_{wf} [m³/day]
$(Q_o)_{max}$	Maximum oil flow rate under zero wellbore pressure [m³/day]
$\bar{p}_r$	Present average reservoir pressure [bar]
p_{wf}	Wellbore pressure [bar]

In the case of Wiggins (1993; see Equation **2.4.17**), a combination of four different groups of relative permeability and fluid properties were used to generate IPR curves for hypothetical oil reservoirs with the help of a computer model. Its formulation was similar to Vogel's and the equal data (p_b, Q_o, p_{wf} & $\bar{p}_r$) must be available to perform the calculations [6].

$$Q_o = (Q_o)_{max}\left[1 - 0.52\left(\frac{p_{wf}}{\bar{p}_r}\right) - 0.48\left(\frac{p_{wf}}{\bar{p}_r}\right)^2\right] \qquad \textbf{2.4.17}$$

In addition to the standard equation created by Wiggins (1996), he derived an equation for oil wells to predict the performance. It advances the original equation and exists in two versions. One version is for saturated oil reservoirs when the reservoir pressure is below the bubble point pressure, whereas the other version is for reverse reservoir conditions.

In 1970, Fetkovich (**2.4.18**) continued the mathematical approach of Muskat and Evinger (1942) to describe the IPR behaviour of the pseudosteady-state flow. For the saturated region ($\bar{p}_r \leq p_b$), the oil flow rate can be written as:

$$Q_o = \left(\frac{kh}{(\mu_o B_o)_{p_b}\left[\ln\frac{r_e}{r_w} - 0.75 + s\right]}\right)\left(\frac{1}{2p_b}\right)(\bar{p}_r^2 - p_{wf}^2) = \frac{J}{2p_b}(\bar{p}_r^2 - p_{wf}^2) \qquad \textbf{2.4.18}$$

The expression $\frac{J}{2p_b}$ is defined as constant C and in the literature it is also known as the performance coefficient. In the case of isochronal well tests, these are tests wherein different

production rates are used to produce but at equal time steps; the formulation of Fetkovich is used to describe the relationship. The resulting equation is known as the back pressure curve (see Equation **2.4.19**) [7; 6].

$$q_o = \mathrm{C}\left(\bar{p}_r^2 - p_{wf}^2\right)^n \qquad \textbf{2.4.19}$$

Where

C	Back pressure curve coefficient or performance coefficient
n	Curve fitting coefficient

As a last method for vertical well performance, that of Standing (1970) should be mentioned. In this case, the PI (**2.4.6**) is introduced to the Vogel equation, and afterwards rearranged (see Equation **2.4.20**) [6].

$$\mathrm{J} = \frac{(Q_o)_{max}}{\bar{p}_r}\left[1 + 0.8\left(\frac{p_{wf}}{\bar{p}_r}\right)\right] \qquad \textbf{2.4.20}$$

$$\mathrm{J}_p^* = 1.8\left[\frac{(Q_o)_{max}}{\bar{p}_r}\right] \qquad \textbf{2.4.21}$$

In equation **2.4.21** J_p^*, the so-called Standing's zero-drawdown PI is defined. As a final expression, Equation **2.4.22** is obtained where the future implemented reservoir conditions are denoted with the subscript "f" by the reservoir pressure [6; 9].

$$Q_o = \left[\frac{J_f^*(\bar{p}_r)_f}{1.8}\right]\left\{1 - 0.2\left[\frac{p_{wf}}{(\bar{p}_r)_f}\right] - 0.8\left[\frac{p_{wf}}{(\bar{p}_r)_f}\right]^2\right\} \qquad \textbf{2.4.22}$$

2.4.3 Horizontal Well Production

Vertical or slanted wells are the industry standard; however, the oil and gas industry has pushed their technical limits repeatedly, thereby achieving the drilling and completion technology required to perform horizontal wellbores. Over recent decades, horizontal wells have increased in importance in every part of the industry. High efficiency in thin reservoirs zones (reservoir thickness < 50 ft.) [10] or thick reservoirs with poor horizontal but high vertical permeability [10], for heavy oil reservoirs [11], wells with coning problems [11], and different EOR methods such as CO_2 flooding [11] is a significant contributing factor to the success of horizontal wellbores. The aim of horizontal wells is to increase productivity [12],

reduce coning effects in the wellbore [13], increase sweep efficiency [14], and intersect and drain vertical-fracture networks more effectively [15].

However, some disadvantages exist in the application of horizontal wells. First, the costs of horizontal wells are higher compared with vertical wells. For infill wells, costs are between 0.4 and 1.3 times higher, and for newly drilled wells, the range is from 1.5 to 2.5 times the cost of vertical ones [11]. When a reservoir is separated into more than one pay zone with high differences in depth, multiple horizontal wells must be drilled [11].

As already described in the vertical well performance chapter, the PI is an effective tool for evaluating the performance of wells. For horizontal wells, it is also possible to calculate a specific type of PI, which is discussed in the next chapter.

For a basic vertical well, a circular drainage area around the wellbore is assumed (see Figure 13), and if the 3D-shape of this drainage area is examined, it is similar to a cylinder where the wellbore is at its centre. When production is from highly deviated or horizontal wells, the drainage area will change from a cylindrical to ellipsoidal shape (see Figure 12 and Figure 13). The gravitational force compresses the cylindrical shape from the vertical wells and flattens the shape, which results in an ellipsoidal drainage area.

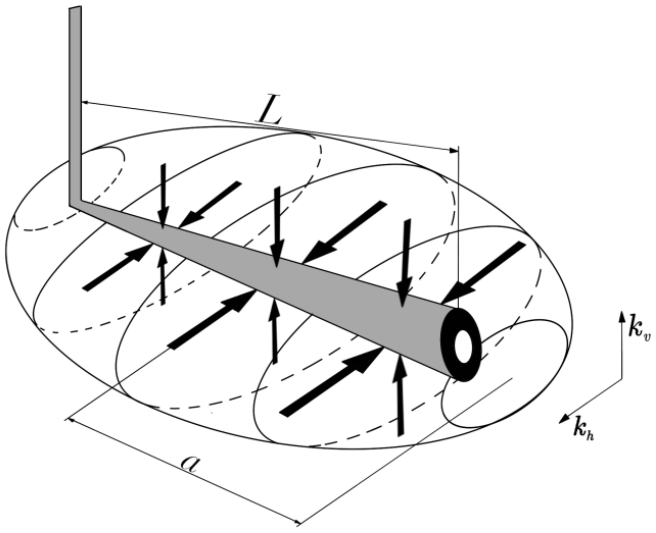

Figure 12: Ellipsoidal drainage shape of a horizontal wellbore; modified after [10]

The horizontal section is drilled over a length L into a reservoir with a horizontal permeability k_h and a vertical permeability k_v. The "a" in Figure 12 is related to the half major axis of the drainage profile. For a horizontal well of both types, radial and laminar flows can exist; therefore, the behaviour may appear similar to an extensively fractured well.

In the literature, several authors have announced measuring similar IPRs for horizontal wells compared with the predicted IPRs following Fetkovich or Vogel. They have also reported that the productivity of horizontal wells is up to four times higher than that of vertical wells [6].

To evaluate the differences between vertical and horizontal wells, Joshi (1991) compared both types in an identical reservoir with equivalent permeabilities and identical height. Figure 13 presents their geometries. Joshi proposed two methods with different methodological approaches to calculate the drainage area.

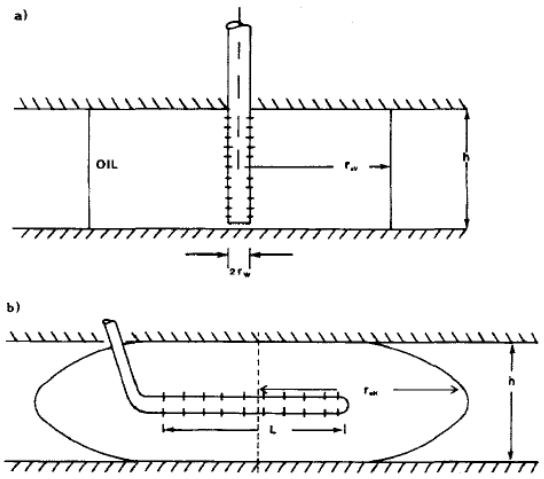

Figure 13: Schematics of vertical- and horizontal-well drainage volume [12]

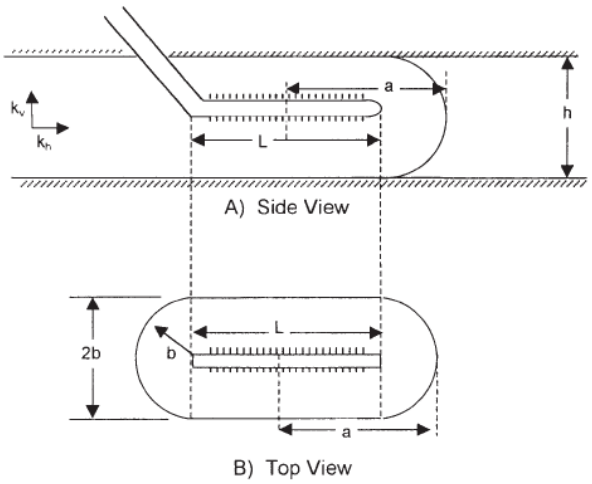

Figure 14: Horizontal geometry and well drainage area [6]

One method proposed that the geometry exists out of two half circles (radius b) at each end of the horizontal section as well as a rectangle (**2.4.23**), whereas the second methods assumed that the horizontal drainage area is represented by an ellipsoid (**2.4.24**).

$$A = L(2b) + \pi b^2 \qquad \textbf{2.4.23}$$

$$A = \pi ab \quad with \quad a = \frac{L}{2} + b \qquad \textbf{2.4.24}$$

Where

A	Drainage area [m²]
L	Length of horizontal section [m]
b	Half minor axis of an ellipse [m]
a	Half major axis of an ellipse [m]

Both variants provide different values for the drainage area; thus, Joshi noted that an average of the two should be measured [6].

The calculations of the inflow performance of horizontal wells are divided into steady-state single-phase flow and pseudosteady-state two-phase flow conditions. First, this paper will examine the steady state flow regime. At this point, an analytical solution to the flow rate equation (**2.4.25**) is a simple yet valid technique. A limit of this equation is that the reservoir pressure does not change at any point in the reservoir at any time.

$$Q_{oh} = J_h \Delta p \qquad \textbf{2.4.25}$$

Where

Q_{oh}	Horizontal flow rate [m³/day]
Δp	Pressure drop, drainage boundary to wellbore [bar]
J_h	PI of horizontal well [m³/day/bar]

Several methods exist for calculating the PI for horizontal wells as well as for vertical wells. Two of the most crucial methods are Joshi's method (1988-1991) and the model of Babu and Odeh (1989).

The horizontal well performance of Joshi (1991) depends on the geometrical dimension of the ellipse, which is introduced into the equation by R and a (see **2.4.26** & **2.4.27**)

$$R = \frac{a + \sqrt{a^2 - (L/2)^2}}{(L/2)} \qquad \textbf{2.4.26}$$

$$a = (L/2)\left[0.5 + \sqrt{0.25 + (2r_{eh}/L)^4}\right]^{0.5} \quad \textbf{2.4.27}$$

Where the drainage radius of a horizontal well is defined as r_{eh}[6]:

$$r_{eh} = \sqrt{\frac{A}{\pi}} \quad \textbf{2.4.28}$$

Where

A	Horizontal drainage area [m³]
r_{eh}	Horizontal drainage radius [m]

As a last property parameter, factor B must be introduced:

$$B = \sqrt{\frac{K_h}{K_v}} \quad \textbf{2.4.29}$$

Where

K_h	Horizontal permeability [mD]
K_v	Vertical permeability [mD]

Combining Equations **2.4.26, 2.4.27,** and **2.4.28** into the PI equation for vertical wells, Joshi presented the PI for horizontal wells in isotropic reservoirs (**2.4.30**).

$$J_h = \frac{hk_h}{\mu_o B_o[\ln(R) + \left(\frac{h}{L}\right)\ln\left(\frac{h}{2r_w}\right)]} \quad \textbf{2.4.30}$$

If the reservoir has anisotropic properties, such as different horizontal and vertical permeabilities, Joshi introduced the factor B (**2.4.29**) to consider both permeabilities k_v & k_h [12].

$$J_h = \frac{hk_h}{\mu_o B_o[\ln(R) + \left(\frac{B^2 h}{L}\right)\ln\left(\frac{h}{2r_w}\right)]} \quad \textbf{2.4.31}$$

The aforementioned method of Joshi is valid only for wells that are placed at the reservoir centre on a vertical plane. To improve his work, Joshi used Muskat's [16] formulation for decentralised wells (**2.4.32**) [12]

$$q_h = \frac{2\pi k_o h \Delta p}{\mu_o B_o \left[\ln(R) + \frac{h}{L}\ln\left(\frac{(h/2)^2 - l_\delta^2}{h r_w/2}\right)\right]} \qquad \textbf{2.4.32}$$

The productivity relation of Joshi (1988) was extended by Economides et al. (1990). This led to a mathematical expression in which a combination of the pseudo-steady state in the vertical area and steady state in the horizontal plane are found [10]. The equation is as follows:

$$q = \frac{kh\Delta p}{B\mu\left[\ln\left(\frac{a + \sqrt{a^2 - (L/2)^2}}{L/2}\right) + (\frac{I_{ani} h}{L})\ln\left(\frac{I_{ani} h}{r_w (I_{ani} + 1)}\right)\right]} \qquad \textbf{2.4.33}$$

where I_{ani} represents the permeability ratio that was also presented in **2.4.29** with the symbol B.

Basically, the production of a well depends on its drainage area. In the case of vertical wells, the production rate increases in a normal case in a directly proportional manner to the wellbore radius. In this case, a slanted or horizontal well with a higher production can also be represented by a simple vertical well with a large drainage radius. The effective wellbore radius is dependent on the dominant skin factor and is defined in Equation **2.4.34**. The more negative the skin factor of the wellbore, the higher the effective radius and the resulting production [12] will be.

$$r_{we} = r_w \exp(-s) \qquad \textbf{2.4.34}$$

Where

r_{we}	Effective wellbore radius [m]
r_w	Wellbore radius [m]
s	Skin factor [-]

Underlying the mathematical approaches of Joshi (1988) and Economides (1990), Babu and Odeh (1989) determined an equation for the inflow of a horizontal well. The goal was an easy and practicable tool for field engineers; it is valid for wells in a box-shaped drainage area where the wellbore is eccentric. Figure 15 illustrates the geometrical construction.

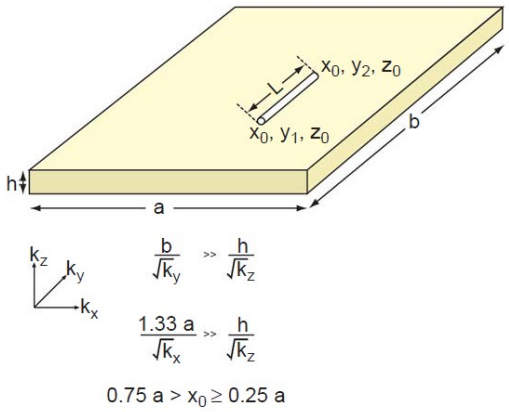

Figure 15: Rectangular drainage area with a horizontal well following the model of Babu and Odeh [7]

They used one of the inflow equations for vertical wells and modified it as follows to generate the following horizontal inflow equation (**2.4.35**) [17]:

$$q = \frac{b\sqrt{k_x k_z}(\bar{p}_r - p_{wf})}{B\mu\left[\ln\left(\sqrt{A}/r_w\right) + \ln(C_H) - 0.75 + s_r\right]} \qquad \textbf{2.4.35}$$

This led us to the general form of the productivity index J (**2.4.36**)

$$J = \frac{b\sqrt{k_x k_z}}{B\mu\left[\ln\left(C_H\sqrt{A}/r_w\right) - 0.75 + s_r\right]} \qquad \textbf{2.4.36}$$

Where

s_r	Skin resulting from partial penetration
C_H	Geometric factor
B	Formation volume factor [-]
μ	Viscosity [mPa.s]
k_x, k_x, k_z	Permeability in x, y, z direction [mD]

Factors s_r and C_H are complex geometrical factors that depend on the penetration length of the horizontal well and width of the drainage area [17; 7]. The main differences between the model of Joshi and that of Babu and Odeh is that Babu and Odeh's model can also work with wells that are not centred in the reservoir area; furthermore, it is based on a semi-steady state assumption with no-flow boundaries.

2.5 Gas and Water Coning

Coning is an undesired effect in which gas from a gas cap or water from the bottom of the reservoir reaches the perforations of a producer well. Coning can occur in both vertical and horizontal wells. Moreover, coning is related to the water or gas breakthrough because of production rates that are too high. When a water or gas face reaches the perforation, the oil production will decrease the more the water or gas fraction increases.

As a result of coning, a newly created production environment (e.g., reservoir fluid with CO_2 or H_2S) can increase corrosion at the completion. Furthermore, this aggressive media will lead to costly workovers and/or disposal costs of the produced corrosive fluid. The working principles of coning are controlled by three forces, which are responsible for the development of the unwanted reservoir effect.

The least influential force is the capillary force; its effect is so small that it is neglected most of the time. The second factor is the gravitational force. Gravitational force is the reason for density separation of fluids and is directed vertically (in a Y-direction in Figure 16). The third factor is the viscous force. This term is related to the fluid flow in the reservoir, which is triggered by the pressure gradient. The viscous force is described by Darcy's Law (**2.4.3**) [6].

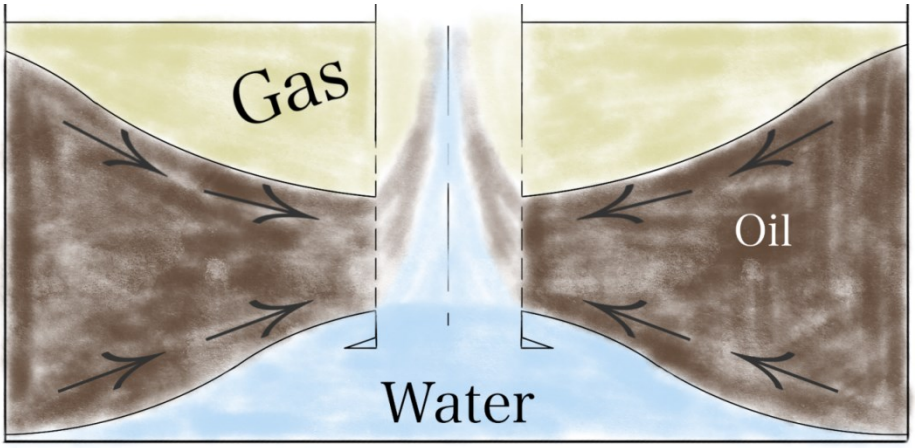

Figure 16: Illustration of water and gas coning

The nonconing state of the reservoir is described as a balance between viscous and gravitational force. A stable cone develops if the gravitational force is smaller than the viscous force (dynamic), resulting in a high probability of decreased production or even total loss of production.

This thesis examines three horizontal wells in the Bockfließ area, which have extremely high water cuts (see Table 2) and very low gas contents.

Table 2: WC of horizontal wells in the Bockfließ Area (Source: GDB)

		BO 204	BO 205	BO 208	
Water Cut	WC	~ 99%	~ 80 %	~ 98 %	%

Because a lower pressure drawdown in horizontal wells is necessary for production, as well as in OMV wells the WCs are already this high, water coning has no relevant influence in these wells [18]. Nevertheless, coning occurs in some wells in Austria. In a later chapter, production data of horizontal wells as well as some data from specifically selected vertical wells are used to evaluate the performance of the redevelopment wells. The Bockfliess 202 well is a vertical well where coning occurs, and therefore, it will not be considered as a comparative value in water cut comparisons.

2.6 Completion

In general, wellbore completion is the connection between the surface and the reservoir from which production is sought, and it is divided into upper and lower completion.

This chapter discusses lower completion, which is the interface between the zones of interest and the wellbore itself. Its configuration depends on the type of fluid (i.e., oil, water, or gas), formation properties being consolidated or unconsolidated, and reservoir properties such as pressure and temperature. Referring to Figure 17, we define two main categories of completion, open hole (OH) and cased hole.

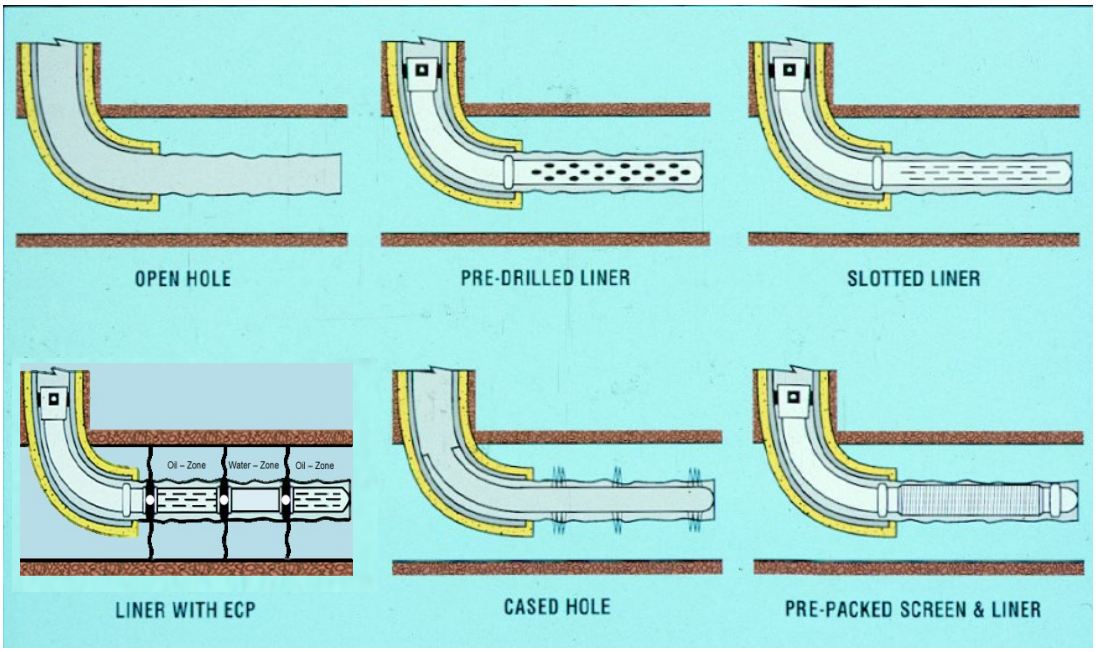

Figure 17: Different reservoir completion methods; modified after [19]

2.6.1 OH Completion

Barefoot or OH completion is the oldest, simplest, and cheapest completion type. It is preferred in hard formations such as limestone or dolomite, where the geological structure is stable and the borehole is not at risk of collapse. The casing and cement can stop in front of the reservoir and the remaining path is drilled without any additional stabilising equipment except for drilling fluid. Or as seen in Figure 17, one possibility is that the casing and cement reaches until the target formation and the residual horizontal section is completed without cement or support of a casing.

OH completions have advantages such as their simple design; however, some problems exist too. Table 3 lists the advantages and disadvantages of OH completion.

Table 3: Open hole completion properties

	Advantages	Disadvantages
Open-Hole/ Barefoot Completion	Low costs No artificial restrictions →360° open to the formation face Recompletion is possible Less to no formation damage due to shorter fluid exposure	Poor inflow control Damage repair is difficult Wellbore stability problems High water/gas breakthrough risk Limited injection options

In OH completion, the possibility exists to use so-called pre-drilled or slotted liners. To make sand production manageable, a combination of production tubing with gravel pack/sand control screens can be used [20; 7].

Slotted liners are used to support the formation and prevent borehole collapse. In additional to their geometrical support, it is possible to optimise the slots in terms of size and shape to control inflow into the wellbore. Nevertheless, slotted liners are normally not used for sand control, but they allow the application of packers to isolate less optimal reservoir zones (zonal isolation; ZI), and therefore optimise production.

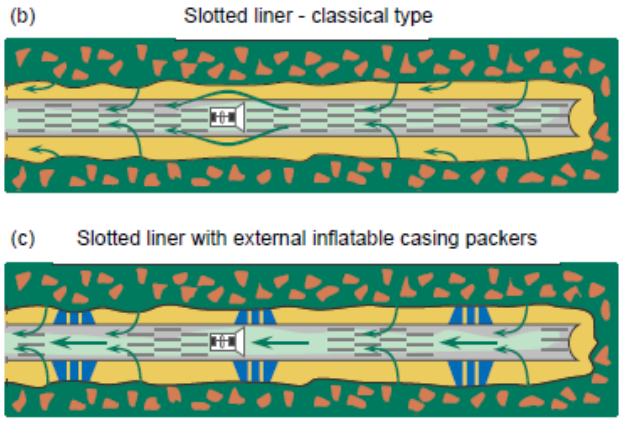

Figure 18: Schematic of a slotted liner without external packers (top) and with external packers (bottom) [21]

Because of the geometry of pre-drilled liners, they have a higher inflow and are not so sensitive to the plugging of holes compared with the slotted configuration. Table 4 summarizes the advantages and disadvantages of slotted or pre-drilled liner completion [19; 22; 7].

Table 4: OH-Slotted-/Pre-drilled Liner Properties

	Advantages	Disadvantages
Slotted-/ Pre-Drilled Liner Completion:	Low costs Safer against borehole collapse than pure OH completion Inflow restrictions are minimal More efficient removal of filter cake through circulating More applicable for coiled tubing and other working strings (low μ)	Less to no flow control Zonal isolation is difficult Crossflow potential Workover is difficult (liner pulling for remedial work) Mitigated liner strength caused by slots, holes → collapse Ineffective sand control Recompletion is very difficult

In addition to standard completion with slotted or pre-drilled liners, new technologies are available on the market that were introduced with well Bo 208 for the first time in OMV's history. Inflow Control Devices (ICDs) and other related technologies belong to so-called "intelligent" completion technology and are discussed in Chapter 2.8.

To reduce the disadvantages of crossflow with slotted or pre-drilled liners, perforated liners in combination with external casing packers (ECPs) are used. ECPs are discussed in Chapter 2.7.

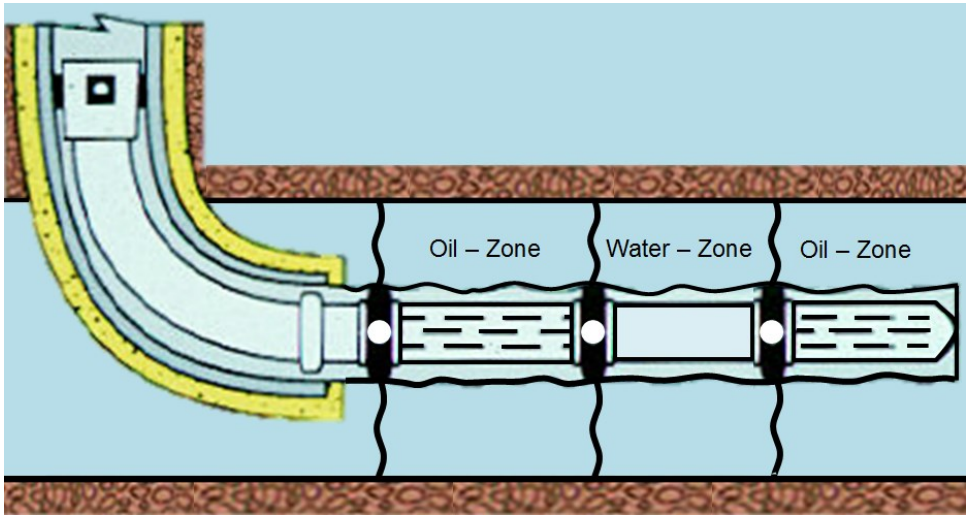

Figure 19: OH completion with a slotted liner and external casing packers; modified after [19]

Through the integration of packers, the possibility of efficient isolation between different production zones and no productive or water/gas bearing zones is provided as seen in Figure 19. Additionally there are other techniques available. Inflow control into the wellbore can be done by a variety of configurations.

For example is the combination of packers with sliding sleeves, various types of screen, blank sections (i.e., pipes without slots or holes), and even inflow control devices a good alternative. Although ECPs provide some improvements compared with basic OH-slotted/pre-drilled completion, some disadvantages can occur with their use.

To place ECPs in the correct location, logs and calipers have to run. Although ZI is possible, if high permeable zones exist around the packers or poorly consolidated formations, the flow may occur around it and result in borehole instabilities that can negatively influence sealing abilities. Furthermore, this type of completion is more expensive than others.

2.6.2 Cased Hole Completion

In cased hole completion with perforations, a liner or casing is placed in the reservoir and cemented. Subsequently, the zones of interest are perforated again to create communication between the reservoir and production string.

The penetration depth of these perforations depend on the nearest wellbore damage area and are placed on the most effective spots to avoid weak formations and nonproductive zones. Because of the availability of sliding side doors (sliding sleeves), it is possible to shut the perforated zones on or off separately, thereby improving the overall productivity; this is the same procedure as in OH completion with slotted/pre-drilled liners and ECPs.

Table 5 summarises the advantages and disadvantages of cased hole completion.

Table 5: Cased hole completion properties

	Advantages	Disadvantages
Case Hole Completion:	Excellent flow control Excellent zonal isolation High wellbore stability Pass near wellbore damage through perforations Necessary for hydraulic fracturing Production logging is possible	High costs of completion (e.g., casing and cement) Perforation costs Limited applications (not in naturally fractured formations) Highly limited formation exposure Liner cementing slightly reliable

A summary of the advantages and disadvantages between OH and cased hole characteristics is provided in Appendix A.

2.7 Inflow Control

Horizontal wells are characterised by a generally lower pressure drawdown compared with vertical wells over the reservoir contact zones. Due to the length of the horizontal production section, an influential pressure drop occurs in the pipe itself. To produce oil from the end of the horizontal area (toe section), the oil must overcome the pressure threshold in the pipe. However, the oil at the beginning of the horizontal section is not exposed to this pressure, and therefore, the flow rate in the heel section is much higher [23].

One feature of inflow control measurements is that they separates different zones from each other, which prohibit the annular flow around the wellbore in case of a water or gas breakthrough. OH completions are highly effective because of the maximised reservoir flow potential, but with regard to their ability to control the subsurface flow, much improvements are necessary. Over the last decade, OH ZI in combination with inflow control devices or PL/SL has become increasingly crucial to recover the control of OH production.
Further regularly used methods for ZI are ECPs, gravel packs (GPs), and cementing of pipes [24]. Cementing is a standard method for ZI, but the cement can cause skin problems near the wellbore. A schematic configuration of an ECP is presented in Figure 20. The inflation process can be performed using mud (via wash pipe) or cement [25].

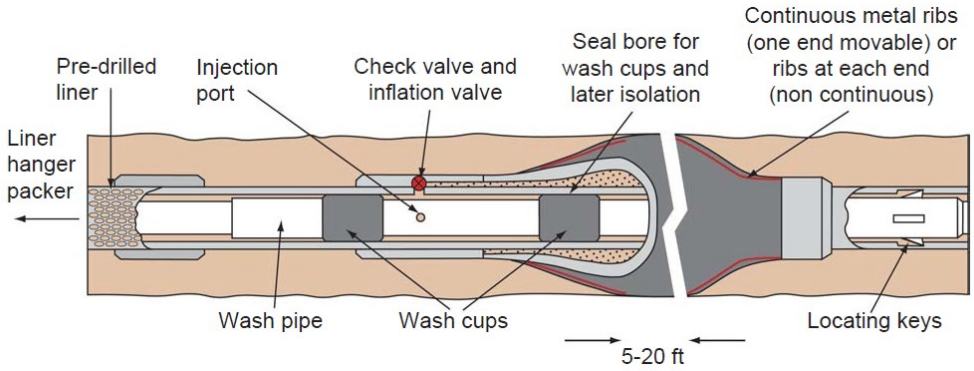

Figure 20: External casing packer [7]

Swellable elastomer packers (SEPs) are more relevant these days. The vulcanised elastomer on the outside of a steel pipe reacts with the completion fluid or reservoir fluid and expands. This swelling of the elastomer is a thermodynamic absorption process and the overall amount of swelling depends on the chemical composition of the elastomer, the predominant fluid salinity and the prevailing temperature of the fluid where the packer is placed. The driving force behind it is the similarity of the solubility parameter of the fluid and the polymer. The closer these parameters are to each other, the higher the affinity between the

packer and fluid. The rubber will expand until a level of equilibrium is developed and then remains constant. Properties such as tear strength, hardness, tensile strength, elongation at break and modulus decrease during the swelling process, but the sealing ability between the casing and wellbore increase. Figure 21 shows a centralised SEP and Figure 22 shows a decentralised SEP.

Figure 21: SEP (centralised) [7]

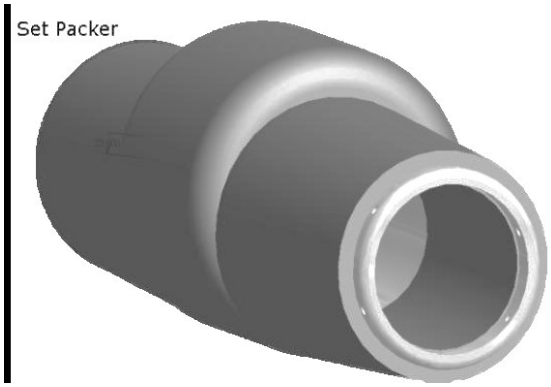

Figure 22: SEP (decentralised) [24]

Compared with ECPs, SEPS are more simply constructed and possess fewer or no moving parts, which can cause failure of the sealing equipment. Furthermore, the overall costs of ECPs are higher in terms of capital cost and installation expenditure. A disadvantage of SEPs is that the final swelling status requires some time. For the installation of this kind of packers, knowledge of the given chemical conditions is decisive. Beside temperature, CO_2 and H_2S concentration must be known, to design a complex elastomer that fits to these conditions and a reliable function is provided. Factor influencing the performance of an elastomer downhole are also the possibility of contact with completion fluid or close contact with solvents as for example methanol or xylene. Furthermore, transport and storage of the packer and prevention of contamination are of the utmost importance.

2.8 Inflow Control Technology

In horizontal wells, the pressure distribution differs from the toe to the heel. This pressure difference causes irregular influx into the wellbore, which can result in various production-related problems such as water or gas coning and higher velocities in some parts of the horizontal section; these higher velocities can lead to erosion and further corrosion problems.

To overcome these problems and smooth the pressure distribution, ICDs were invented. Different possibilities exist for controlling the influx into a wellbore; for example, a simple sliding side door or sliding sleeve (SS), inflow control valves (ICVs), or ICDs [26; 27; 7]

The basic idea behind this completion component is to restrict the flow in areas with higher permeability or where other fluids (e.g., water or gas) occur and increase the pressure drop in these sections. The Norwegian company Norsk Hydro introduced the advanced technology of ICDs in the early 1990s, which they used to improve the performance of a giant gas field with small oil rims named the Troll Field in Norway [28].

In this field, the ICDs worked quite impressively for enhancing productivity, but generally, standard ICDs have one problem: all adjustments for flow regulation must be performed in advance of the installation. Over time, the fluid properties of a reservoir change, and water or gas coning begins to occur (see Figures 23 and Figure 24). Normal ICVs have no adaptability to this situation, resulting in an additional requirement for passive flow control devices (FCDs) or proactive FCDs, because the settings of these devices are based on reservoir simulations and cannot be changed afterwards or during production without quite large expenditures.

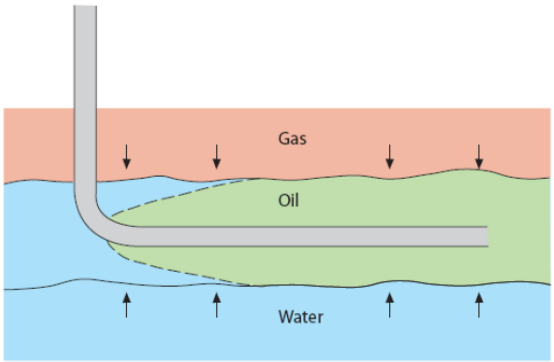

Figure 23: Horizontal coning problem [26]

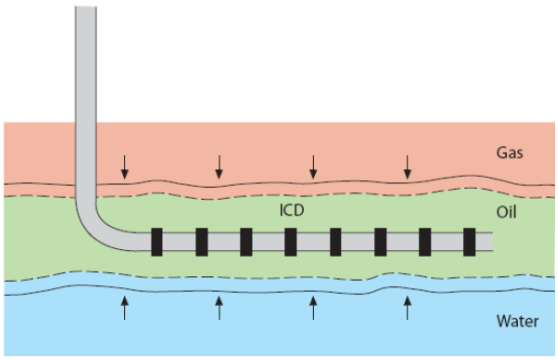

Figure 24: Equalised pressure distribution with ICDs [26]

Over the years, ICDs have been permanently optimised, and additional new types of FCDs have been created. Thus, it is now possible to use components that not only restrict the flow through density differences, but also through viscosity differences. Nowadays, other newly developed autonomous ICDs (AICDs), which are designed to perform without any further wellbore interventions and regulate the fluid restriction on their own, are used in industry.

In the E&P industry, few companies currently have special sectors for ICDs. Companies such as Schlumberger, Halliburton, Baker Hughes, Weatherford, Tendeka, and HP Well Screen are the most well-known.

2.8.1 ICVs

ICVs are remotely operated completion components controlled from the surface; they are used to partially or fully choke the inflow into the wellbore and are known in industry as so-called active control components or interval control valves. They are effective at stopping water or gas breakthrough completely when it occurs, but they are limited to the number of zones that they can be operated in. Installation of ICVs is complicated and they are provided with electrical and/or hydraulic power as well as a data transfer cable to each unit from the surface.

In general, ICVs have additional measurement components such as pressure or temperature sensors and flow metres, and therefore, they belong to the more expensive elements of inflow control. As a basic part of so-called smart wells, it is important to identify the "perfect" location for ICVs. Reservoir parameters such as porosity, permeability, viscosity, and other fluid and rock properties must be identified during the planning phase to position the ICVs in the right and most effective spot [29].

2.8.2 ICDs

ICDs pertain to the group of passive smart completion components. A typical ICD tool is illustrated in Figure 25. There, the reservoir fluid flows around the production section. The oil streams through the screens, which are wrapped around the so-called base pipe, and leads the oil directly to the ICD. Within the ICD, numerous orifices control the influx of fluid [23].

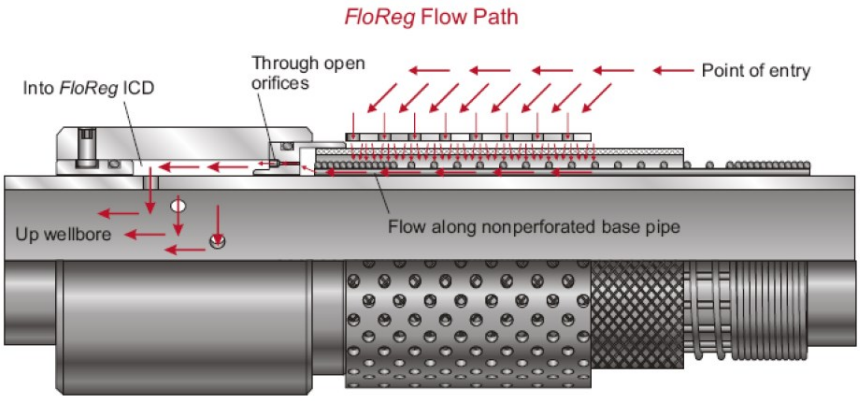

Figure 25: Weatherford FloReg inflow control device [23]

In industry at present, there are three basic types of ICD and one hybrid type. They create a pressure drop through flow restriction as well as through an increase of friction. Figure 26 presents the main ICD types with three-dimensional computer-aided design images using the SOLIDWORKS® software package [30].

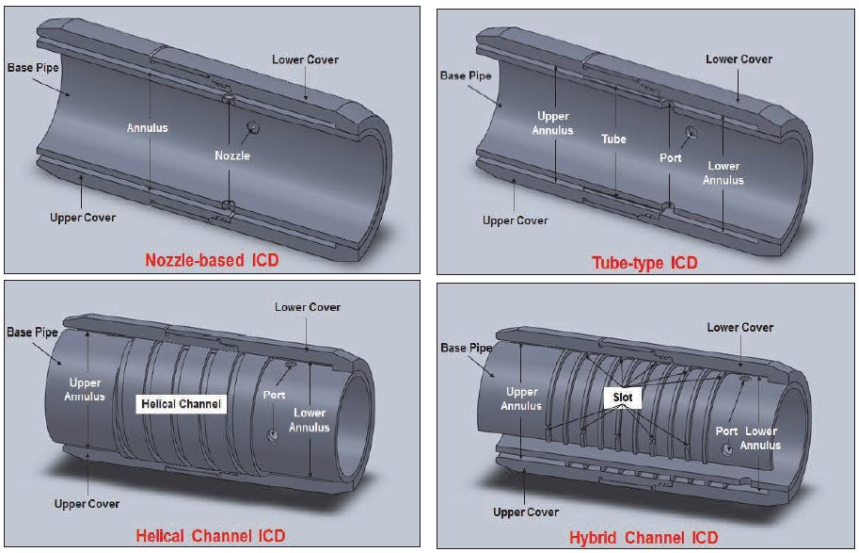

Figure 26: Images of the four main types of ICD [30]

2.8.2.1 Nozzle-Based ICDs

Nozzle-based ICDs are designed to restrict flow. Fluid enters at the screen, flows towards the orifices, and leaks into the pipe. The number of nozzles and their diameters are set according to the pressure drop required to reach the production rate. This pressure drop at the nozzles is a function of the flow rate and is based on Bernoulli's equation (**2.8.1**):

$$\Delta p = \frac{1}{2}\rho v^2 = \frac{\rho Q^2}{2A^2} \qquad \textbf{2.8.1}$$

Where

ρ	Density [kg/m³]
v	Velocity [m/s]
Q	Flowrate [m³/s]
A	Nozzle cross section [m²]

Nozzle-based ICDs are active well completion components (self-regulating), which is an advantage because reservoir uncertainties such as permeability and fluid composition change over time [31] before readjusting themselves.

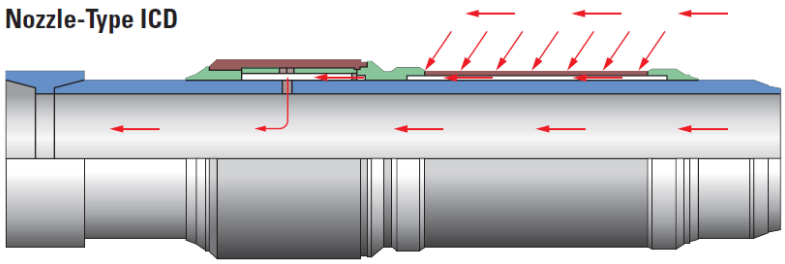

Figure 27: Nozzle-based ICD [31]

The flow restriction depends on the number of nozzles and orifices that are integrated in the horizontal section, and therefore, the pressure drawdown over the whole horizontal section depends more on velocity and fluid density than on viscosity. One problem of this type of completion is the possibility of erosion caused by high velocity at the nozzles.

2.8.2.2 Helical Channel ICDs

The working principle of this ICD is not restriction of the flow path compared with the nozzle ICDs; instead, an extended travel path is responsible. The red arrows in Figure 28 demonstrate the fluid flow from the reservoir towards the ICD. After the liquids pass the screens, they move in the direction of the channels.

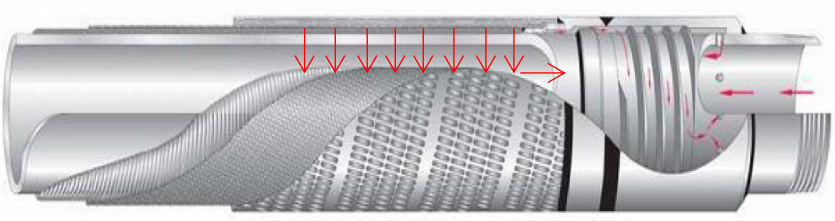

Figure 28: Baker Hughes helical channel ICD [31]

The helical channels restrict fluid flow through their geometry, and guide the reservoir fluid to the inside of the ICD chamber. Compared with the nozzle-type ICDs, the helical channels are more difficult to adjust at the well site and also more time consuming, which results in higher costs [31]. The helical channels increase the length that the fluid has to travel, and with this, the velocity decreases. As a result, this type of ICD is less susceptible to erosion because of lower streaming velocities.

2.8.2.3 Hybrid Channel ICDs

A further development of the helical channel ICD is the slot-type ICD, which is a so-called hybrid ICD. To reduce the pressure drawdown dependency from the viscosity of the helical channels, the channels were modified with slots of different sizes. These slots introduce a predefined differential pressure and flow rate through their size and geometry.

The slots are positioned at different distances, which force the fluid to change direction when it moves through the channels. The number of channels is responsible for the velocity change, and therefore for the occurring differential pressure. A construction drawing of a hybrid type ICD is seen in Figure 29. This hybrid type has slots modified with water swelling rubber, which decreases the diameter of the slots if the activating fluid passes through. The forced direction change and diameter reduction of the hybrid ICD are seen in Figure 30.

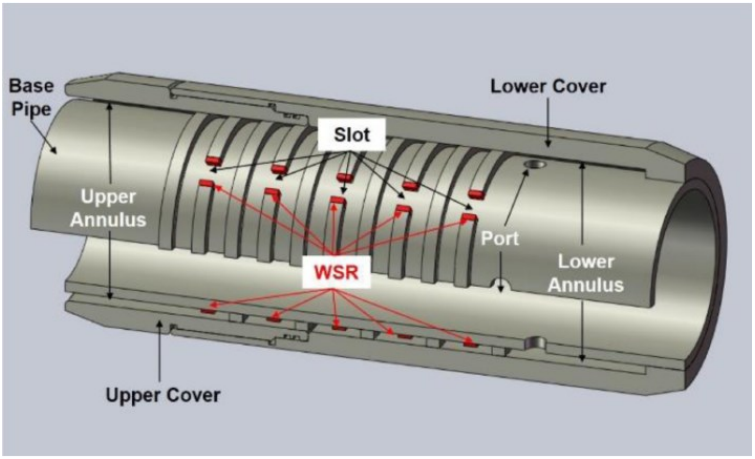

Figure 29: Hybrid-type ICD [30]

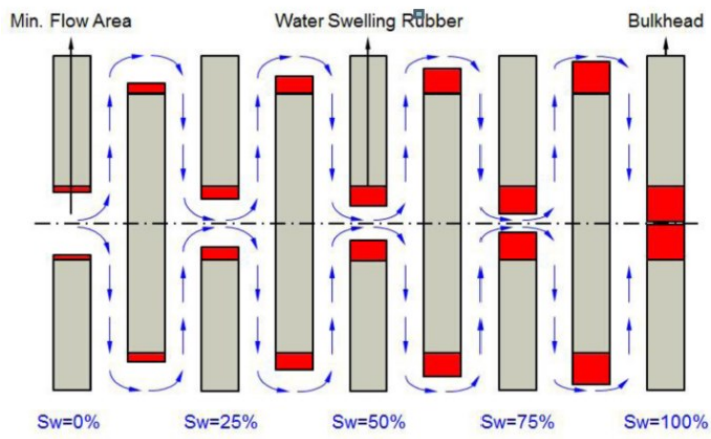

Figure 30: Working principle of water swelling rubber in a hybrid ICD [32]

2.8.2.4 Tube-Type ICDs

In tube-type ICDs, the pressure drop is created by several long tubes with predefined geometry in terms of diameter and length. The resulting pressure drop follows Bernoulli's equation (**2.8.1**) with an additional pressure term that includes the length of the tubes. The longer the tubes, the more equal the behaviour, which is similar to the helical channel-type ICDs; the relationship between tube length and fluid flow behaviour is more conditional on the viscosity of the reservoir fluid than on the density.

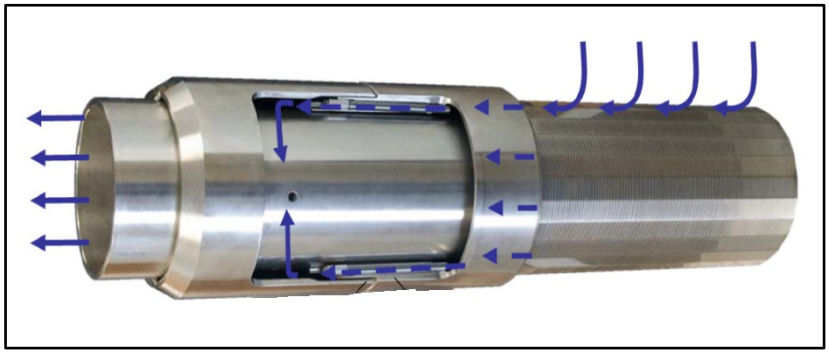

Figure 31: Tube-Type ICD [33]

Figure 31 presents an EquiFlow™ ICD manufactured by Halliburton. The blue arrows on the right side identify the entry point of the fluid. It moves between the screen and base pipe to the tubes (dotted blue arrows) and further to the orifices in the ICD.

2.8.3 Autonomous ICDs

Autonomous ICDs (AICDs) are the next development stage from passive ICDs. As the name suggests, they are completely self-regulating and able to control the fluid flow without any external control unit. AICDs combine the technical function of passive control devices with an active regulation part.

In recent years, numerous types of AICD have been designed and built; for example, Baker Oil Tools created a flapper-type AICD, Halliburton created a ball-type AICD, and Statoil created a swellable-type AICD and disc-type AICD.
The following section describes the main types of AICD and ends by focusing on the disc-type AICDs of by Tendeka. OMV Austria used them at well BO 208 and they are of interest to this thesis.

2.8.3.1 Counterweight Flapper-Type AICD

AICDs are intended to eliminate the dependency of external energy sources (batteries) on the requirement of energy lines from the surface. Flapper-type AICDs are based on the Archimedean principle. The valve is a density sensitive ICD, which is installed into each screen (or the necessary screens) of the horizontal or highly deviated production well.

In a reservoir, different fluids exist with higher and lower densities. The flapper valve is designed as in Figure 32. The green spot on the upper side of Figure 32 represents the location of counterweights. Before flapper valves were equipped with a counterweight, the flappers were made from synthetic foams. This foam had a very low density, which resulted in effective opening/closing behaviour of the valve when the density changed, but the valve was limited in its application. The origin of this limitation is based on the structure of the foam. The synthetic foam can react with fluids from the reservoir and the foam structure is susceptible to collapse due to pressure that is too high. Therefore, the counterweight alternative was developed [34].

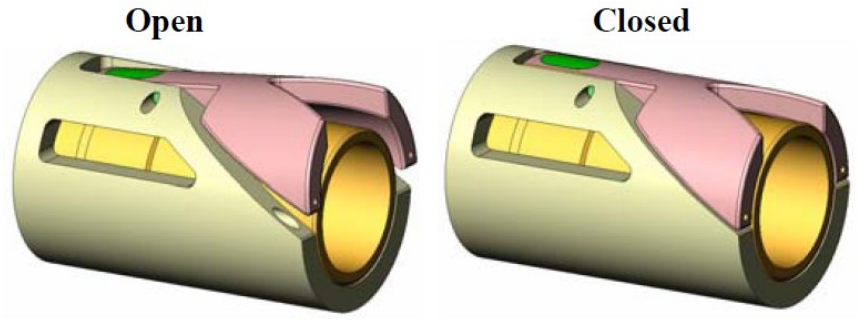

Figure 32: Flapper valve AICD with counterweight [34]

The counterweight allows the application of higher dense materials (alloys) that withstand the extreme conditions in a reservoir. A further advantage is the possibility to modify the valve specifically for each section/application in the wellbore. A negative aspect of this AICD is the position of the flapper valve, which must always be on the top side of the wellbore to ensure its function. Therefore, the flapper valve is built into a rotatable housing with additional sealing rings to ensure valve tightness.

To control water influx from the bottom of the reservoir, the same principle was applied. The differences are that the valve is mounted on the bottom side and the working direction of the flapper valve is inverted. Fluids with lighter densities will not move the lever, but when water occurs in the production, due to the higher density, the flapper valve will be forced to move. The buoyancy forces moves the flapper and closes the valve (see Figure 33).

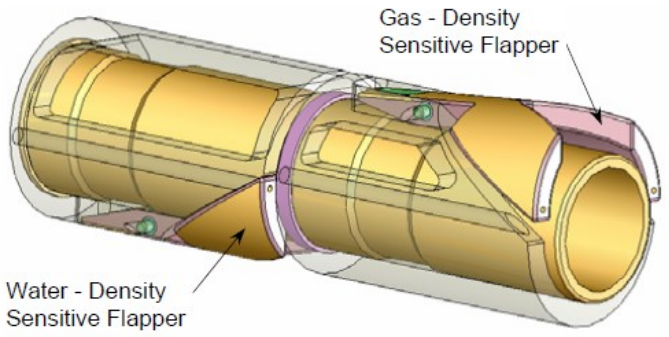

Figure 33: Flapper valve AICD for water and gas [34]

The flapper type has, in the case of excess gas production, an orifice to bleed the gas. This bypassed gas creates a backpressure that allows continuous production from the other screens. When gas coning does not exist anymore, the valve will reopen again and production from the disabled area is reinstated.

2.8.3.2 Ball-Type AICDs

Ball-type AICDs work similarly to flapper valves. They are density sensitive valves in which small balls are used as inflow control elements, or rather, sealing elements. The device can be realised to limit water or gas production. The diameter of the balls differs in terms of optimal ball to orifice ratio; a larger ball diameter leads only to a reduction of the flow.

Regarding the oil type, the floating balls lie on the lower part of the device, and at the moment the water saturation increases, the density of the fluid also increases. This forces the spheres to start rising upwards and seal the nozzles where the oil normally flows through (Figure 34). When the water saturation decreases, the sealing balls start to lower, and oil production resumes again [35].

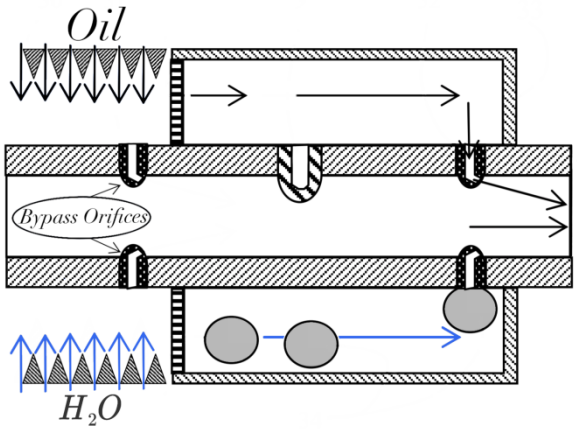

Figure 34: Ball-type AICD for water production; adapted from [35]

In the case of the gas controlling unit, the balls are designed to float on oil. When gas appears on the top and the process of gas coning begins, the density of the oil decreases. On the basis of the lower density, the balls move down and seal the nozzles on the top of the ICD. This is the reverse floating mechanism, as in the water controlling ball AICD. Figure 35 shows the buoyancy effect when the density decreases due to increasing gas content during production [35].

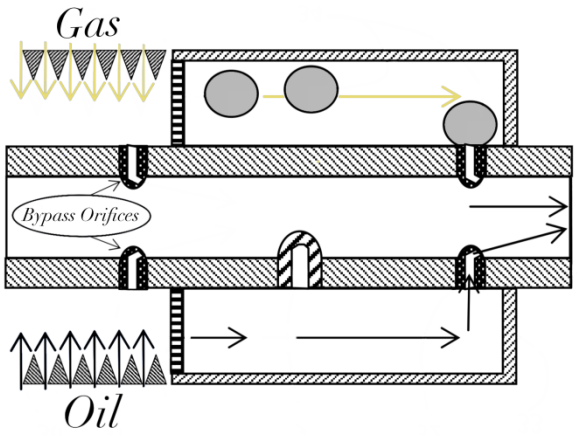

Figure 35: Ball-type AICD for gas production; adapted from [35]

Additionally, the bypass orifices maintain the overall production of the horizontal or highly deviated section. When all active controlled nozzles are plugged by the sealing balls, the flow through the bypass conserves the pressure drop inside the production area.

2.8.3.3 Swellable-Type AICDs

As the name suggests, a swellable material is used to control the flow of water in this type of AICD. This type combines the restriction effect of nozzle-based ICDs (Figure 27) with swellable elastomers. The basic pressure drop occurs due to the geometry of the nozzle. A reduced diameter forces the fluid from a larger flow area (inflow into the ICD) through the small diameter of the nozzle and creates a resistance against the flow. To improve this static behaviour, swellable rubber is integrated into the nozzles, which reacts with the increasing amount of water [36].

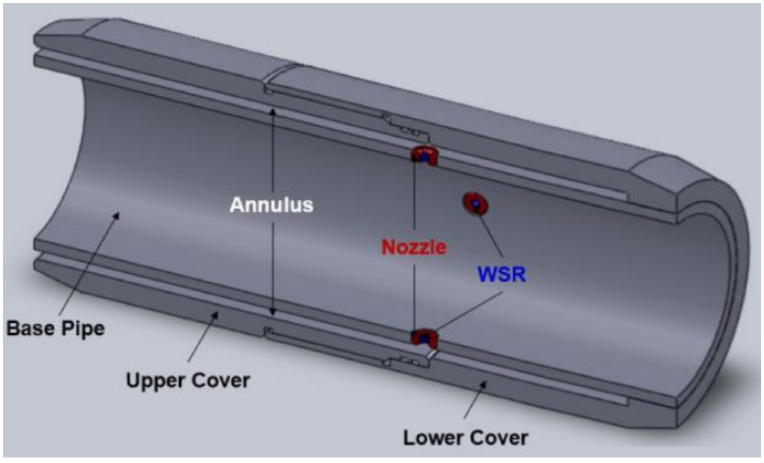

Figure 36: Swellable-type AICD [36]

Once there is a water breakthrough in one area of the horizontal section, the water "activates" the autonomous part of the control device. The higher the water saturation in the fluid, the smaller the diameter of the nozzles becomes. The swelling process is demonstrated in Figure 37.

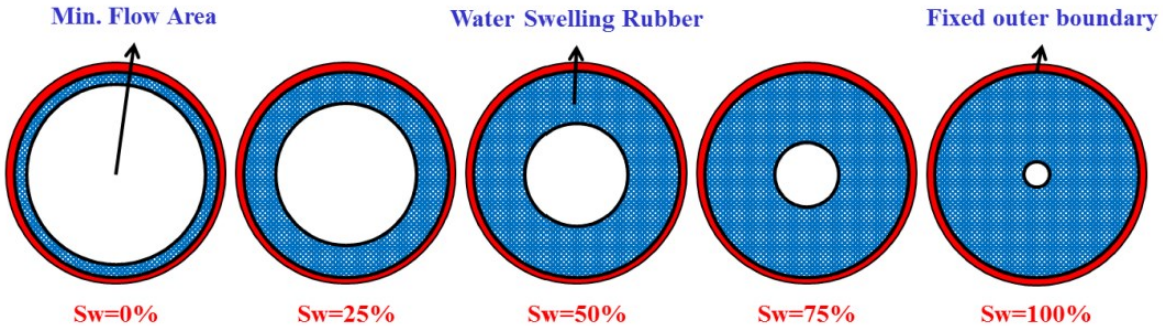

Figure 37: Restriction of inflow nozzles depending on water saturation [36]

Once the water saturation reduces, the diameter will increase again and the flow restriction will be minimised. An additional advantage is that the rubber requires some time to react; thus, the AICD will swell only if the amount of water is significantly higher.

2.8.3.4 Disc-Type AICDs

Disc-type AICDs were invented by Statoil in 2007 [37]. This type of advanced ICD is also known as the rate controlled production (RCP) valve. Since its invention, numerous disc-type AICDs have been created. This thesis focuses mainly on a product of Tendeka that was used in the completion of well BO 208.

A PT team from OMV Austria in cooperation with Tendeka selected the FloSureTM TR7 AICD screen design. This device works on Bernoulli's principle, which states that the sum of the static pressure, dynamic pressure, and friction loss along a streamline is constant. The specific geometry is used to create a flow restriction with a moving disc. This disc levitates inside the AICD housing (see Figure 38 and 39). Halvorsen [38] and Mathiesen [39] described an enormous improvement in the functionality and mechanical integrity of the valve by redesigning the original rate controlled valve.

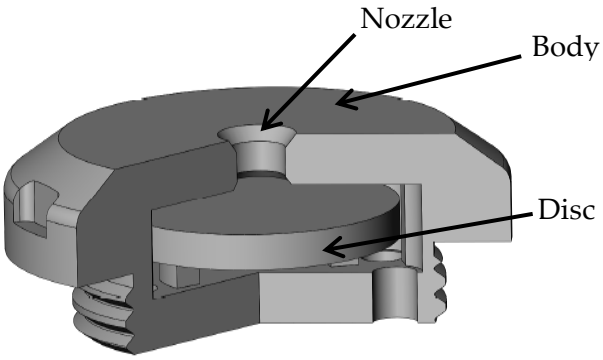

Figure 38: Levitating disc [40]

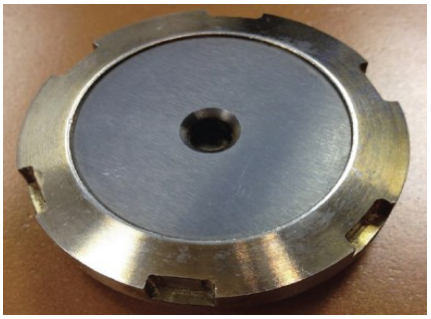

Figure 39: Disc-type AICD [40]

The AICD by Tendeka is available in various configurations, which vary from 2.5 mm to 10 mm in diameter and 1–2 valves per joint. The ability to vary dimensions results in a large flux range per joint of the production section [40]. OMV selected three configurations, which are discussed in a later chapter.

Next, this paper examines the choking mechanism of RCP valves. They are based on Bernoulli's principle through the exclusion of compression and elevation effects [41].

$$p_1 + \frac{1}{2}\rho {v_1}^2 = p_2 + \frac{1}{2}\rho {v_2}^2 + \Delta p_{friction\ loss} \qquad \textbf{2.8.2}$$

Where

p_1	Static pressure [Bar]
$\frac{1}{2}\rho {v_{1,2}}^2$	Dynamic pressure [Bar]
$\Delta p_{friction\ loss}$	Friction pressure loss [Bar]

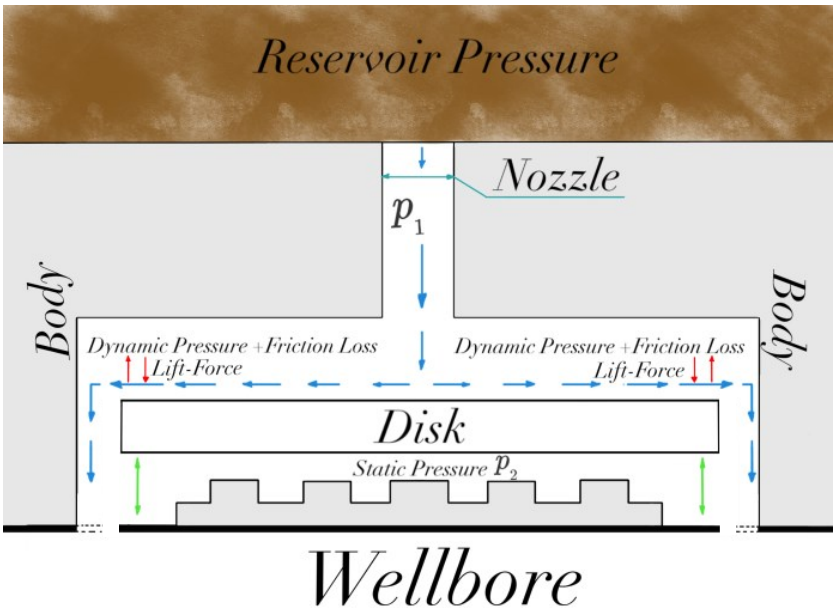

Figure 40: Acting forces on AICD disc; modified after [41]

Dynamic pressure loss is caused by the viscous drag force and hydraulic lift force. The drag force is the resistive force, which acts on an object when it moves through a fluid such as oil or water. In this case, the principle is used that the fluid flows around the disc and the created force attempts to move the disc.

$$F_D = \frac{1}{2}\rho u^2 C_D A \qquad \textbf{2.8.3}$$

Where

F_D	Drag force [N]
ρ	Density [kg/m³]
u	Flow velocity [m/s]
C_D	Drag coefficient [-]
A	Reference area [m²]

The drag force acts in the opposite direction of the relative flow velocity, and as Equation **2.8.3** states, is proportional to the density and square of the flow velocity of the fluid. The smoothness of the surface and the area also affects the magnitude of the force.

The lifting force acts perpendicular to the direction of the relative fluid flow. When a medium flows around a geometric shape, a pressure difference is created on the opposite sites of the body. As Bernoulli's principle describes, the velocity of a fluid is inversely

proportional to the pressure, and at regions with high velocity, the pressure is lower and vice versa. The lift force is calculated as follows:

$$F_L = \frac{1}{2}\rho u^2 C_L A \qquad \textbf{2.8.4}$$

Where

C_L Lift coefficient [-]

The force that acts in the centre point of the disc is also referred to as stagnation pressure (the Bernoulli Effect). This pressure pushes the cylindrical plate towards the seats and the resulting differential pressure between the inlet side (reservoir) and the stagnation pressure forces the disc to move up to close it.

The elevation of the disc is therefore dependent on the fluid rate, density, and viscosity of the fluid. The viscosity controls losses in friction pressure, and when the produced oil has a high viscosity, friction pressure is increased and the disc is pressed away from the nozzle. This leads to an increased oil flow. When oil has a lower viscosity and dense water starts to occur in the fluid, the friction pressure is reduced and the velocity increases. This increase directly affects the force equilibrium, and the disc is aspirated to the upper housing and reduces the flow rate.

Gas, with its low viscosity, causes very high velocities, and the disc will be forced strongly against the top of the housing. As a result, the gas flow is restricted significantly. The decrease in flow rate with decreasing viscosity is demonstrated in Figure 41.

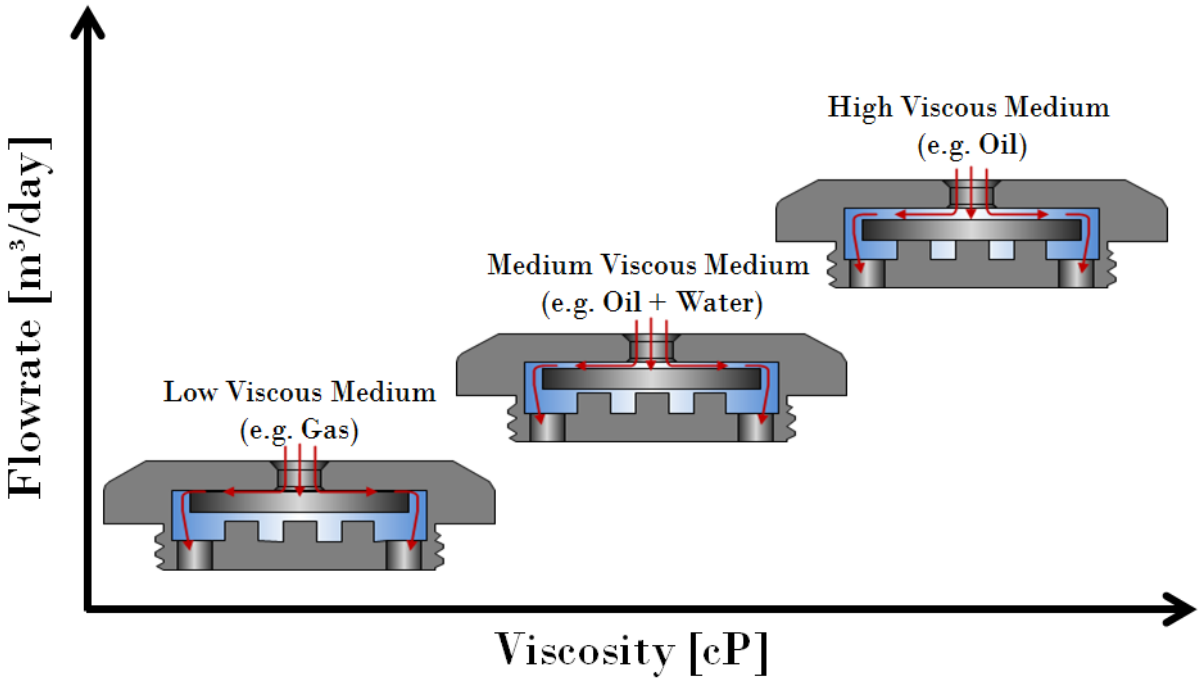

Figure 41: Flow rate dependence of viscosity [40]

A great advantage of this hovering technique is that there are no mechanical moving parts involved. There are no springs, membranes, or other parts to control the fluid flow, which reduces the risk of malfunctions.

The detailed parameters of the AICD used for well BO 208's completion are discussed in the following chapter.

2.9 Computer Applications/Software

This chapter describes the basic functions and applications of the used software. All of the programmes were used to gather data from the observed wells and perform analyses to compare the performances of the wells after the redevelopment. Microsoft Office programmes are not discussed.

2.9.1 GDB

The Gewinnungsdatenbank (GDB) is the name of the internal main database of OMV Austria, based in Gänserndorf. The database was created in 1998 and is based on Oracle®; it acts as storage for all kinds of production and treatment data of OMV's approximately 1000 oil and gas wells in Austria. The software is maintained by the internal IT department, and the reservoir as well as production department use this tool equally.

The GDB, features numerous data about wells; therefore, a filter tool is implemented for effective searching. The following picture (Figure 42) shows the main screen of the GDB without any filter applied.

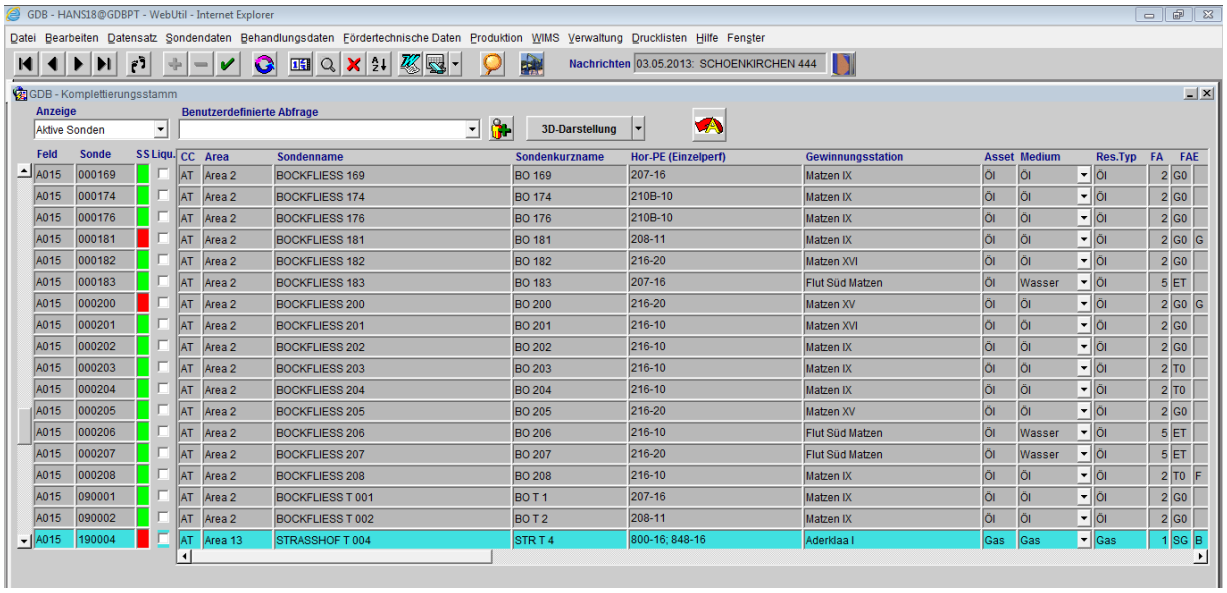

Figure 42: Main screen of the GDB

The database is programmed so that the special keys (F1–F10) perform shortcuts for the user. "F7" activates the filter function and allows the user to define the following parameters:

- Feld (Field)
- Sonde (Well)

- Area (Area)
- Sondenname (Well name)
- Sondenkurzname (Well-abbreviated name)
- Hor-Pe (Einzelperf) (Horizon-Perforation, Single-Perforation)

After defining one or more of these entry fields, the main screen will only display the desired wells (see Figure 43).

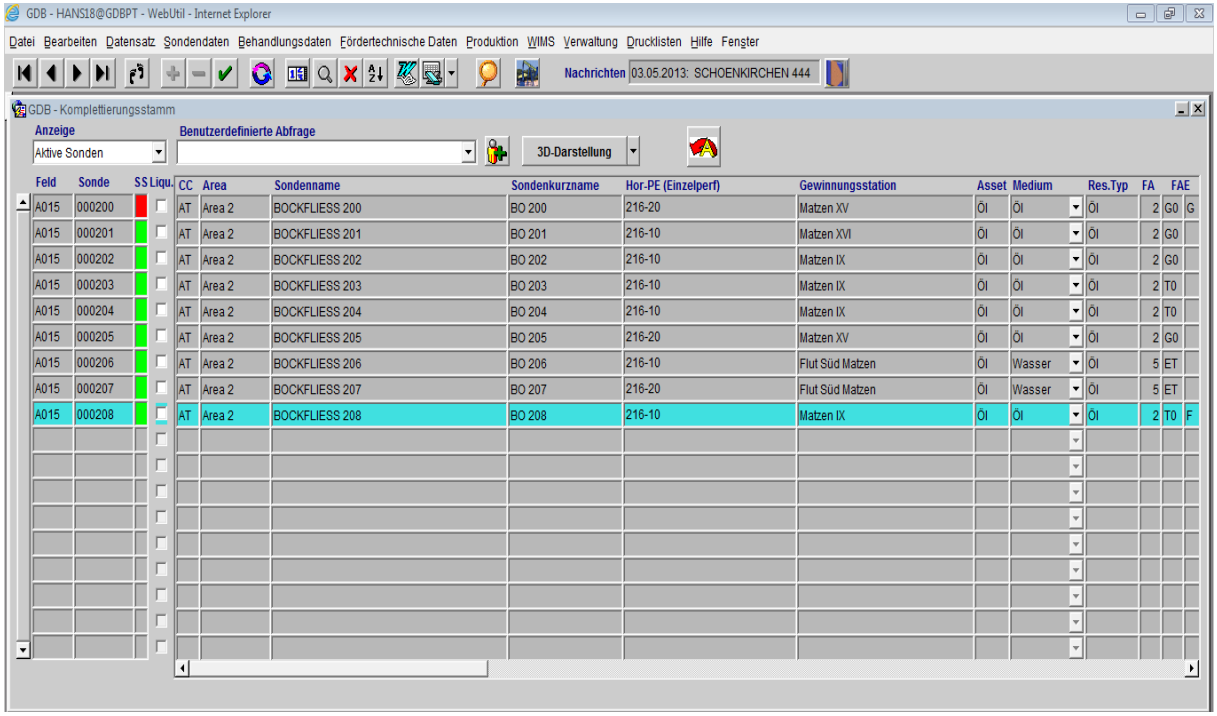

Figure 43: GDB-filtered main screen

Because this thesis investigates the performance of three different horizontal wells, the production and pressure data are necessary. These data are available via the tab "Produktion" and further "Tagesproduktion-/ or Monatsproduktion-Technisch" (see Figure 44). The data of wells BO 204, BO 205, and BO 208 were filtered and exported into MS Excel to perform further calculations. In Figure 44, the logged production data of well BO 204 are seen as representative.

Tagesproduktion R3

Land: AT Obj.Typ: Sonde Feld: A015 Sonde: 000204 Sondenname: BOCKFLIESS 204 FA / FAE: 2 T0

Hor-PE (Einzelperf): 216-10 (16. TORTON) Area: Area 2 GWST: Matzen IX Medium: Öl

Änd.	Datum	Brutto [m3]	Zielrate [m3]	H2O %	Dichte-BH	Dichte	GÖV	Gas [m3]	Öl Ges. [t]	ZR H2O Inj. [m3]	H2O Ges.[m3]	Liftgas [m3]	Prc
	14.02.2018	2.064,4	2.100	99,07	0,905	0,905	229	4.388	17,3		2.045,3	0	
	29.01.2018	2.102,8	2.100	99,05	0,905	0,905	229	4.592	18,1		2.082,7	0	
	28.01.2018	2.102,8	2.100	99,05	0,905	0,905	248	4.982	18,2		2.082,7	0	
	25.01.2018	2.109,5	2.100	99,06	0,905	0,905	281	5.539	17,9		2.089,8	0	
	24.01.2018	2.109,5	2.100	99,08	0,905	0,905	282	5.495	17,6		2.090,0	0	
	22.01.2018	2.109,3	2.100	99,05	0,905	0,905	269	5.382	18,1		2.089,3	0	
	20.01.2018	2.104,5	2.100	99,04	0,905	0,905	239	4.833	18,3		2.084,3	0	
	19.12.2017	2.093,9	2.100	99,02	0,905	0,905	255	5.251	18,6		2.073,3	0	
	18.12.2017	2.094,4	2.100	98,99	0,905	0,905	228	4.812	19,1		2.073,4	0	
	16.12.2017	2.088,7	2.100	99,01	0,905	0,905	246	5.117	18,8		2.068,0	0	
	15.12.2017	2.099,9	2.100	98,99	0,905	0,905	215	4.559	19,2		2.078,7	0	
	14.12.2017	2.159,2	2.100	99,03	0,905	0,905	243	5.075	18,9		2.138,3	0	
	12.12.2017	2.157,9	2.100	99,04	0,905	0,905	241	5.012	18,8		2.137,1	0	
	10.12.2017	2.160,2	2.100	99,02	0,905	0,905	234	4.944	19,1		2.139,1	0	
	09.12.2017	2.160,3	2.100	99,04	0,905	0,905	241	4.997	18,7		2.139,5	0	
	24.11.2017	2.156,4	2.100	99,01	0,905	0,905	239	5.135	19,4		2.135,0	0	
	23.11.2017	2.158,9	2.100	99,00	0,905	0,905	237	5.113	19,5		2.137,4	0	
	22.11.2017	2.160,9	2.100	99,01	0,905	0,905	234	5.024	19,4		2.139,4	0	
	21.11.2017	2.165,7	2.100	99,01	0,905	0,905	267	5.715	19,3		2.144,3	0	

Datenumfang gesamter Zeitbereich

Figure 44: Production data of well BO 204

2.9.2 NETOOL™

To simulate ICD completion, some simulation programmes are available, of which NETool™ is one of the most common. It is used to evaluate the initial well performance under different well completion configurations and can be combined with an Eclipse simulation model to observe the well performance change over time [42]. This software is mainly used for horizontal or highly deviated wells with long reservoir contacts and multilateral and/or advanced wells, as well as wells that are drilled through thin pay intervals or multiple zones [43–45].

NETool™ allows numerical simulations of multiphase fluid flow on the inside and around complex completions (near wellbores) under steady-state conditions. Nodal analysis is critical, and the NETool™ software package links Artificial Lift (AL) software applications with reservoir simulations. In Appendix B, Figure 63 shows the first window of the program after launch. On the left side, it is possible to choose between 'gridless' or 'with reservoir model'.

The gridless model does not require a reservoir model; thus, it allows entering the wellbore data manually or loading them from a spreadsheet or log file. The reservoir model option requires a correctly defined reservoir model with PVT data, porosity, permeability, and

reservoir dimensions. Reservoir grid files can be imported (e.g., Eclipse 100-type) to simulate the most realistic inflow compared with standard nodal analysis programmes, which only work with concentric annuli in a standard tank or with basic PI models. Appendix B shows a symbolic photograph of a possible reservoir with well completion including the seen trajectory.

The programme covers the near wellbore regions and the wellbore itself with a two-dimensional grid of nodes, which is similar to conventional reservoir simulation software packages. This tool is used to calculate the PI for the three horizontal wells with different completions and compare their results with the original production history, which has been recorded since production began.

3 Horizontal Infill Wells

The following chapter covers general HSSE aspects of OMV, wellbore stability considerations, well-specific data including reservoir data, and the surrounding well data, which are used to compare horizontal wells with vertical wells. The investigated wells are drilled in the 16th TH in the geological area referred to as Westscholle (the Bockfliess Area in Figure 2). In 2013, the redevelopment started with the main purpose of accelerating and increasing the oil production in the 16th TH. The locations of the wells are designed so that no interferences with already existing wells occur.

3.1 HSSE and Wellbore Integrity

In October 2017, on Global HSSE Day, OMV Austria launched their new HSSE Strategy 2020 – 'Zero Harm – No Losses'. The overall mission is not only to protect the people, but also assets and the environment. As an international company, OMV moved one step further to creating a sustainable HSSE culture within the company and their environment. The most important points to achieve this are:

- Health
    - Improve the ability to work through integrated health management
- Safety
    - Build on sustainable safety for people and plant
- Security
    - Protect people and assets against emerging malicious intentional threats
- Environmental
    - Minimise environmental footprints throughout the entire lifecycle

To ensure high quality related to these HSSE topics, OMV has implemented their own HSSE management system. The working principle follows international standards, such as ISO 14.001 and OHSAS 18.001, and is implemented under the following process cycle:

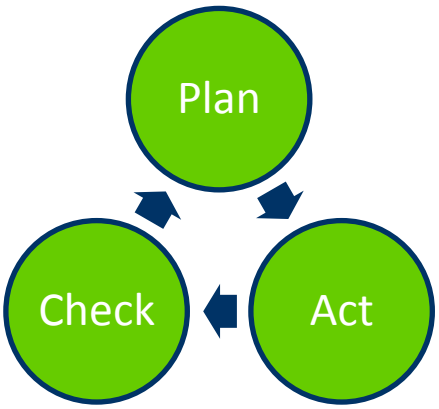

Figure 45: HSSE – Act Cycle according to OMV. Source OMV Austria E&P

In the oil and gas industry, wellbore integrity and safety during the complete E&P cycle is mandatory. In 2013, to ensure the wellbore stability of the three horizontal wellbores in sand formation, a geomechanical study was conducted. To create the geomechanical model, four different offset wells were used, as well as (if available) an analysis of multi-arm calipers and image logs. This study also comprises a wellbore stability analysis for the 16th TH reservoir and its cap rock strength and structure, so that MW is assured to not exceed the formation strength.

The locations of the four used offset wells are shown in Figure 46 and are used as representative geomechanical assumptions not only for well BO 204, but also for the later drilled BO 205 and BO 208 [46].

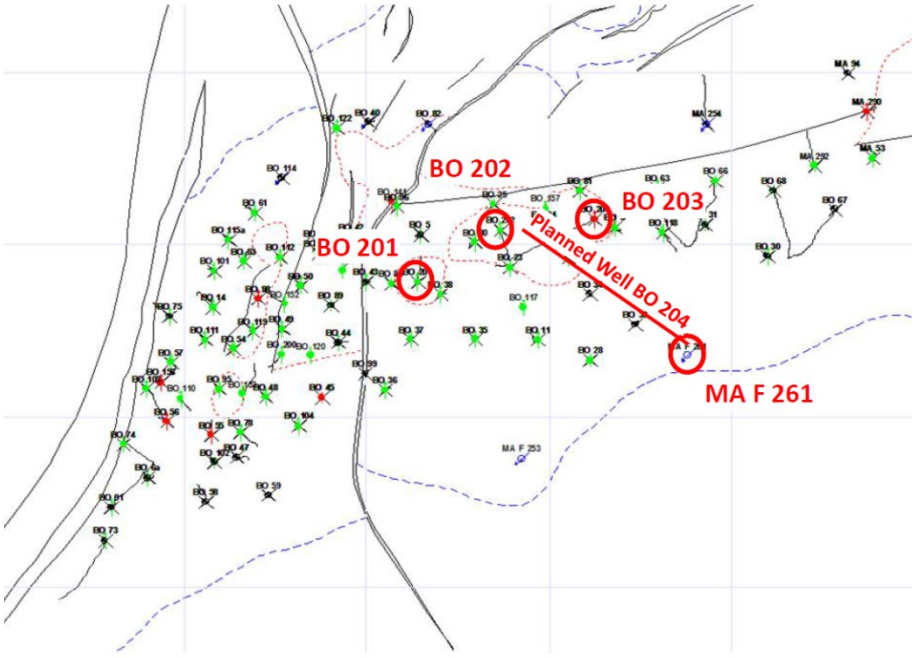

Figure 46: Offset well position for geo-study [46]

In addition to the log data, a variety of daily drilling reports were available. A maximum reservoir pressure was estimated by the petroleum geologist up to a value between 120 and 135 bar. Therefore, a worst case scenario for the geomechanical study was calculated with a reservoir pressure of 120 bar [46]. To increase the amount of data for the investigated area, approximately 10 LOTs and 2 new FITs were run between 2009 and 2013. Both types of tests are conducted below the casing shoe. Important to mention is that the results of these tests are only valid for the near casing shoe region and can differ in other depths of the reservoir. A LOT is used to determine the fracture pressure of the open formation while the FIT is used to test the strength of the formation to a designed pressure. Furthermore, six step rate tests positioned on the same well site as the planned BO 204 were analysed.

Out of the results of the different tests for the offset wells, the vertical stress or overburden gradient was identified by integrating the existing density logs and exponential trend lines. The graph below (Figure 47) indicates similar vertical stress behaviour and an SG at the depth of the reservoir of approximately 2.2.

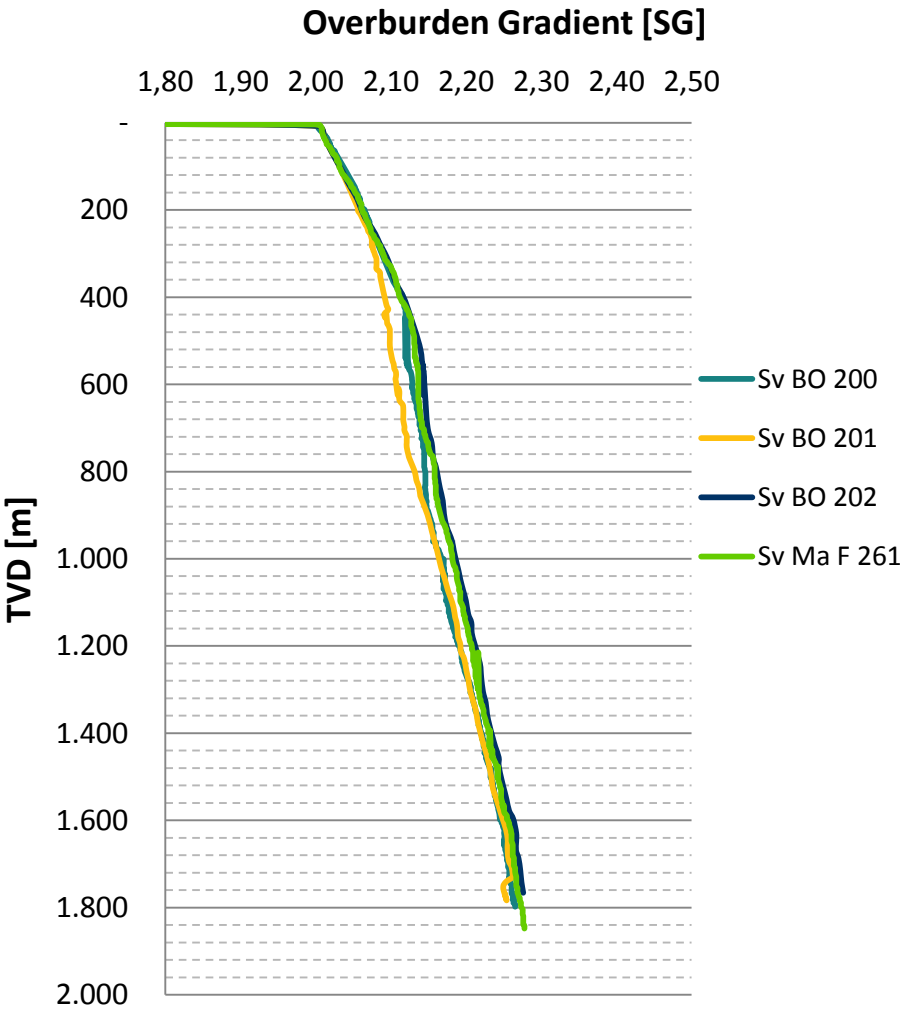

Figure 47: Overburden gradient graph; modified after [46]

As previously described, no exact pore pressure measurements of the target reservoir were available; therefore, a p_{res} of 120 bar (approximately 0.75 SG depending on depth) was assumed. The higher reservoir zones were ignored, and because of the primary focus on the 16th TH, all other formation pressures were assumed to be hydrostatic.

The least principal stress determination was applied to calculate the effective stress at the depths where the leak-off tests were performed. The effective stress ratio (ESR_{Shmin}) is calculated for every available leak-off or extended leak-off test. It is critical for understanding the stress regime of the target formation; otherwise, if the pressure limits are surpassed, a loss of mud during the drilling operation or other hazards could cause high costs. To evaluate the mechanical properties of rock, an old core sample from well BO 157 (approximately 43 years old) and a 15-year-old core from well MA 84a were used [46].
To improve the result of the geomechanical model, or at least to verify the authenticity of the values, several different daily reports (drilling, geological, and final reports) were used. The reports were screened for typical indicators of rock mechanical problems such as loss of fluids, tight spots, stuck pipes, and ballooning [46].

Based on the results of the geomechanical study of the 16th TH, this study proposed some recommendations. Because only old core samples from BO 157 were available, verification with the model showed that the UCS were going to be too low if the rock properties of the model were calibrated with these samples. The following parameters were evaluated for the final geomechanical model [46]:

- Normal faulting stress regime $S_v > S_{Hmax} > S_{hmin}$
- Overburden gradient (@ reservoir) $S.G = 2.25$
- Hydrostatic pore pressure in the overburden
- Pore pressure $p_{pore} = 120\ bar$
- Effective stress ratio $ESR_{Shmin} = 0.55$
    - 1.58 sg @ reservoir
- Effective stress ratio $ESR_{SHmax} = 0.85$
    - 2.03 sg @ reservoir
- UCS in the reservoir 10 to 50 MPa

To ensure wellbore stability, mud weights of 1.05 – 1.15 SG were suggested, where were based on drilling experience of previous wells in the region.

Bockfliess 204 and 208 were drilled and had OH completion because no signs of a gas cap existed in the target zone. Different to the other two wells, Bockfliess 205 was cased and cemented, and afterwards it was perforated to keep a possible gas outcome under control. As previously described, a redevelopment project being conducted in the Bockfliess area. Figure 48 presents the region of interest with the three horizontal wells.

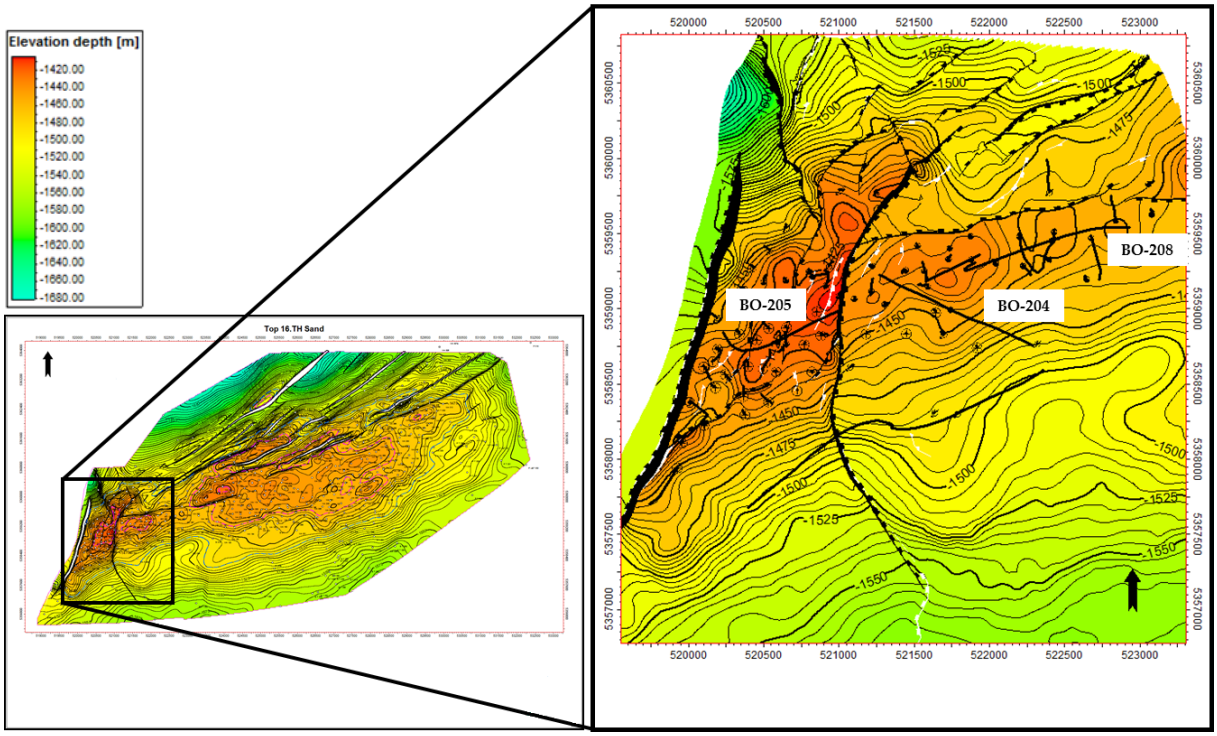

Figure 48: Overview of the horizontal well location; modified after [47]

The following subsections present more detailed descriptions of the observed wells. In addition to BO 204, BO 205, and BO 208, some vertical wells are used to compare oil production behaviours and the development of the water cut.

3.2 BO 204 – Slotted Liner with Blank Pipes and ECPs

Well BO 204 was planned by a multidisciplinary team from OMV Austria in 2013. As a target region, the uppermost zone of the 16th TH was identified and investigated as the most saturated oil zone. The subsurface production target was defined by following a specific geological zone in the 16th TH-1. The final depth of the horizontal well was planned to reach 2480 m MD [48]. The defined wellbore corridor is seen in Figure 49:

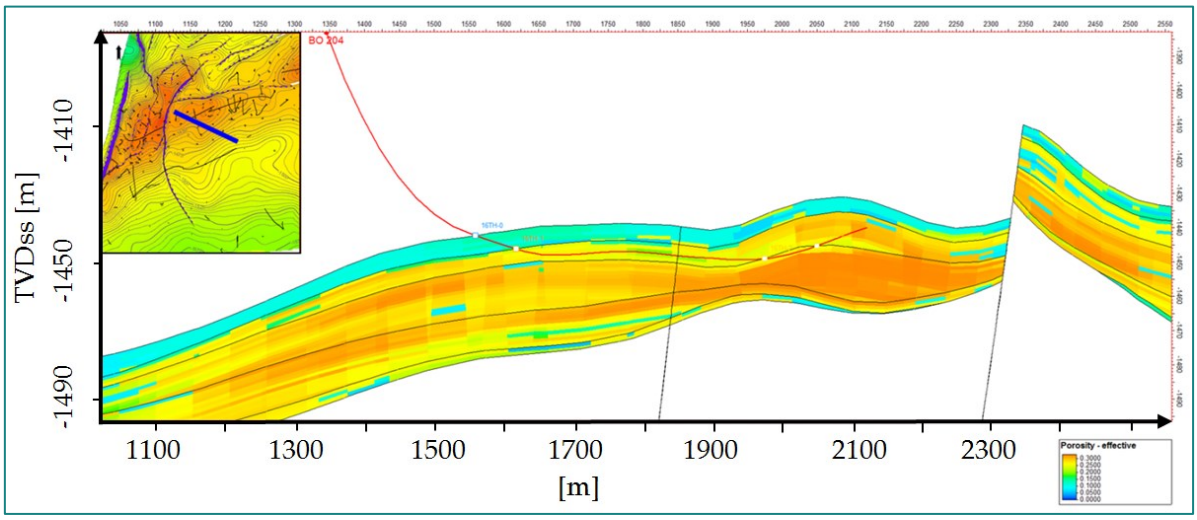

Figure 49: Wellpath of BO 204 with present geological information; modified after [47]

From a preliminary log report, the thickness of the hydrocarbon bearing interval from the 16th TH was estimated at approximately 481.6 m MD and is located between 1958.8 – 2443.1 m MD in the target section. Based on petrophysical log interpretation ranges, the expected porosity was between 15% and 30 %. The average water saturation was approximately 25%, except for the interval between 2333 – 2394 m MD where a water conductive zone was drilled through with high water saturation up to nearly 75 %.

Generally, the formation has very low shale and clay contents with exception of the interval between 2138 – 2195 m MD. This area has low resistivity and low porosity, and therefore, it is a region of low oil and gas saturation [49; 48].

The following table provides an overview of the layer in which the horizontal well is placed as well as the layer above the HC reservoir.

Table 6: Layer overview of Bockfliess 204 – 16th TH-0 [50]

16TH-0								
Top [mMD]	Bottom [mMD]	Top [mTVDSS]	Bottom [mTVDSS]	Thickness [mMD]	Thickness [mTVD]	Por [V/V']	SW [V/V']	Fluid [-]
1954.8	2443.3	1444.8	1445.9	485.4	4.3	0.25	0.26	Oil

Table 7: Layer overview Bockfliess 204 – 16th TH-1 [50]

16TH-1								
Top [mMD]	Bottom [mMD]	Top [mTVDSS]	Bottom [mTVDSS]	Thickness [mMD]	Thickness [mTVD]	Por [V/V']	SW [V/V']	Fluid [-]
1958.5	1969.2	1445.1	1445.8	10.7	0.7	0.15	0.32	Oil
1970.8	1971.1	1445.9	1445.9	0.3	0.0	0.10	0.41	Oil
1971.6	2443.3	1445.9	1442.6	471.7	3.4	0.25	0.26	Oil
1954.8	2443.3	1444.8	1445.9	485.4	4.3	0.25	0.26	Oil

The bore string takes course approximately 500 m along the top layer to maximise reservoir exposure.

To produce the attic oil from the reservoir, the well was completed with a slotted liner in an open-hole section. To eliminate possible crossflow or annulus flow in the OH area, swellable ECPs were used. To reach the production depth, the following casing configurations were used:

Table 8: Casing configuration of BO 204 [49]

Casing [in]	Depth-Top [m]	Depth-Bottom [m]	Weight [kg/m]	Quality [-]	Couplings/ Threads [-]
18 5/8	0.00	30.00	130.21	J-55	BUTT
13 3/8	0.00	533.04	81.10	J-55	BUTT
9 5/8	0.00	1952.19	69.94	L-80	BUTT
7	1839.74	2478.00	34.23	L-80	VAGT

During the well planning phase, the complete wellbore was designed so that an ESP could be installed. Therefore, a casing diameter of 9 5/8" was selected so that a variety of ESP diameters could fit into the wellbore. Additionally, the wellbore was drilled with a dog leg severity of a maximum of 3° per 30 m, down to a TVD of approximately 1500 m to ensure

that the ALS equipment is able to reach its correct operation depth and don't get stuck before. The position in the wellbore where the ESP was placed is referred to as the 'tangent section' and features a DLS = 0° per 30 m over the complete length of the ESP, including some additional metres of length as a reserve [48]. The tangent section was placed between 1440 m and 1519 m MD [51]. The ESP reaches from approximately 1453 m MD up to 1491 m MD, and therefore, it is in an optimal position between the tangent section. The submersible pump configuration has a length of approximately 40 meters. The operation length of an ESP is defined by the number of stages, pump length, and motor length, and each part must be selected by the PT.

Following the main objective of the redevelopment (to increase and accelerate production), the production technologist installed an ESP with a gross production rate of 300 – 500 m^3/day at first. In the next phase of the wellbore, an ESP with a much higher production rate of about 2000 m^3/day was installed.

The actual ESP configuration is stored in the GDB and included as a screenshot in Figure 66 (Appendix C) to show the complete configuration. The critical parameters of the ESP are that the overall configuration has a maximum diameter of 6", consists of two compression pumps with 35 stages each, and has two motors of type REDA Maximus 562 (5.62" = 142.7mm housing OD).

The most promising production zones were identified using well logs and possible crossflow was disabled by ECPs. As a result, three production intervals were created with varied lengths [49].

1. Production interval 1978.3 – 2135.0 m MD
2. Production interval 2222.6 – 2291.3 m MD
3. Production interval 2418.7 – 2478.0 m MD

These production intervals have a total length of 284.7 m, and with this, the following pipe configuration was determined. The downhole configuration of the 7" slotted liner is presented in Appendix D in Figure 68, where the SL and BP configurations are presented. The slotted segments lengths are as follows [49]:

1. Slotted segment 138 m
2. Slotted segment 50 m
3. Slotted segment 47 m

Therefore, all three production interval sections are covered to 83% by slotted liner segments, and the residual length is assembled with blank pipe segments and ECPs to prevent any unwanted crossflow or water production. The resulting production data from this reservoir region are discussed in the Production Data Analysis chapter.

3.3 BO 205 – Cased Hole with Perforations

The intention of horizontal well BO 205 was to increase the production rate from the 16th TH by penetrating the reservoir layers directly beneath the assumed GOC. The GOC is located on top of the 16th TH-2, which is a relatively high stratigraphic zone with 300–350 m of net sand. Due to the possible presence of a gas cap and weak areas within the formation, OMV performed a cased hole completion. The ZI used cement to ensure that no gas production occurs unintentionally.

The routing of the horizontal section was majorly driven by the geological structure and presence of structural highs. Another crucial point was to avoid already known complex fault areas and prevent interaction within drainage radii from existing wells. The desired production of attic oil (the same as BO 204) should be accompanied by as little gas from the gas cap as possible. The fluid contact level between the gas and oil is calculated to be no deeper than – 1422.6 m TVDSS, and therefore, the whole well path design was planned to be maintained in the range of 1.5–2 m TVD below the contact zone [52]. The geological cross section of the location where the well is planned is seen in Figure 50.

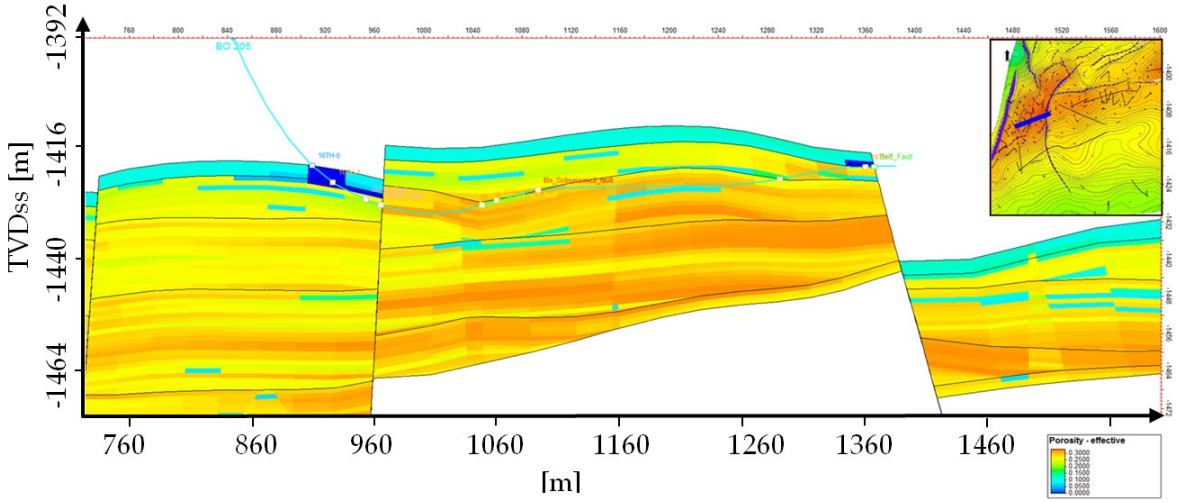

Figure 50: Wellpath of BO 205 with present geological information; modified after [47]

Because of a miscommunication between the contractor and OMV, a mistake in the reference depth of the well was given. As result of this communication problem, the first part of the horizontal section (heel section) landed too low in the 16th TH-2 region. Timely discovery of this mistake prevented this situation from becoming worse, and resulted in a final course of the wellbore with an approximately 290-m MD at the top of the 16th TH-2 and approximately 145 m MD in the 16th TH-1 zone [47]. The expected average porosity ranges from 22% to 30% and generally increases with depth. In the target region, the average water saturation was expected at approximately 15%, and in the lower regions of the 16th TH-2, this value was up to 60%. The vertical permeability K_V was expected to range from 15 to 1500 mD and the horizontal permeability K_H was expected to be higher in a range between 25 and 2500 mD [52].

The following table provides an overview of the layers in which the horizontal well is placed, and additionally, the surrounding oil bearing horizons.

Table 9: Layer overview of Bockfliess 205 16th TH-1 [53]

16TH-1								
Top [mMD]	Bottom [mMD]	Top [mTVDSS]	Bottom [mTVDSS]	Thickness [mMD]	Thickness [mTVD]	Por [-]	SW [-]	Fluid [-]
1801.3	1819	1426.6	1428.5	17.7	1.9	0.29	0.17	Oil
1913	1946.9	1425.2	1427.4	33.9	2.2	0.30	0.13	Oil
1947.2	1948	1425.2	1425.2	0.8	0	0.21	0.14	Oil
1913	1948	1425.2	1427.4	34.7	2.2	0.25	0.13	Oil
2145	2211.6	1420.3	1422.9	66.6	2.6	0.28	0.14	Oil

Table 10: Layer overview of Bockfliess 205 16th TH-2 [53]

16TH-2								
Top [mMD]	Bottom [mMD]	Top [mTVDSS]	Bottom [mTVDSS]	Thickness [mMD]	Thickness [mTVD]	Por [-]	SW [-]	Fluid [-]
1819	1913	1427.4	1428.5	94	1.1	0.31	0.11	Oil
1948	2145	1422.9	1425.2	197	2.3	0.30	0.12	Oil

The exposure length between the bore string and the reservoir was defined as approximately 300 m MD as a completion objective [52]. To ensure safe production and an optimal ZI between the reservoir areas, the horizontal section was cased, cemented, and perforated to produce the attic oil, block high water saturation zones out, and minimise early gas

production from the gas cap. To reach the production depth, the following casing configurations were used:

Table 11: Casing configuration of BO 205 [54]

Casing [in]	Depth-Top [m]	Depth-Bottom [m]	Weight [kg/m]	Quality [-]	Couplings/ Threads [-]
18 5/8	0	21.5	-	-	-
13 5/8	0	607	-	-	-
9 5/8	0	1798	69.94	L-80	BUTT
7	1692	2238	34.23	J-55	VAGTRN

Similar to BO 204, this wellbore was planned so that ESPs of larger diameter would fit into the tubing string when the production with the SRP is not sufficient enough anymore. Therefore, a casing section with a diameter of 9 5/8" was integrated into the wellbore. The requirements in the tangent section and the DLS are equivalent to those of BO 204.

The tangent must be placed as deep as possible in the wellbore with regard to positioning of the ESP with a minimised distance between the pump intake and reservoir. A deviation of 3° per 30 m as maximum deviation down to a depth of 1400 m TVD is indispensable to run the ESP in hole. Proactive evaluation of the necessary pump size results in a minimum length of the tangent section of approximately 75m (long is even better). As result of the drilling procedure, the tangent section was finally located between 1490 m and 1589 m MD, which resulted in a length of 99 m [55].

At the beginning of the production cycle, an SRP was installed in the wellbore. This SRP was specified after API Specification 11AX and its short description is 40-375-TH-22-4.
To understand this short description, a general introduction into sucker rod pump designation is provided as follows. Basically, all sucker rod pumps are named after API specifications, and therefore, a worldwide industry standard for the oil and gas industry is provided. The specification has the general form of:

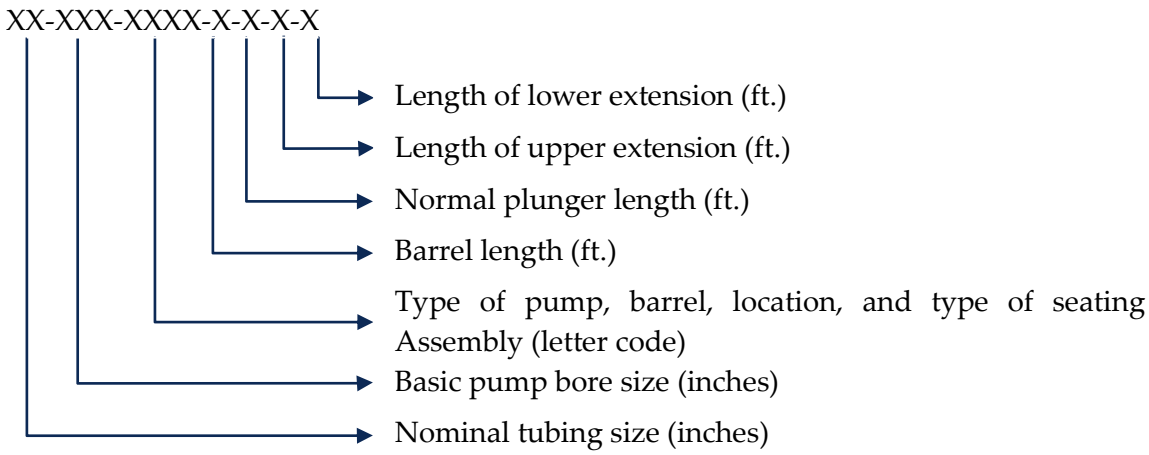

This means that in the case of well BO 205, the SRP has a configuration of:

- 4 1/2″ of nominal tubing size
- 3 3/4" of basic pump bore size
- TH stands for heavy wall, travel barrel, bottom hold-down
- Barrel length of 22 feet
- Barrel extension of 4 feet

To identify the exact position of the oil or gas bearing zones in the horizontal section, a cased-hole neutron log was performed prior to the perforation activities. As result of this log, a potential perforation length was identified between 1800 – 2210 m MD. The connection between the production string and the reservoir was restored with specially designed perforation guns. The perforation guns have the following specifications: 3 3/8″, TCP, DP, 6 spf, and 24 g. This code indicates the following configurations:

- Diameter 3 3/8″
- Completion technique TCP (tubing-conveyed perforation)
- Charge performance DP (deep penetrating, but a smaller hole at the casing)
- Shot density 6 spf (shots per foot)
- Charge 24 grams of powder (explosive)

The perforated section length was planned to measure 75–120 m MD, and the perforation process began at the toe section of the wellbore to ensure the success of the perforation process.

1. Perforation interval 2010–2050 m MD
2. Perforation interval 2080–2120 m MD
3. Perforation interval 2170–2200 m MD

The overall length of the horizontal section with an MD of approximately 290 m at the top of the 16th TH-2 and approximately 145 m at the 16th TH-1 is covered to 25 % by perforated intervals.

The production data produced thus far in this wellbore completion configuration are discussed in the Production Data Analysis chapter.

3.4 BO 208 – AICD Completion

The last horizontal well to be discussed in detail is BO 208. In the course of the redevelopment project of the 16th TH, various completion technologies were used to improve production. With BO 208, OMV Austria introduced the first intelligent completion method to their technical portfolio. The use of AICDs introduced a technique that for the first time is able to change the proportion of oil, water, and gas in the gross production rate by itself without any additional interventions (WO).

This drilling campaign connected two conjectural undrained local structural highs with a main focus on the wellbore remaining in the 16th TH-1 reservoir zone. The geological cross section before drilling based on pre-existing information of other wells and seismic data is presented in Figure 51.

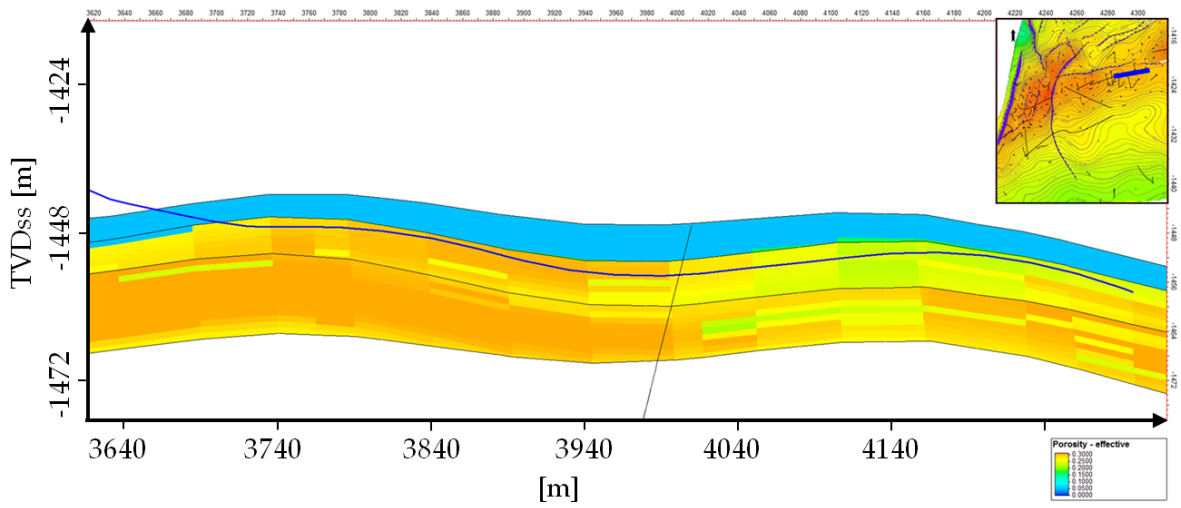

Figure 51: Wellpath of BO 208 before new information from the drilling campaign [47]

The general reservoir parameters were expected to be as follows: a reservoir temperature of 60°C (@ - 1450 m TVDSS) and an average reservoir pressure of 120 bar at a depth of 1641 m. Because the target zone is also the 16th TH-1, the average porosity (20–30%), average water saturation (from 16% at the top to 60% at the bottom), and permeability values (K_V = ~15 to ~ 1500 mD & K_H = ~ 25 to ~2500 mD) in the same range as the previously discussed wellbores [52].

During drilling, it was recognised that the geological model deviated from the factual situation; therefore, the project team had to adjust the drilling path. In Figure 52, the geological cross section with the additional newly gathered data during logging while

drilling (LWD) are presented, including the final wellpath of BO 208. When the original and the new cross section are compared, the geological target section is clearly identified to be positioned several metres deeper than was originally planned. Because of this significant difference, the initial water saturation was much higher at BO 208 than at any other well.

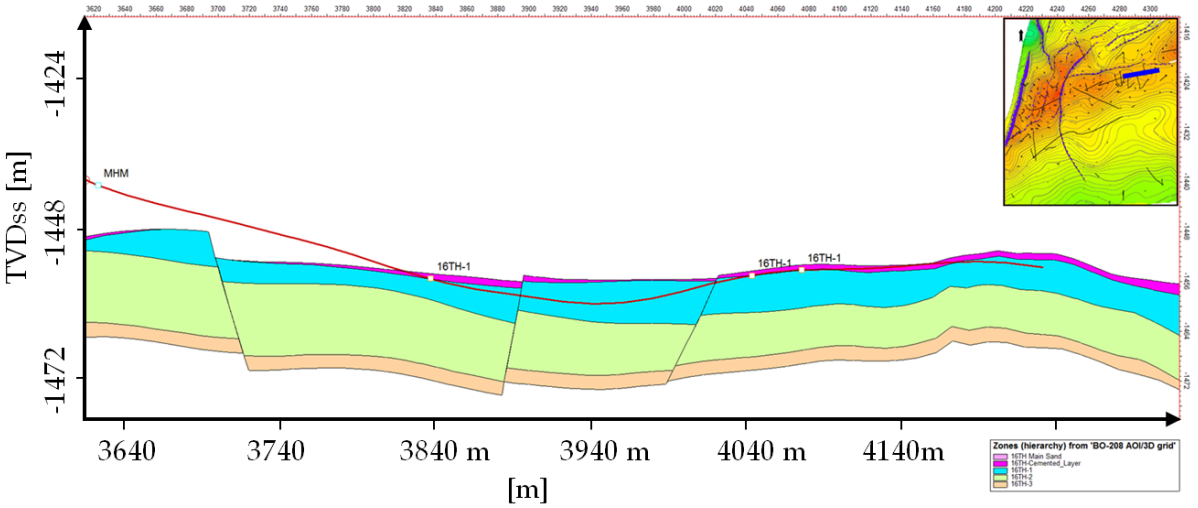

Figure 52: Wellpath of BO 208 with present geological information [47]

Thus, the geological formation was different than presumed, and the planned drilled-through layers also changed. The following table provides the updated horizons.

Table 12: Layer overview of Bockfliess 208 – 16th TH-1 [56]

16TH-1								
Top [mMD]	Bottom [mMD]	Top [mTVDSS]	Bottom [mTVDSS]	Thickness [mMD]	Thickness [mTVD]	Por [V/V']	SW [V/V']	Fluid [-]
2131.2	2145.3	1455.6	1456.5	14.2	0.19	0.19	0.29	Oil
2147.5	2338.1	1455.0	1456.6	190.6	0.27	0.27	0.34	Oil
2131.2	2338.1	1455.0	1456.6	204.8	0.23	0.23	0.31	Oil

Table 13: Layer overview of Bockfliess 208 – 16th TH-2 [56]

16TH-2								
Top [mMD]	Bottom [mMD]	Top [mTVDSS]	Bottom [mTVDSS]	Thickness [mMD]	Thickness [mTVD]	Por [V/V']	SW [V/V']	Fluid [-]
2370.3	2496.8	1452.9	1454.2	126.5	1.3	0.20	0.36	Oil

Due to the anticipated formation strength (Geomechanical Study of BO 204) and a nearly free gas target region, a multidisciplinary team from OMV Austria decided to complete this wellbore as an OH in combination with blank pipes, ECPs, and the newly introduced AICDs. The completion configuration regarding the casing and line diameter is stated as follows:

Table 14: Casing configuration of BO 208 [57]

Casing [in]	Depth-Top [m]	Depth-Bottom [m]	Weight [kg/m]	Quality [-]	Couplings/ Threads [-]
18 5/8	0	27.5	-	-	-
13 3/8	0	498.89	-	-	-
9 5/8	0	2025.5	69.94	L-80	TenXP
7	1915.70	2118.53	34.23	J-55	VAGT
6 5/8	2118.53	2444.0	29.76	L-80	BUTT

As with BO 204 and BO 205, this wellbore integrated a casing measuring 9 5/8". The requirements for a tangent section (max. 3°/30 m MD) and a DLS = 0° are similar to the other wells, which is to provide a broad range of options in terms of ESP sizes. Based on the survey data of the drilling report, the tangent section was placed at a depth between 1457 m and 1534 m MD [58]. Therefore, the ESP was placed at a depth of 1467 to 1509 m MD for optimal production conditions.

Similar to BO 204 and BO 205, well logs with additional interpretations regarding porosity and water saturation were used to identify the most promising oil zones. The total horizontal length exposed to the potential reservoir measures approximately 405 m [47]. With the collected information from the logs, three potential production zones were identified and equipped with AICDs [57].

1. Production interval 2130.40 – 2233.41 m MD
2. Production interval 2291.98 – 2338.29 m MD
3. Production interval 2373,36 – 2419.39 m MD

As was the case for BO 204, the nonproductive zones were also excluded with blank pipes and ECPs.

As previously described, different sizes of AICDs are available. To evaluate the correct amount, position, and dimension of the ICDs, the production team investigated the water

saturation information from the existing logs in more detail. Information such as porosity, permeability, water saturation, and other reservoir parameters of the horizontal section were used to calculate the mobility of oil and water. These values were used to identify five categories of horizontal completion zones:

- Category 1 Blind pipe
- Category 2 Packer
- Category 3 Oil with low mobility value
- Category 4 Oil with medium mobility value
- Category 5 Oil with high mobility value

Because Categories 1 and 2 are self-explanatory, Categories 3 to 5 were adjusted with three different diameters of AICD. In cooperation with Tendeka, the production technology team chose the following three configurations to cover the possible oil mobility values:

- Single AICD – 2.5-mm nozzle diameter
- Double AICD – 10-mm nozzle diameter
- Twin Doublet AICD – 10-mm nozzle diameter

Through different combinations of these valves, the three mobility categories (3–5) were realised. Category 3 was implemented as single 2.5 mm AICDs, Category 4 (medium oil) as a 10+10 valve combination, and Category 5 as a twin 10+10 valve combination.

The ALS at BO 208 was realised with an ESP consisting of three compression pumps with 67 stages each. To have the possibility of higher production rates in the later production cycle, the pumps were chosen as ‘mixed flow’ stage-type pumps. This is a combination of pure radial flow (small flow rates) and pure axial (very high flow rates) centrifugal pumps. To have enough power downhole, two motors of types M456 UT-AC and M456 LT-AC (where UT indicates an upper tandem and LT describes a lower tandem pump) were used. The power ratings for these motors are equal and provided at a frequency of 50 Hz as follows:

Table 15: Motor Nameplate Data – Pump BO 208. Source OMV Austria E&P

Motor Series	[-]	456
Rating Factor	[%]	100
Motor HP @ 50 Hz	[HP]	204.8
Motor - Current	[A]	67
Motor Voltage @ 50 Hz	[V]	1966

In the following picture, the pump performance curve of the installed pump of BO 208 is shown. This curve characterizes the performance of ESP pumps and in this case describes the performance of a particular pump per stage. On the left vertical axis the discharge head is given in feet per stage and on the right vertical-axis, the efficiency of the pump depending on the flowrate and the brake horsepower is displayed. The horizontal axis on the bottom indicates the flowrate in barrels per day (or m³/day). In the chart, the best efficiency point or BEP is indicated with the dotted arrow line.

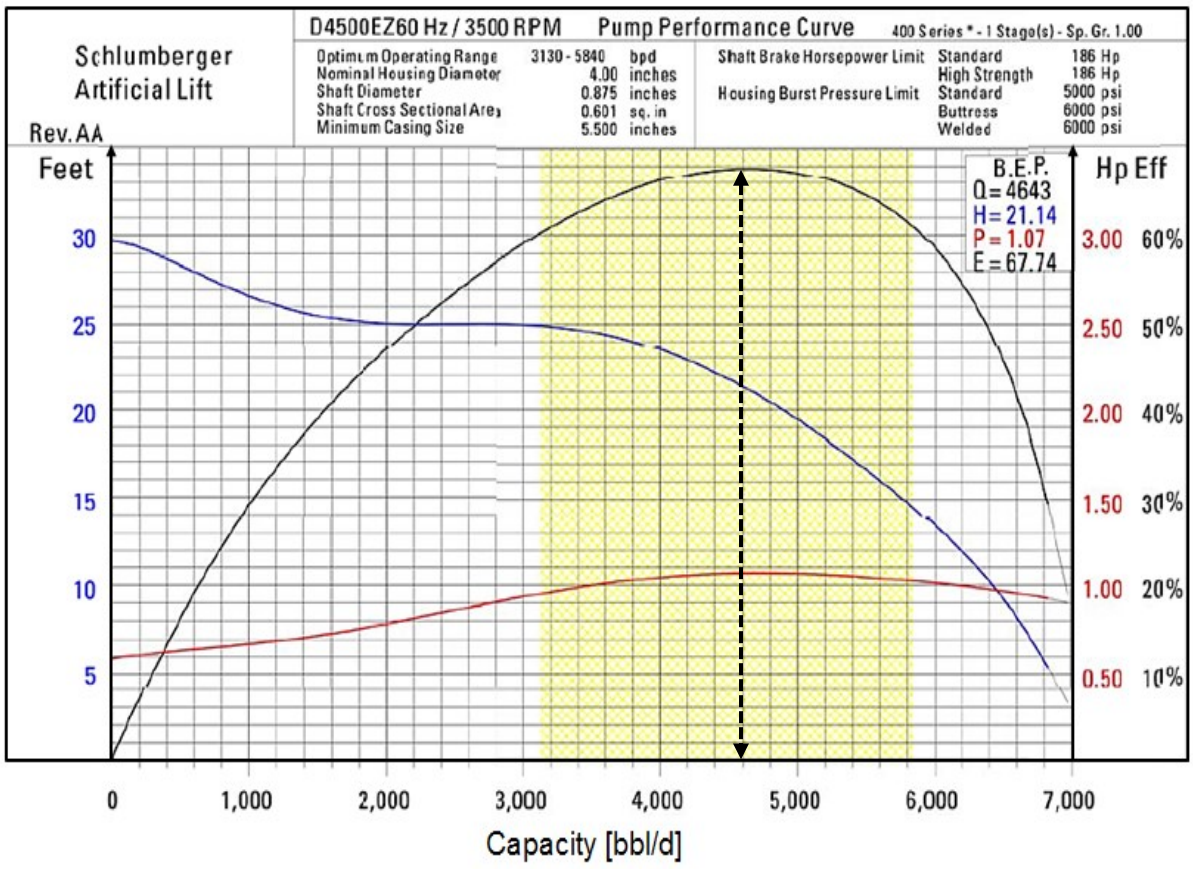

Figure 53: BO 208 – Pump Performance Curve. Source OMV Austria E&P

The actual ESP configuration of BO 208 is represented as screenshot out of OMVs software GDB, which is seen in Appendix C, Figure 67.

To evaluate the performance of the wells, I chose some vertical wells, which are in the close area of BO 204, BO 205, and BO 208. These wells are discussed in subsequent chapters, and the important parameters are summarised in a table.

3.5 Wells for Comparison

In addition to the three horizontal wells, six vertical wells were selected for comparison. These wells are located near the new infill wells and have a similar spatial position to their production zones. The vertical wells are mainly cemented, perforated, and equipped with ESPs or SRPs. In the following table, the most important information concerning these wellbores is listed. To ensure accuracy of the data, it was decided that the selected production would be in taken from March 2018 as the latest data values from the GDB.

Table 16: Wellbore summary

Wellname [-]	Field [-]	Well Type	ALS-Type [-]	WC [%]	Density [kg/m³]	Depth [mTVD]
BO 31	A015	Vertical	ESP	99.22	905	1675.00
BO 68	A015	Vertical	ESP	98.44	905	1720.18
BO 200	A015	Vertical	SRP	96.46	905	1704.00
BO 201	A015	Vertical	SRP	94.98	905	1756.00
BO 202	A015	Vertical	SRP	80.00	905	1770.00
BO 203	A015	Vertical	ESP	98.95	905	1724.30
BO 204	A015	Horizontal	ESP	99.12	905	1632.74
BO 205	A015	Horizontal	SRP	81.14	905	1627.65
BO 208	A015	Horizontal	ESP	98.26	905	1650.31

The following chapter discusses the available production data. These data are pressure and temperature data from the reservoir, ESP sensor data such as pump intake pressure (PIP) and pump discharge pressure (PDP), and different fluid levels from Sonolog measurements.

At the sucker rod pumps and the electrical submersible pumps where no sensors were installed, the dynamic and static fluid levels from measurements were used to calculate the well flow pressure. To ensure correct results, the original data had to be quality checked as well because no valid data were sorted.

One major challenge determined during analysing the data for this master thesis was that during fluid level measurements, the levels were often distorted by the presence of foam in the annulus. This foam forged the measurement results and had to be eliminated by checking for example pump installation depths and previous existing fluid level trends.

4 Production Data Analysis

This chapter describes the production data analysis and provides the results from theoretical calculations; furthermore, the NETool™ simulations are compared with the existing production history of the observed wells. First, the cumulative production was examined closely. From December 2013 to January 2014, BO 204 began its production. Nine months later, the next horizontal wellbore (BO 205) was completed and started its production interval in September 2014. At the end of the redevelopment programme, the last horizontal well (BO 205) started its production. As a reference time interval for data comparison, the shortest production interval was chosen. The following analyses were performed for each well within its first 30 months of production to gather comparable results.

During the investigation of the different wells, a significant difference in early stage oil production has been found. Therefore, I stopped further investigations and considered a manner of evaluating the wells in a reasonable way. To improve data analysis and implement a well-specific filter, a vintage analysis of the 16th TH was performed. In the petroleum industry, oil and gas fields are developed over decades, and during its lifetime, the reservoir conditions can change significantly (e.g., reservoir pressure, reservoir temperature, and saturation). A vintage analysis is used to identify specific groups of events and classify oil and or gas wells according to these events.

As data for the analysis, the average oil production rates from the first months of each well were taken. Basically, the 16th TH is divided into three main oil production sections. The first section is defined by the highest oil production from the early stage of the first development of the horizon in 1949 until 1959. After 1959, new wells were drilled with an initial oil production rate that was nearly equivalent to previous wells. The wells from 1959 to 2007 were declared as midlife wells, and those wells drilled after 2007 were grouped as youngster wells. Figure 54 elucidates the vintage analysis; it shows all three groups (mature, midlife, and youngster), the initial average oil production, and the different development dates of the investigated wells.

Notably, in the vintage analysis, the initial oil production's typical decline behaviour of an oil field is visible. High oil production is seen at the beginning of the field development until a plateau oil production is reached, followed by a strong decline.

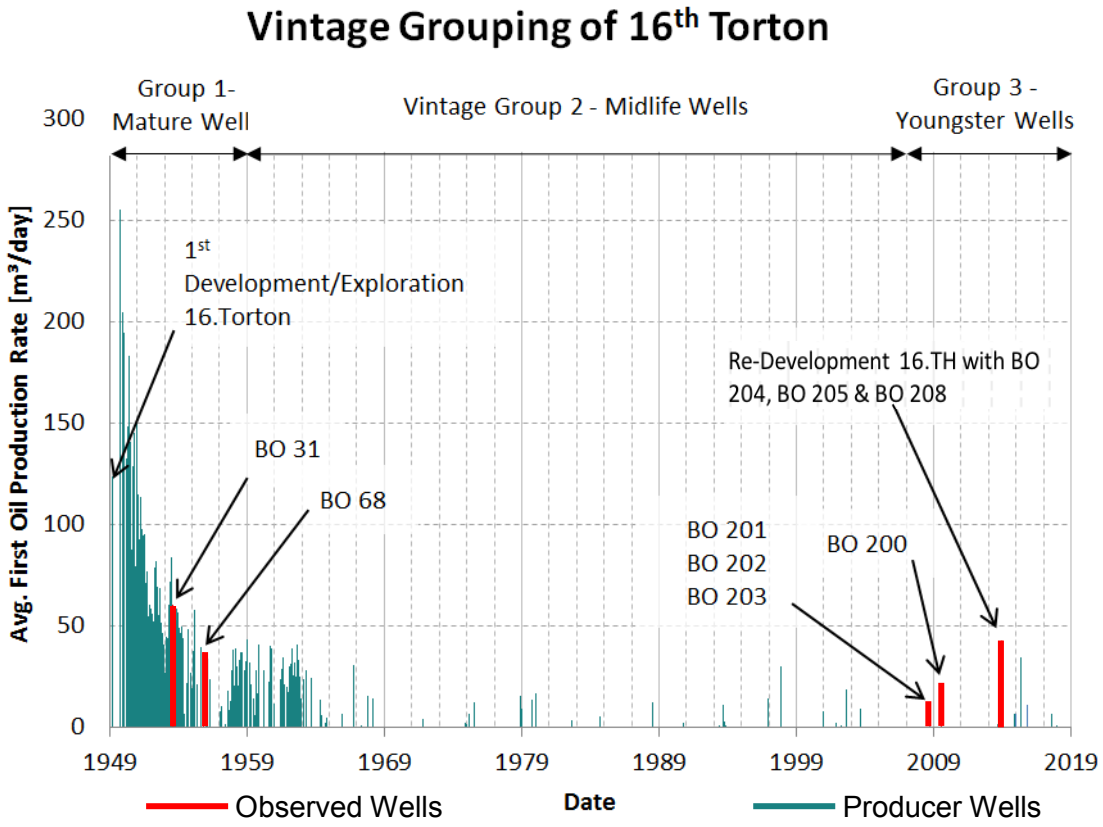

Figure 54: Vintage analysis based on initial oil production

Based on the vintage analysis, wells BO 31 and BO 68 are not compared with the youngster wells from 2007 and after. The initial oil production of these two wells belongs to the earliest stage of the 16th TH production, and therefore are not comparable using all analysis methodologies. In the following subsection, the first relevant production parameter to be examined is the AOF potential of the wells.

4.1 AOF Potential

Based on the theory of 'Well Performance', it is known that the AOF is the maximum capacity that a well can produce (see Equation **2.4.11**) when the well flowing pressure is zero. Normally, the AOF is determined during a well test, but in the case of the observed wells, no actual well test was available. Therefore, the standard Vogel equation was rearranged so that the $Q_{O,max} = AOF$ could be calculated. The reservoir pressure in general is approximately 120 bar at the 16th TH and the well flowing pressure (p_{wf}) was calculated with the latest given value for the static/dynamic fluid level (in the case of the SRP pump) or with the provided PIP data (in the case of the ESP pump).

As a result of the PI of each well, the maximum flow potential was calculated, and based on this, a Vogel–IPR curve was calculated for each well. In Figure 56, the IPR curves of the observed wells are presented. Well BO 204 has the highest calculated open flow potential. The origin of such a high AOF is based on the calculation from the well flowing pressure from the ESP sensor and a very high production rate at this well of about 2000 m³/day.

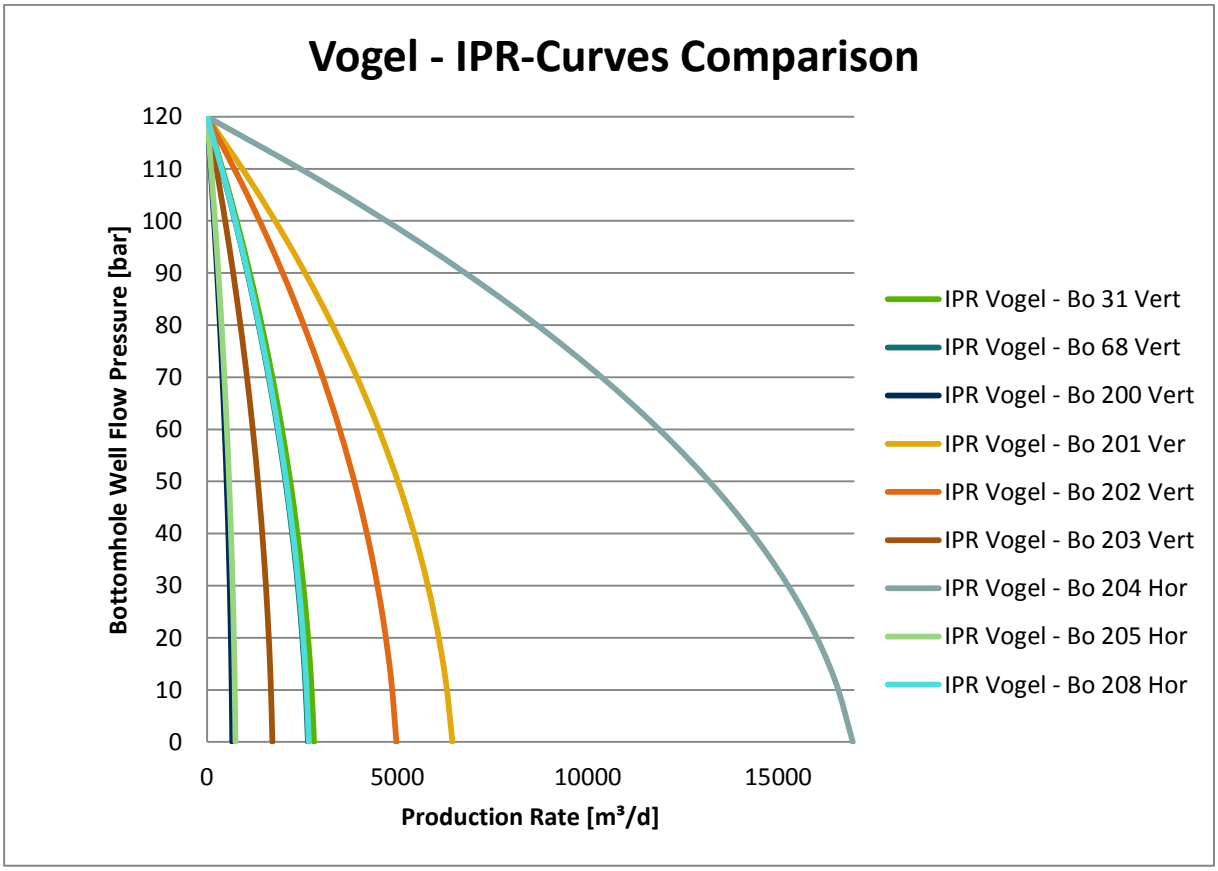

Figure 55: IPR curves of the observed wells

Based on the results of the AOF potential calculation, no possibility exists to evaluate a quantitative answer about the performance of these wells.

For further investigation on the efficiency of the wells, the PI and specific PI was calculated. For this, only the valid parameter of the fluid levels (Sonolog) or ESP sensor data were used.

In addition to the standard PI calculations, which were performed using MS Excel, the three horizontal wells BO 204, BO 205, and BO 208 were rebuilt in NETool™ and static simulations with the initial parameter were conducted.
In the following table, the PIs and specific PIs of the standard calculations are listed.

Table 17: Table of PIs and specific PIs

Wellname [-]	Flowrate [m³/d]	p_{res} [bar]	p_{wf} [bar]	PI [m³/bar/day]	Prod. Interval [m]	PI* [m³/m/bar/day]
BO 31	262.7	120	113.2	38.8	2	19.41
BO 68	163.7	120	105.8	29.6	3	9.88
BO 200	117.5	120	107.6	9.5	11	0.86
BO 201	183.5	120	113.7	29.3	7.67	3.82
BO 202	83.13	120	114.22	14.38	6.72	2.14
BO 203	392	120	103.82	24.23	3	8.08
BO 204	2100	120	103.37	120.27	247.30	0.49
BO 205	90.94	120	111.63	10.86	190	0.06
BO 208	765.22	120	110.77	82.93	289.21	0.29

Table 18: NETool™ results of initial PI

Wellname [-]	Flowrate [m³/d]	PI [m³/bar/day]
BO 204	230	20.44
BO 205	70	40.661
BO 208	300	26.93

During the setup of the NETool™ -simulations, some challenges occurred. One of the first problems is based on the modelling type itself. Because of that, there was no up-to-date Eclipse model available for this reservoir region, I had to work with a static model. This static model was based on the available log data, and from these data, the permeability, porosity, and water saturation parameters were extracted. Based on the static data, the simulation results were only valid for the initial state of the reservoir when the wells were drilled. The change in water saturation or relative permeability over the last 30 months cannot be considered in this simulation, and therefore, the NETool™ data cannot be compared with the up-to-date PIs.

A further problem was based on the production rate. As in the case of BO 204, a very high production rate of more than 2000 m³/day was provided. The static model of the horizontal well cannot be calculated with this high production rate. Based on the simulated intern equations and the position of the first node, the pressure at the first node would be below 0 bar. This result was an error and the programme closed the simulation process.

4.2 Water–Oil Ratio (WOR)

A common tool to evaluate the lifetime of a well is to plot the WOR against cumulative oil production. In the industry, the WOR is used to predict future production and evaluate the expected ultimate recovery (EUR). It is an empirical analysis method in which the abscissa and the ordinate (X-/ Y-axis) are in logarithmic form. In water driven reservoirs such as the 16th TH, WOR interpretation is used to enhance confidence in the forecast of the well performance. OMV's database software GDB has a WOR analysis tool and is used to evaluate the future performance of the observed wells.

In the following figure, the WOR of well BO 204 is shown. As a limit for the production, a water cut of 99.50% was adjusted and unified for all horizontal wells to obtain comparable graphs. The wells are in the same reservoir, and therefore, the reservoir volume for the EUR calculations are equivalent. Based on the different increases of the WOR, a wide variation in time is provided until the EUR is reached.

In the case of BO 204, a permanent increase of the WC leads to a steep ascent of the exponential WOR curve, and therefore, to a relatively fast achievement of EUR.

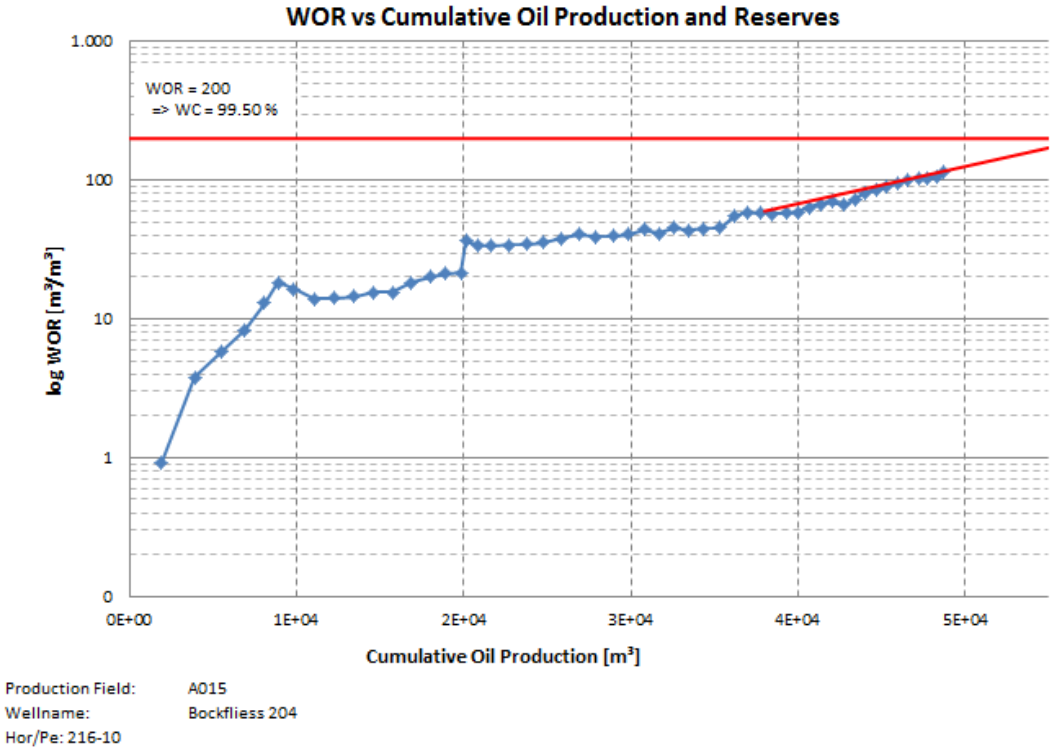

Figure 56 Water–oil ratio of BO 204 from the GDB

In all cases, a different behaviour of the water cut increase is provided, which leads to a tremendous difference in the EUR. BO 204 has the steepest 'constant' rise in water cut compared with the other wells.

The whole forecasting method is dependent on the increase of the WOR in combination with the observed time. The future trend is calculated on data that most promisingly predicts the behaviour of the reservoir in future.

As seen in Figure 57, the increasing WOR is slightly shallower than in Figure 56 (BO 204). This leads to a higher EUR if the oil WOR increases the same proportion than over the previous months.

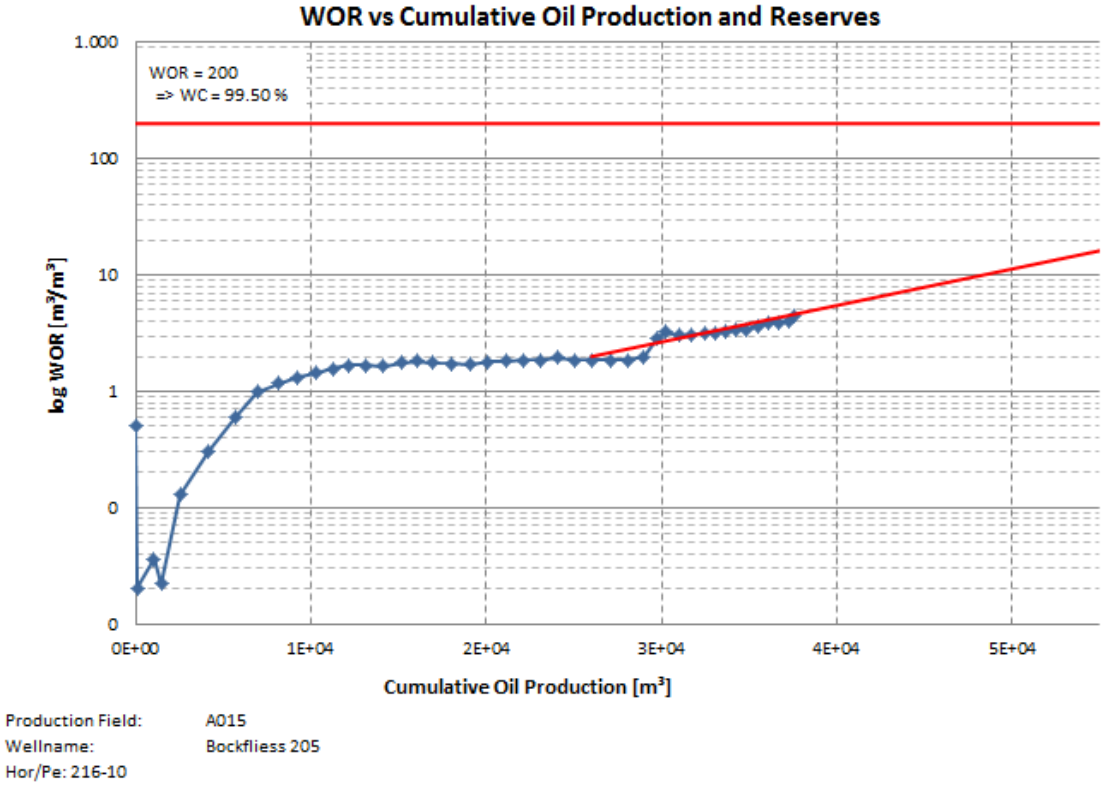

Figure 57: Water–oil ratio of BO 205 from the GDB

The highest EUR of all horizontal wells is shown for BO 208. There, the very low increase and near constant WOR leads to an extreme shallow increase, and therefore to the maximum water cut of 99.5% being reached slowly.

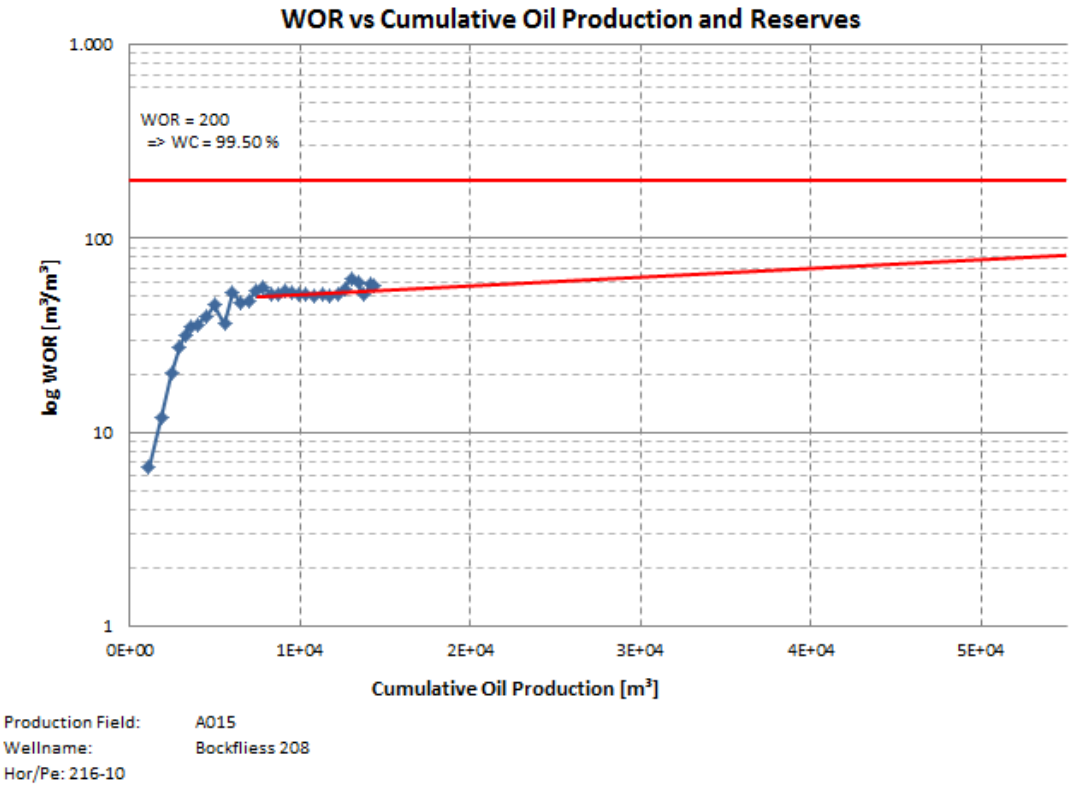

Figure 58: Water–oil ratio of BO 208 from the GDB

As a result of the gathered data and the exponential forecast interpretation of the WOR to the cumulative oil production, BO 205 and BO 208 will have an EUR 1.5 to 2.4 times higher than BO 204

4.3 Water Cut

In a water driven oil reservoir, an increase of the water cut during the production period is considered normal progress. In the Matzen oil field, a very high water cut often higher than 90% exists and acts as a driving force to motivate OMV Austria to improve their technical AL solutions repeatedly.

During my research on the production data, I first examined the water cut of the horizontal wells, which is shown in Figure 59. To make the occurring upwards trend at the water cut visible, both ordinates in the figure are adjusted in 5% steps. BO 204 and BO 208 are displayed on the left y-axis and BO 205 is seen on the right one. Although the existing water cut at BO 205 is lower than at the other wells, it has a distinct increasing trend. At BO 208, the intelligent completion was implemented to self-regulate the occurring water production, and based on the data from Figure 59, a more constant than increasing water cut trend is visible.

Thus, it seems that the AICDs work in the manner that they were constructed for, but without any additional measurements of the production, this is based more on assumptions than on hard facts. Recommendations regarding this are mentioned in the last chapter of this thesis.

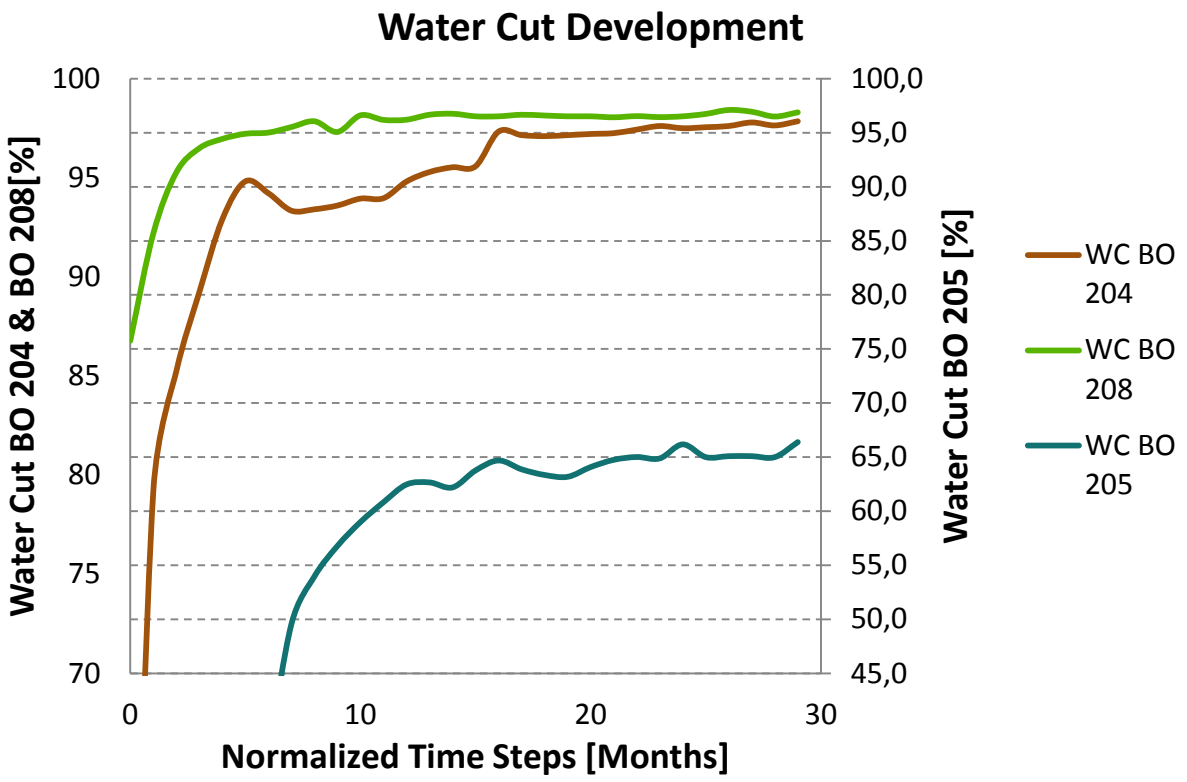

Figure 59: Water cut of horizontal wells. Source GDB

In addition to the comparison of the three horizontal wells, a graphical analysis in which all observed wells were compared was performed (see Figure 60). From a closer look at the trends of the individual curves, each water cut trend can be seen to increase over time, except the water ratio line of BO 208 (see Figure 60). Although BO 208 is positioned in a much deeper location, and a very high initial water cut, the ability of this well to keep a constant water cut is matchless.

The deviation from 'normal' behaviour of the increasing water proportion from BO 208 compared with the other wells (vertical and horizontal) is a clear indicator that the new completion technology has a significant impact on the production behaviour.

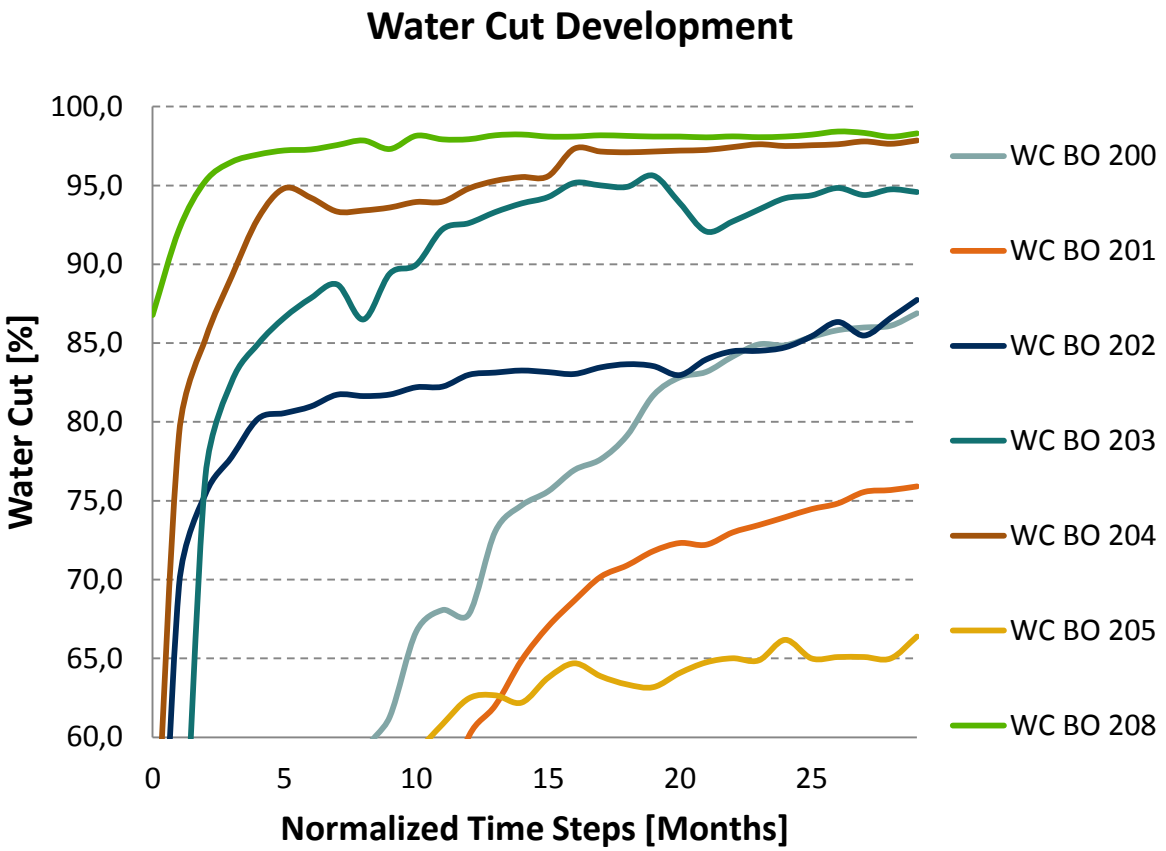

Figure 60: Water cut from all wells. Source GDB

4.4 Production Data

Because of low oil prices in recent years, the oil and gas industry has been under enormous pressure to decrease its operational and capital expenditures (OPEX and CAPEX, respectively). To perform an economic analysis on the observed wells, certain criteria must receive attention. Because all wells are drilled and completed on different dates, the timestamps of the wells were normalised. This normalisation is based on the latest production start date of well BO 208. The required production data were collected on a monthly basis from October 2015 to March 2018.

All available production data (e.g., gross production rate, oil production, water production, water cut, and gas production) were extracted from the GDB for the first 30 months of each well. After all data were time-normalised, it was decided to keep the economic analysis independent of the oil price to neglect the volatility of the market and focus on the technical efficiency itself. The analysis is based on the production volume of oil, gas, and water instead of on price per barrel.

The following picture shows a typical production profile from the 16th Torton and is represented by the production data of BO 205 (Figure 61)

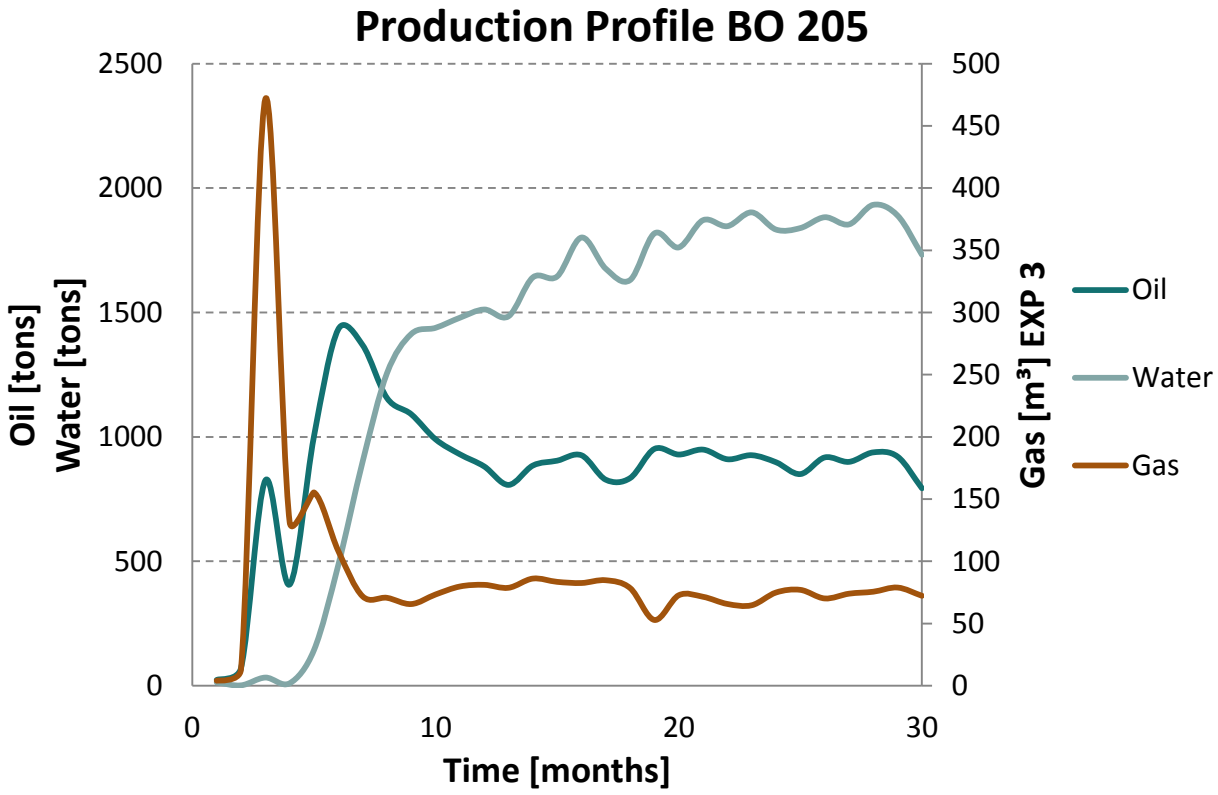

Figure 61: Production profile of BO 205 with Oil, Gas & Water. Source GDB

In the Bockfliess area, very low gas content was predicted based on the known reservoir properties and geological structures. Therefore, only the oil production data, or more accurately, the cumulative oil production of each well was investigated. As stated previously, only the oil wells beginning from BO 200 to BO 208 were compared. BO 31 and BO 68 launched in mid-1950 belong to the earliest development stage of the oil field and are therefore not suitable for comparison.

The required production data were imported into MS Excel to perform the interpretation. Over the first 30 months, significant differences between the observed wells were visible. In the following figure, a comparison of the youngster wells is provided. In addition to the well name, a short name of each individual well type and completion type is provided. The first abbreviation indicates the type of ALS and the second initials name the wellbore type (Vert = vertical or slanted well; Hor = horizontal well). Based on the lowest cumulative oil production data, a factor was derived that indicates the multiplication of the other wells' cumulative production.

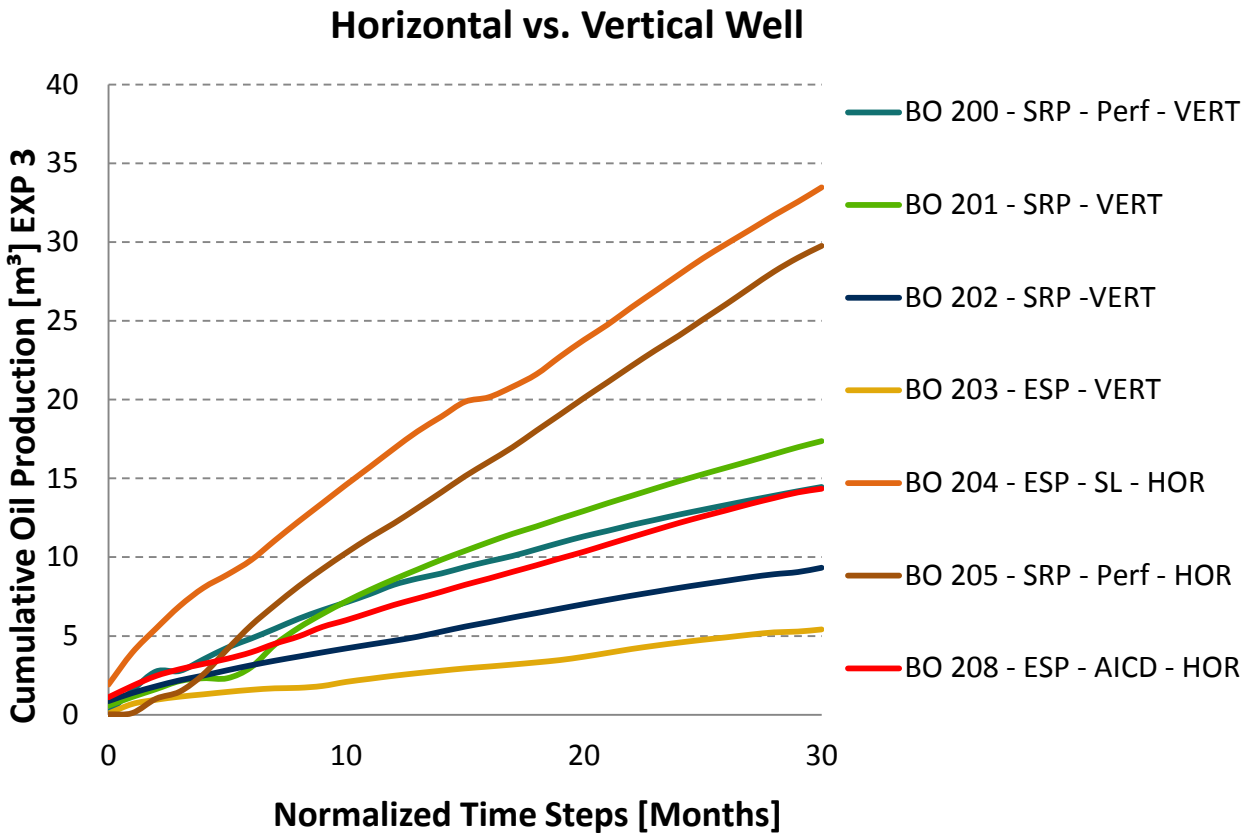

Figure 62: Cumulative oil production comparison. Source GDB

As seen in Figure 62, BO 203 had the lowest cumulative production over the first 30 months. Therefore, this well was chosen as a basis for the following calculations. Visible at first glance in Figure 62 is that the cumulative production of two horizontal wells (BO 204 and BO 205) is much higher than of any other production well. More accurately, the production of BO 205 is approximately 1.7 times and the production of BO 204 is approximately 2 times the cumulative production of the best vertical well (according to this comparison).

Although BO 208 is not one of the top three wells, because of the subseismic faults that caused the partly deeper depth in the reservoir (a very high water cut from the beginning onwards), this well has performed at least 3 times more effectively than the vertical well with the lowest cumulative oil production.

Table 19 provides a list of all wells sorted by their cumulative oil production performance, the values of which are based on the lowest production.

Table 19: Cumulative production factor

Well	Cum. Prod. Factor
BO 204 - H	6,2
BO 205 - H	5,5
BO 201 - V	3,2
BO 200 - V	2,7
BO 208 - H	2,6
BO 202 - V	1,7
BO 203 - V	1,0

The horizontal wells were planned in the same manner; the biggest difference between them is that BO 208 has a geological interpretation. The difference in their performance may result from the incorrect position of BO 208.

Finally, the average vertical and horizontal cumulative production were compared. The result of this analysis showed that a horizontal well in this reservoir region produced approximately 2.2 times more oil over the same time interval than a horizontal well.

Table 20: Comparison of vertical and horizontal well production

Well	Cum. Prod. Factor
Vertical Type	1
Horizontal Type	2.2

5 Lessons Learned and Conclusion

During the past several months, the reservoir settings of the Bockfliess area, the completion configuration of the nine different oil wells and their production data was investigated and analysed.

In chapter 4.1, the AOF and PIs of the wells were calculated and afterwards compared with each other. First, the AOF potential was investigated in combination with the PI and the specific productivity indices. In this thesis, the AOF calculations were performed through the rearrangement of the Vogel equation and the calculated PIs from the different fluid levels. It is important to estimate the maximum deliverability of the reservoir, but, for a comparison of the different wells, in this case this parameter has no significant influence on benchmarking the efficiency of the completion configurations. Due to the high difference in flow rate from ESP to SRP application, the calculated values vary quite widely.

Furthermore, the PIs and specific productivity indices were calculated in three different ways. They were first calculated by using the given equations from chapter 2.4, then by the simulation software NETool™ and finally by the existing production data, which resulted in several different results of PIs and specific PIs. Reasons for these discrepancies are the following:

- Different input data based on the distribution of averaged values
- Log data input instead of single value parameters.
- Discrepancy between recorded data and real data (fluid level measurements)
- Varying number of values for the analysis
- Varying input parameters for the equations

In addition to the already mentioned problems with the parameters, the absence of an Eclipse model that was not up to date for the reservoir region led to different results in the calculations. The newly gathered subsurface information from BO 208 regarding the subseismic faults will be implemented in the existing geological study to improve the simulation. Because this would take years to conduct, the present results of the NETool™ simulation are not representative.

Since the log data for the permeability and saturation values only indicate the initial state of the borehole, the static NETool™ model is possible to use as a first approach. It proved to be possible to evaluate the downhole completion and its behaviour and to quickly provide a

rough estimation of the pressure and production distribution for horizontal wells. It is therefore recommended that the reservoir model should be updated with all the information that was gathered during LWD and that, with this, parts of the analysis within this thesis should be repeated. With the reprocessed reservoir model, the production data can be compared to determine how realistic the simulated results are in comparison with the real data.

During the analysis of the data horizontal wells, it was observed that additional production measurement devices would give a more clear understanding of the horizontal production behaviour. To increase the performance of horizontal completion configuration, it will be necessary to identify the high productive zones. Because of the difference in pressure distribution from the heel to toe section of horizontal wells, the true production from each section is unknown. One existing method besides production logging tools are so called tracers. These tracers can be installed in combination with e.g. slotted liner or AICDs in the horizontal section of the wellbore. Analysis of the tracer marks can tell you afterwards exactly from which region how much oil or water is being produced. OMV has planned to implement this technology (tracers) in BO 208 in near future for further investigations on the efficiency of the AICDs.

Especially at BO 208, the implementation of production measurement devices would provide additional information. Beside the varying production section, OMV would be able to gather data about the real case choke behaviour of each group of AICDs, which is necessary for further wells with similar completion configuration. As the previous chapter showed, BO 208 with its AICDs saw a significant flattening of the water cut curve over time, which can mainly be attributed to the integration of these inflow control devices.

The last chapter of the production data analysis investigated the economics of the different well types. In Figure 62, the cumulative production showed a strong difference between horizontal and vertical producers. Due to the normalization of the time scale, it is evident that BO 208, which had the lowest cumulative production of all observed horizontal wells, still produced approximately 2.5 times more oil in the same amount of time than the vertical well with the lowest production (BO 203). Moreover, the production of BO 208 was in the same range as the top performer of the compared vertical wells (BO 200 and BO 201).

In regards to BO 204 and BO 205, the performance of these horizontal wells was significantly higher than every other well in the same amount of time. Compared with their vertical

counterparts, the production of BO 204 and BO 205 was, respectively, 1.9 and 1.7 times higher during their first 30 months than the best performing observed vertical well (BO 201).

This thesis showed that the overall performance of the selected horizontal wells in comparison with nearby located vertical wells is significant better. Not only is the amount of produced hydro carbons of interest, but also the economic costs of the complete project has to be analysed as well and implemented into the project considerations.

Based on the results of this thesis regarding the completion behaviour, water cut behaviour and cumulative production trend, a clear answer was able to be derived out of it. In homogeneous sandstone reservoirs like the 16th Torton, horizontal wells perform in much better way than vertical ones, and the application of AICDs improve the overall trend of increasing water cuts.

6 Appendix A [7; 59; 20]

Table 21: Advantages and Disadvantages of various Completion Types

	Advantages	Disadvantages
Open-Hole/ Barefoot Completion:	Low costs No artificial restrictions →360° open formation face Recompletion possible Less to no formation damage due to shorter fluid exposure. Full exposure of reservoir zone No cementing or perforating expense Minimize wellbore skin Improve wellbore performance due to a large inflow area	Poor inflow control Damage repair is difficult Wellbore stability problems High water/gas breakthrough risk Limited injection options Unable to control excessive water or gas production Unable to isolate hydrocarbon zones Difficult to do reservoir management Has large potential to produce sand Inability to produce at different zones
	Advantages	Disadvantages
Slotted-/ Pre-Drilled Liner Completion:	Low costs Safer against borehole collapse than pure OH completion Inflow restrictions are minimal More efficient removing of filter cake through circulating Better applicable for coiled tubing and other working strings (low μ)	Less to no flow control Zonal isolation is difficult Crossflow potential Workover difficult (liner pulling for remedial work) Mitigated liner strength due to slots, holes → collapse Ineffective sand control Recompletion very difficult
	Advantages	**Disadvantages**
Case Hole Completion:	Very good flow control Very good zonal isolation High wellbore stability Pass near wellbore damage through perforations Necessary for hydraulic fracturing Production logging is possible Sand production less compared to OH completion Good reservoir management Recomplete and workover possible	High costs of completion (casing, cement, etc.) Perforation costs Limited application (not in naturally fractured formations) Liner cementing slightly reliable Maximum reservoir exposure is less than in OH

7 Appendix B

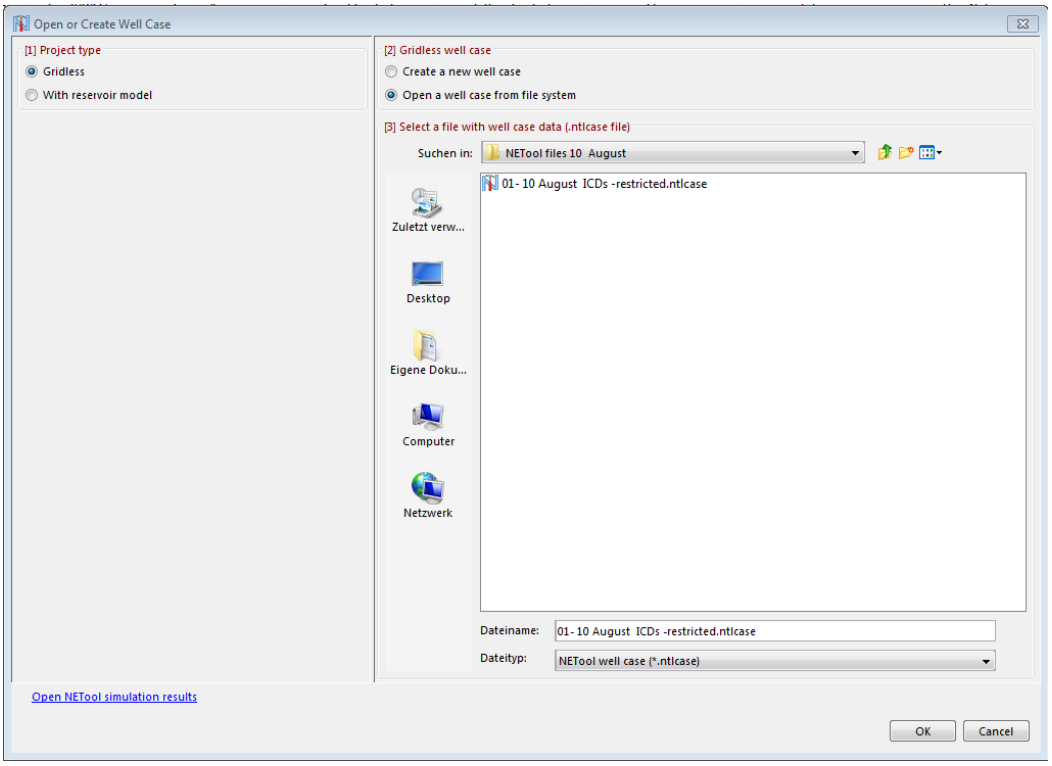

Figure 63: NETool™ Start Window, Project Type Selection. Source NETool™ Software

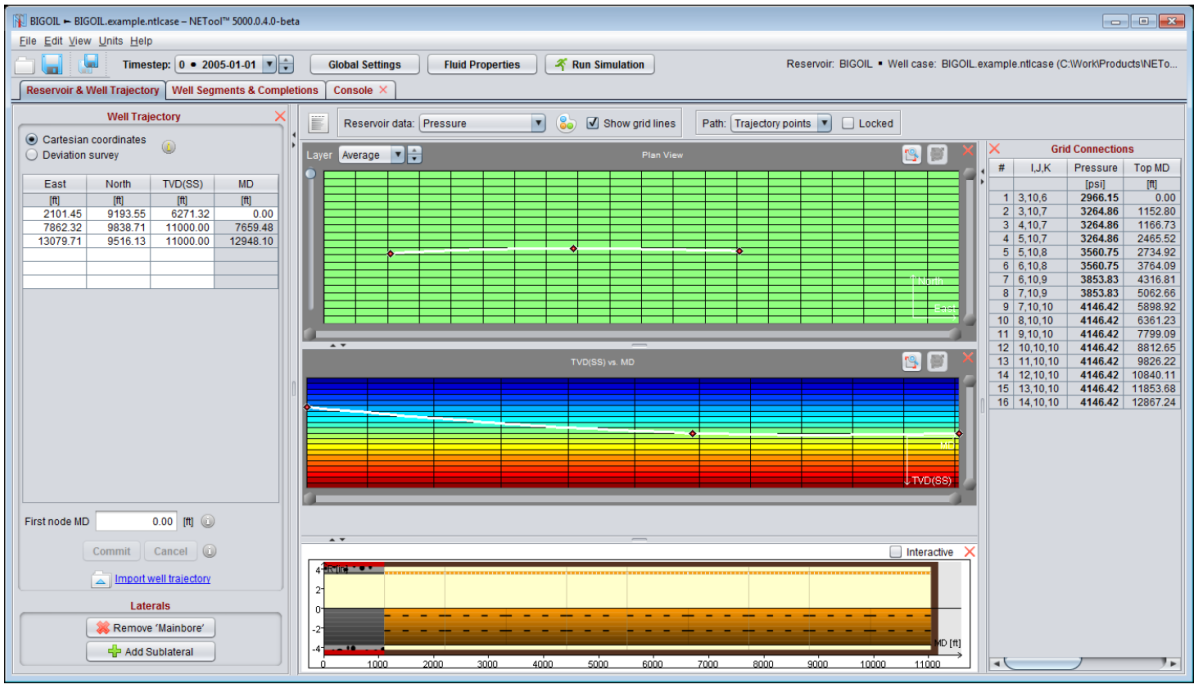

Figure 64: Well Trajectory and Reservoir View [45]

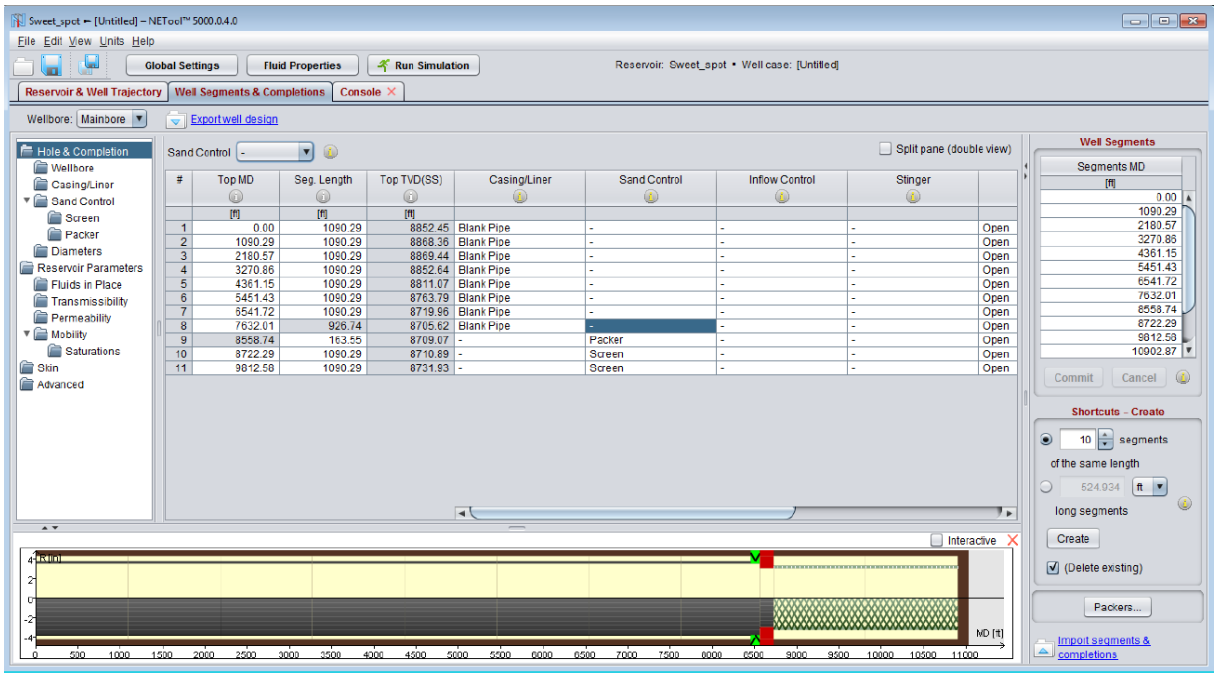

Figure 65: Well Segments and Completion View [45]

8 Appendix C

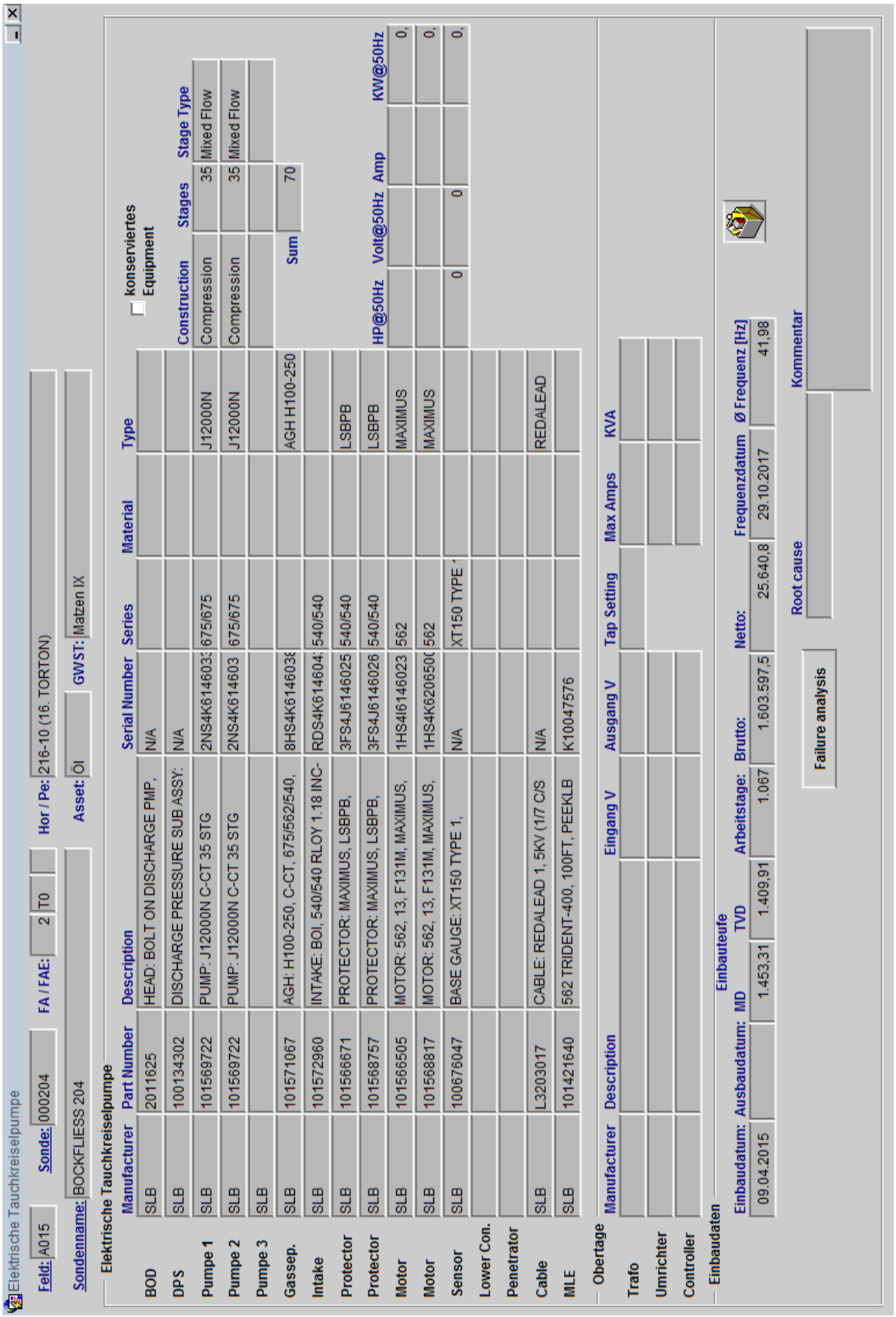

Figure 66: BO 204 – ESP Configuration from the GDB

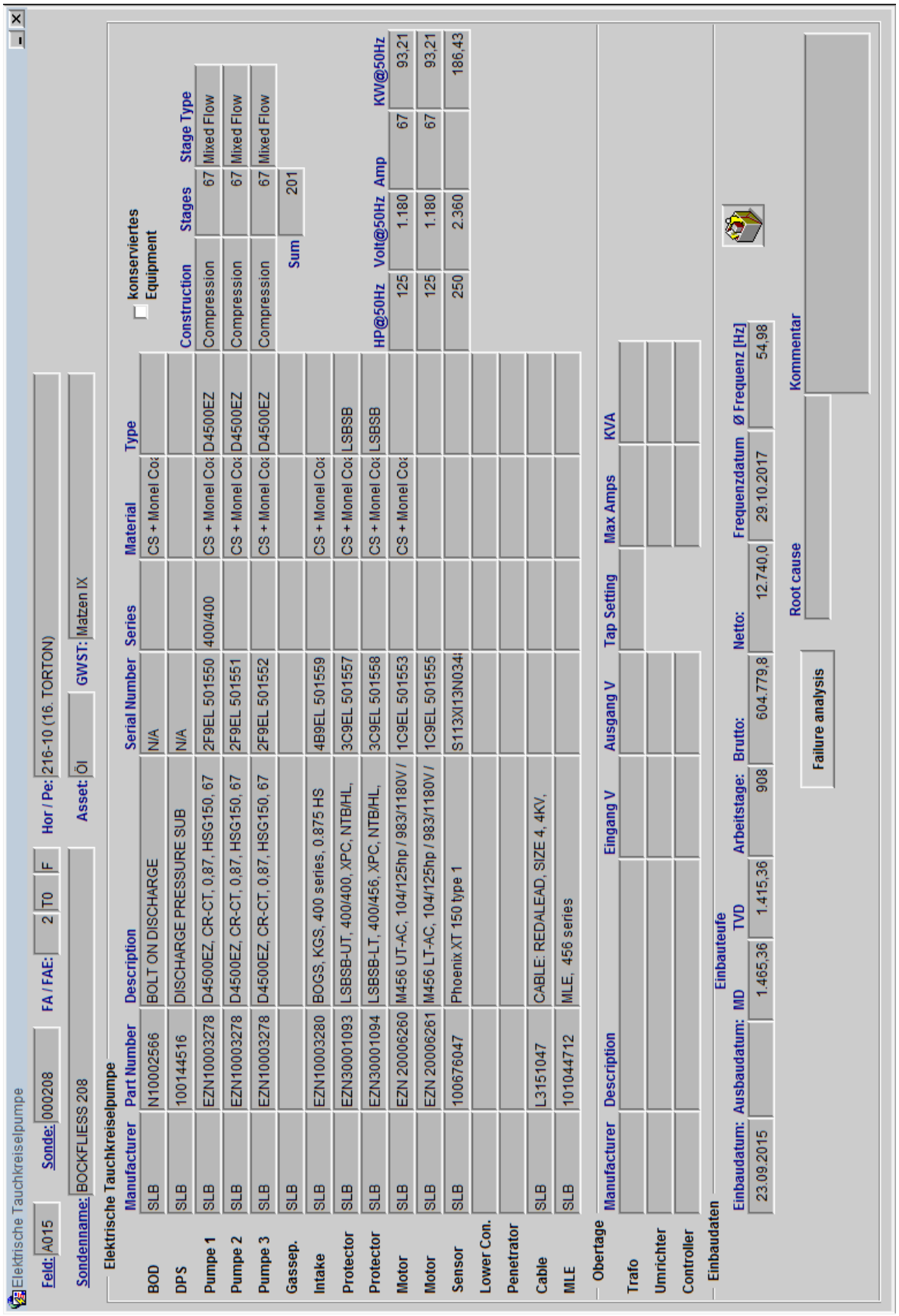

Figure 67: ESP configuration of BO 208 from the GDB

9 Appendix D

9.1 Wellbore Schematic – BO 204

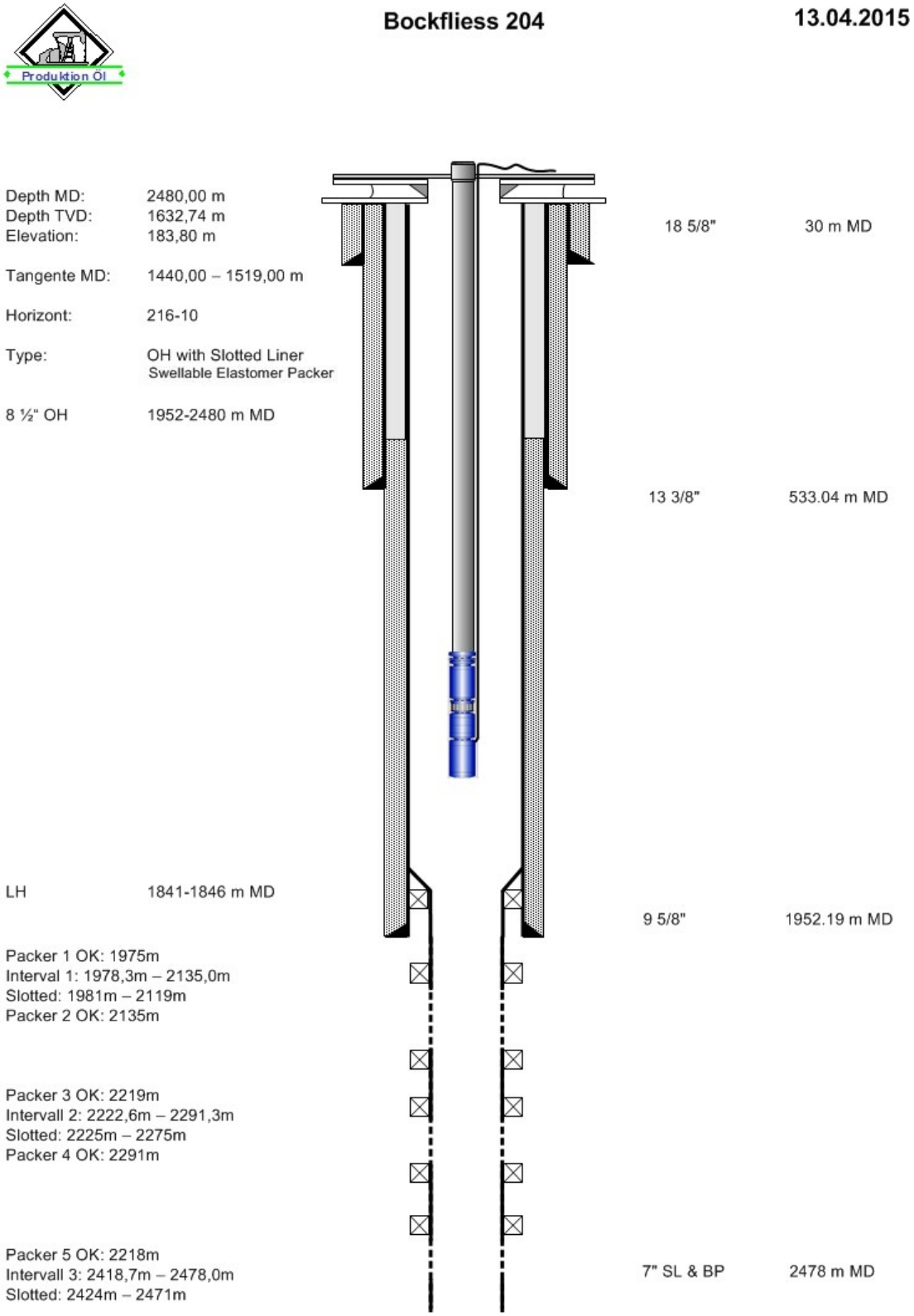

Figure 68: BO 204 Wellbore Schematic. Source OMV Austria E&P

9.2 Wellbore Schematic – BO 205

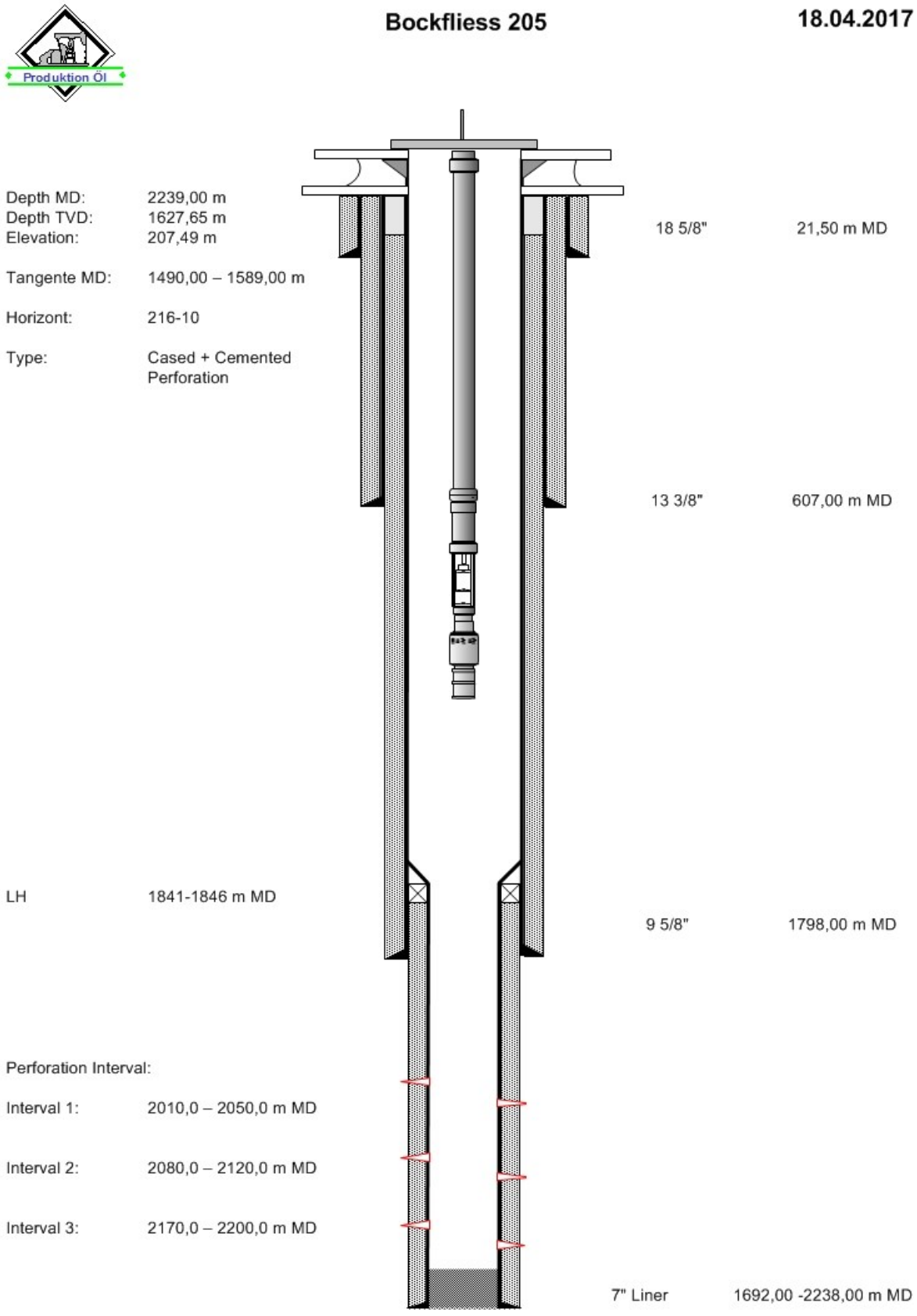

Figure 69: BO 205 Wellbore Schematic. Source OMV Austria E&P

9.3 Wellbore Schematic – BO 208

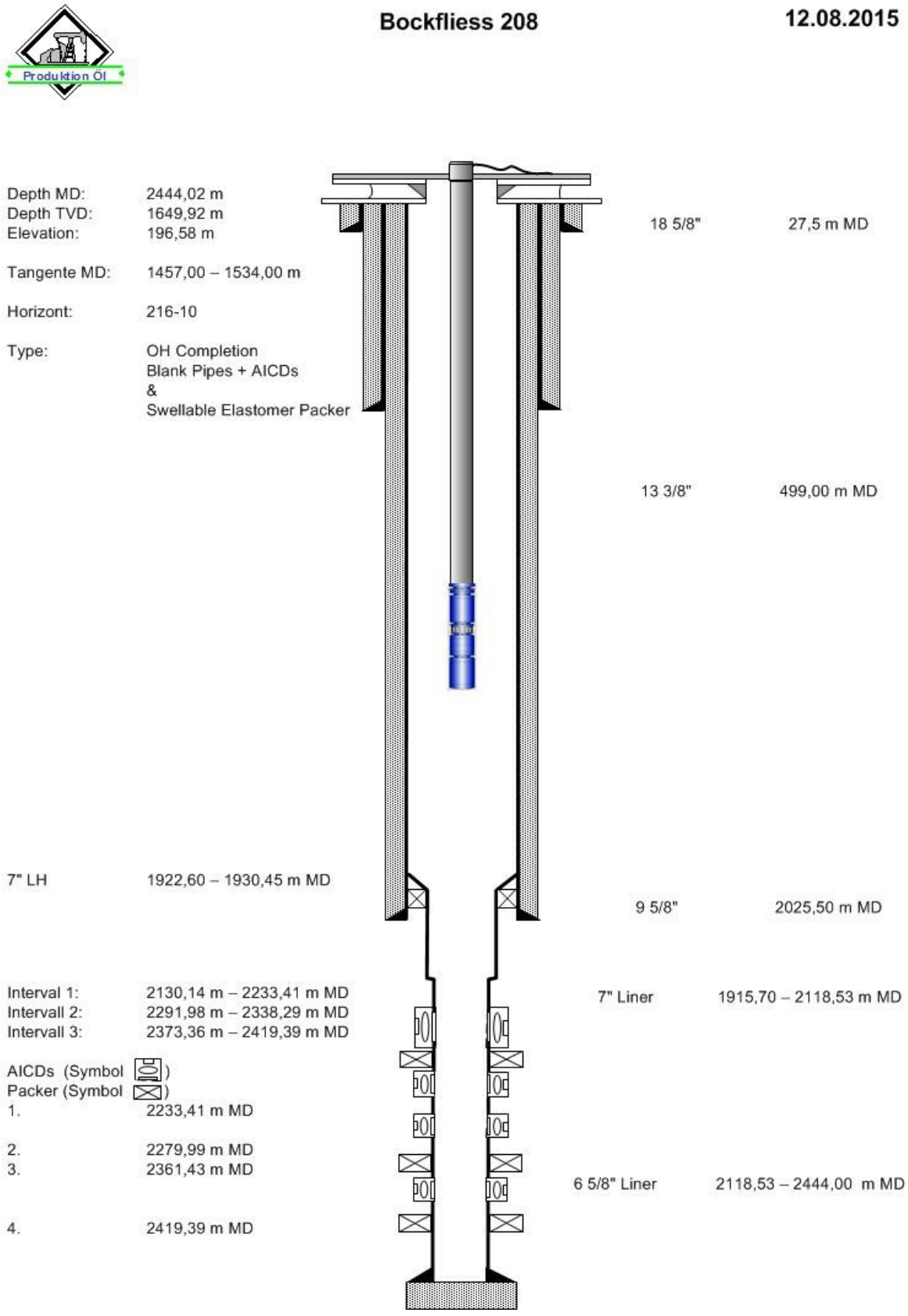

Figure 70: BO 208 Wellbore Schematic. Source OMV Austria E&P

10 Appendix E

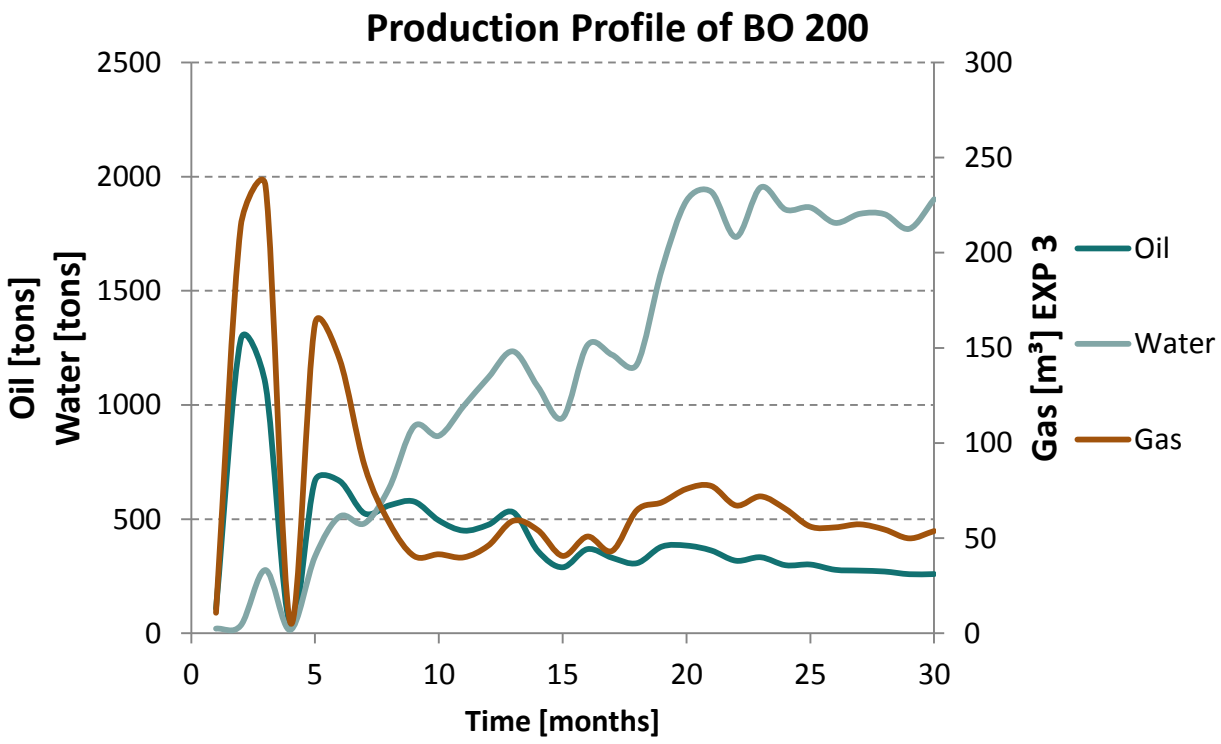

Figure 71: Production Profile of BO 200 with Oil, Water & Gas. Source GDB

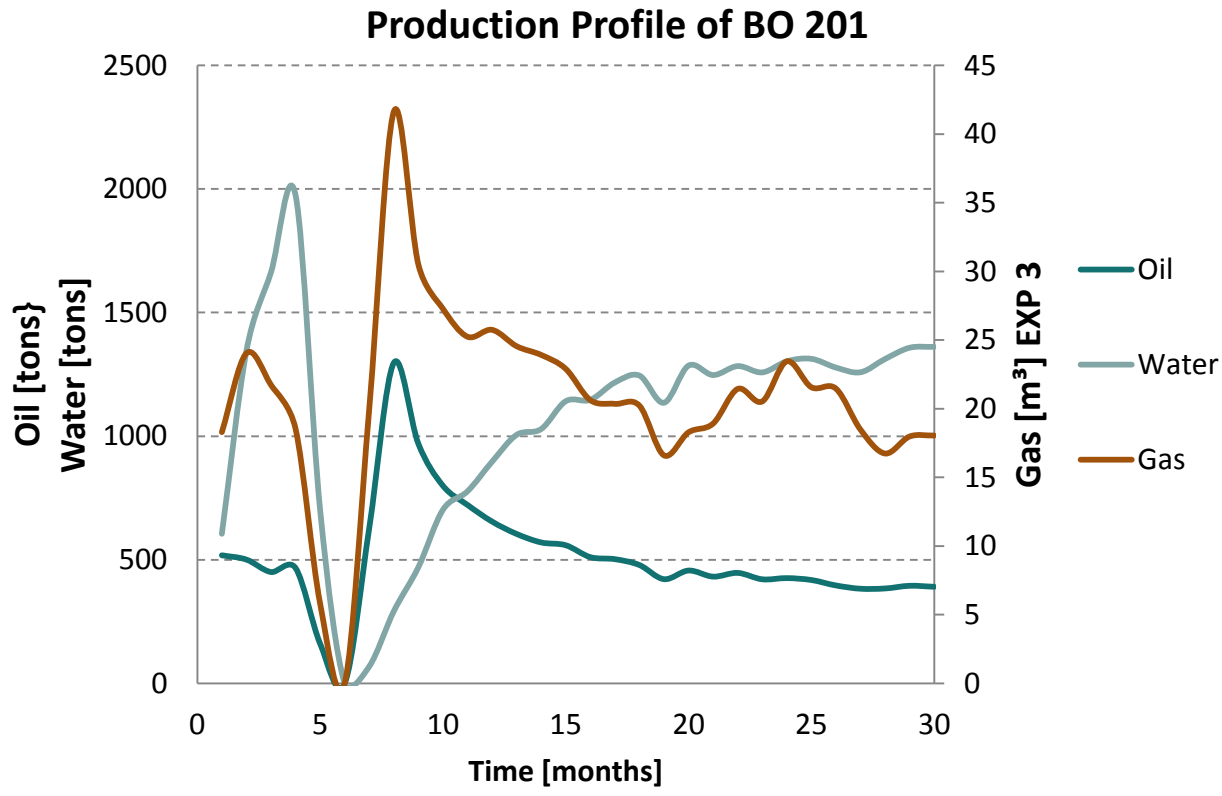

Figure 72: Production Profile of BO 201 with Oil, Water & Gas. Source GDB

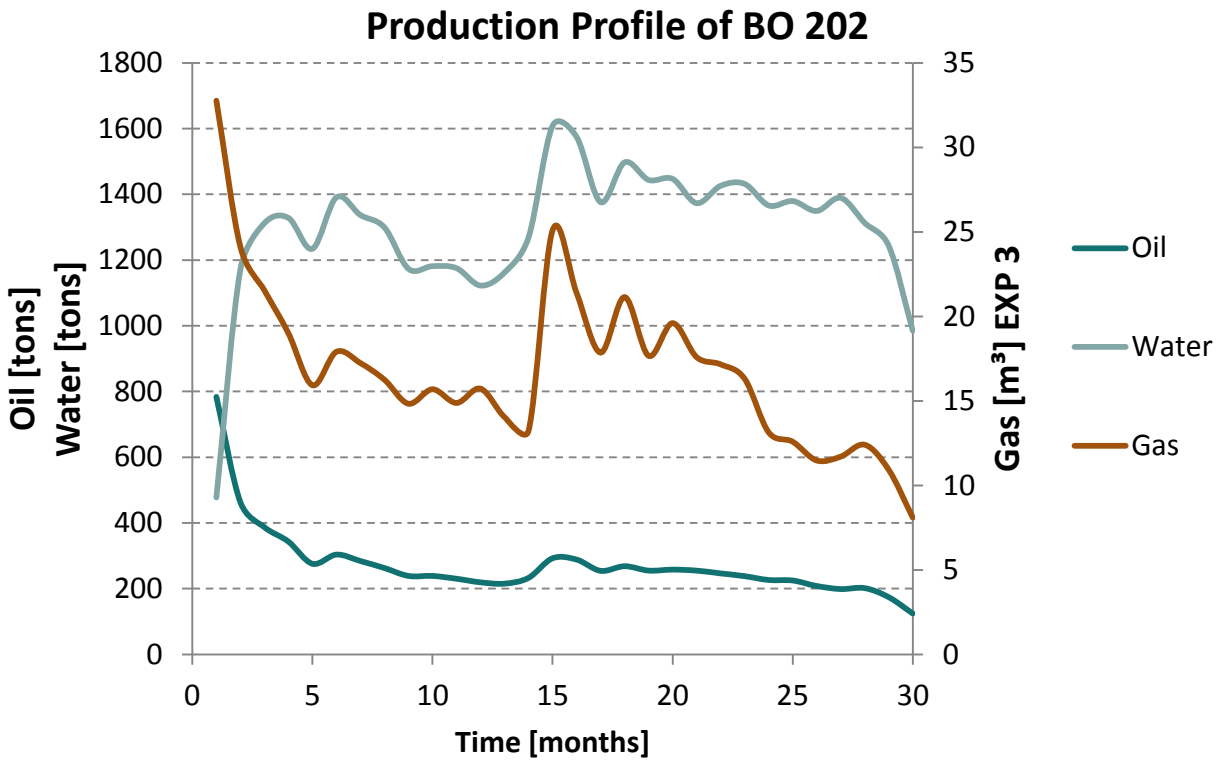

Figure 73: Production Profile of BO 202 with Oil, Water & Gas. Source GDB

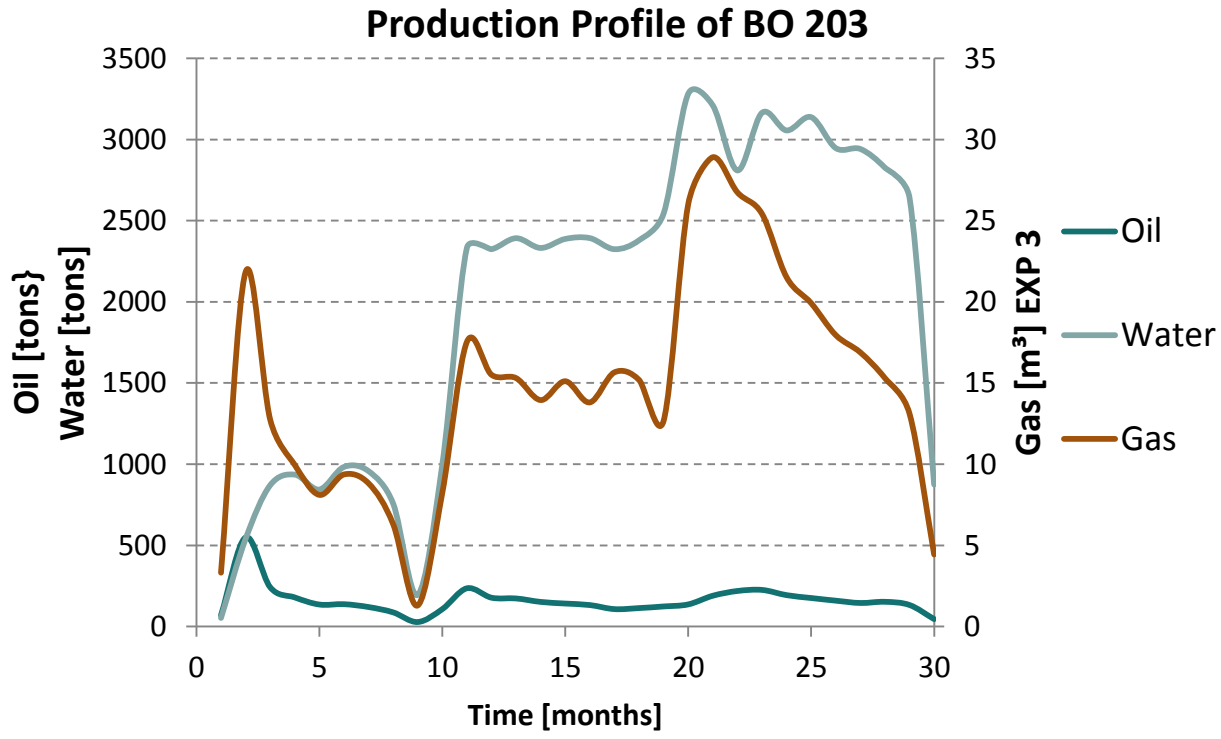

Figure 74: Production Profile of BO 203 with Oil, Water & Gas. Source GDB

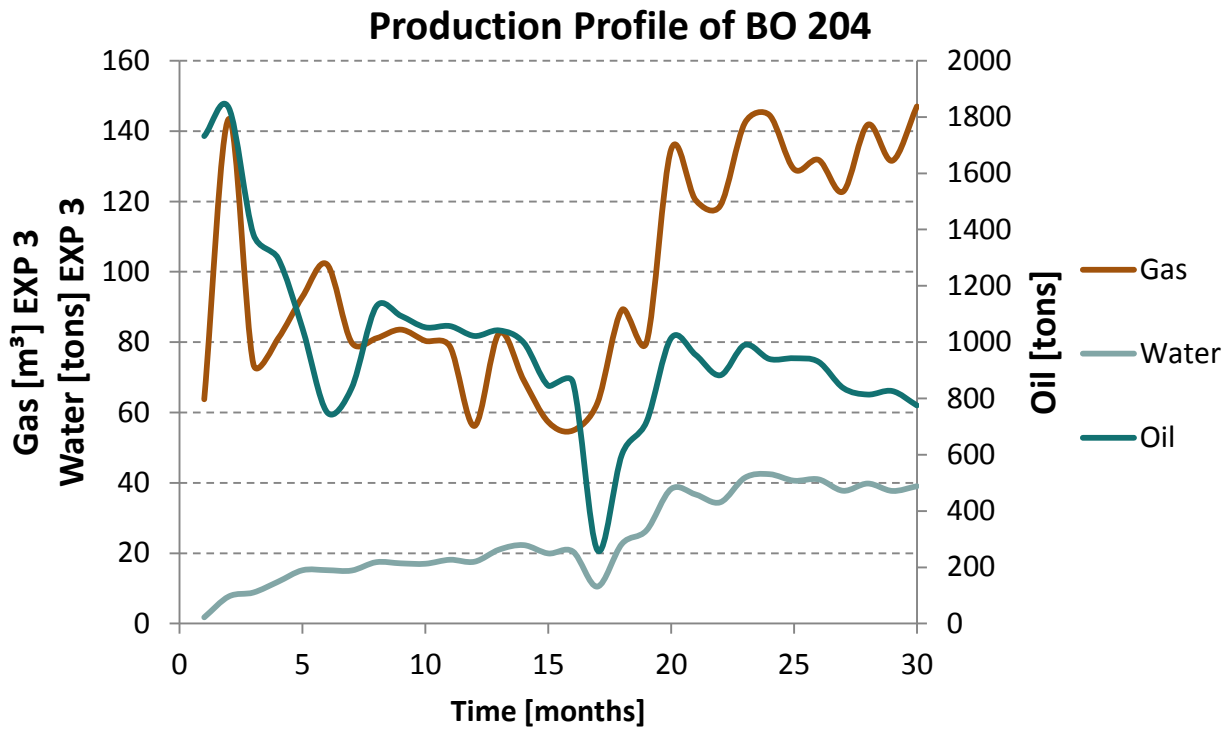

Figure 75: Production Profile of BO 204 with Oil, Water & Gas. Source GDB

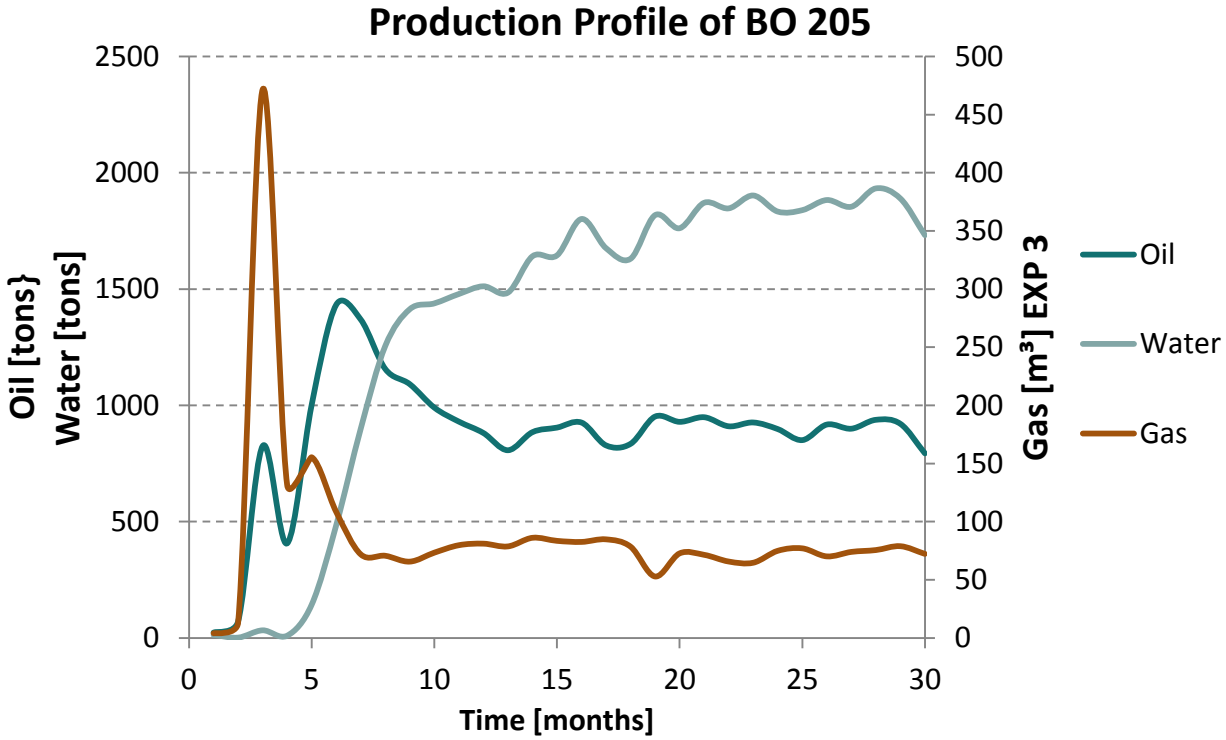

Figure 76: Production Profile of BO 205 with Oil, Water & Gas. Source GDB

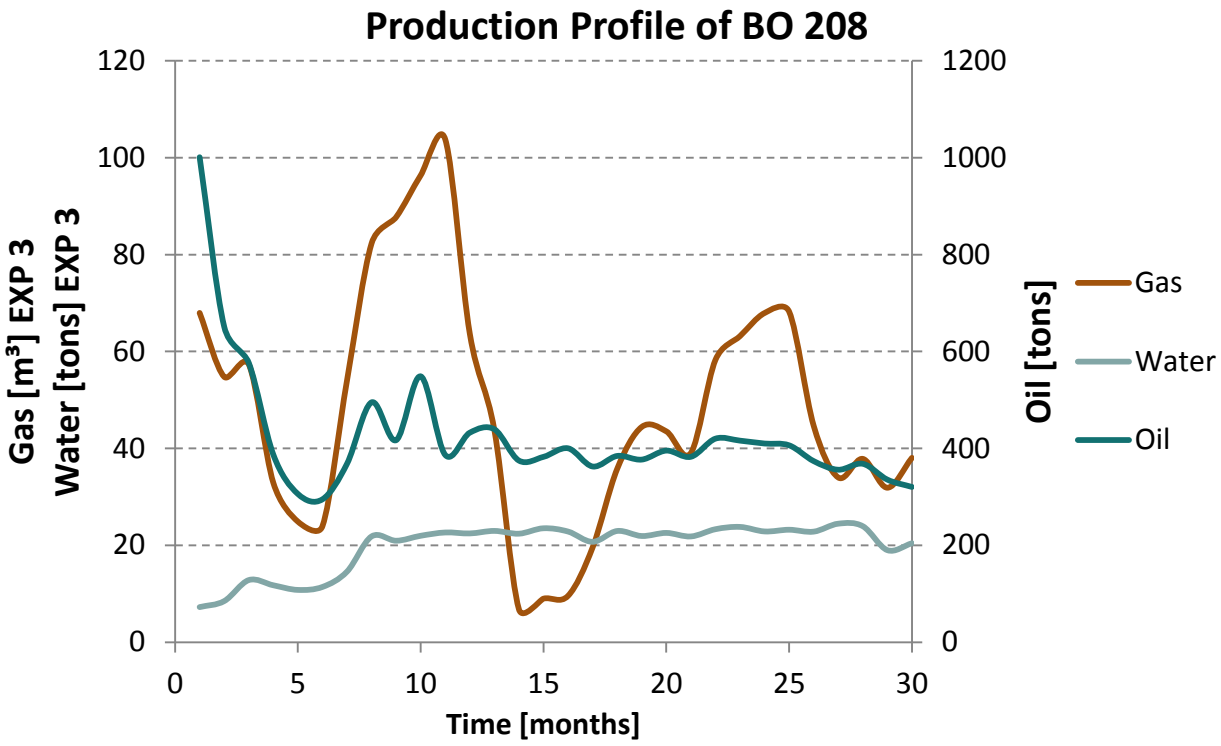

Figure 77: Production Profile of BO 208 with Oil, Water & Gas. Source GDB

11 References

[1]. Proseis AG. 2003. *Matzen Field (Vienna Basin, Austria): Geophysical, Stratigraphic and Petrophysical Evaluation of the 16th Tortonian Oil Reservoir*.

[2]. Kienberger, G. and Fuchs, R. 2006. *Case History of the Matzen Field/Matzen Sand (16th TH): A Story of Success—Where is the End?* https://doi.org/10.2523/100329-MS.

[3]. Giden, I., Kometer, B., Buerssner, P. et al. 2017. *Re-development of an Onshore Mature Oil Field to Double Gross Production by the Use of Sensor-Equipped Electrical Submersible Pumps*. https://doi.org/10.3997/2214-4609.201701595.

[4]. OMV E&P GmbH Laboratory, Paul Toplack, Wolfgang Vollnhofer. *Changes in PVT properties over the lifetime of an oilfield (Matzen)*.

[5]. Beggs, H. D. 1991. *Production optimization: Using NODAL analysis*. Tulsa, Okla: OGCI Publications.

[6]. Ahmed, T. H. 2006. *Reservoir Engineering Handbook*, third. ed. Amsterdam u.a.: Elsevier Gulf Professional Publ.

[7]. Bellarby, J. 2009. *Well completion design*, firstst ed. Amsterdam Netherlands, Boston Mass.: Elsevier.

[8]. Fattah, K. A., Elias, M., El-Banbi, H. A. et al. 2014. New Inflow Performance Relationship for solution-gas drive oil reservoirs. *Journal of Petroleum Science and Engineering* **122:** 280–289. https://doi.org/10.1016/j.petrol.2014.07.021.

[9]. *A Revision Article of Oil Well Performance Methods*.

[10]. Economides, M. J. 2013. *Petroleum production systems*, second. ed. Upper Saddle River NJ u.a.: Prentice Hall.

[11]. D. Joshi, S. 2003. *Cost/Benefits of Horizontal Wells*. https://doi.org/10.2118/83621-MS.

[12]. Joshi, S. D. 1988. Augmentation of Well Productivity With Slant and Horizontal Wells (includes associated papers 24547 and 25308). *SPE-15375-PA*. https://doi.org/10.2118/15375-PA.

[13]. Babu, D. K. and Odeh, A. S. *Productivity of a Horizontal Well Appendices A and B*. https://doi.org/10.2118/18334-MS.

[14]. Mukherjee, H. and Economides, M. J. 1991. A Parametric Comparison of Horizontal and Vertical Well Performance. *SPE-18303-PA*. https://doi.org/10.2118/18303-PA.

[15]. Karcher, B. J., Giger, F. M., and Combe, J. *Some Practical Formulas To Predict Horizontal Well Behavior*. https://doi.org/10.2118/15430-MS.

[16]. Muskat, M. and Wyckoff, R. D. 1937. *The flow of homogeneous fluids through porous media*. Ann Arbor, Mich.: J. W. Edwards, In.

[17]. Babu, D. K. and Odeh, A. S. 1989. Productivity of a Horizontal Well (includes associated papers 20306, 20307, 20394, 20403, 20799, 21307, 21610, 21611, 21623, 21624, 25295, 25408, 26262, 26281, 31025, and 31035). *SPE-18298-PA*. https://doi.org/10.2118/18298-PA.

[18]. Zlodnjak, K. 2016. Anaylsis of real-time ESP data for detecting producer-injector interaction. Master Thesis, OMV.

[19]. Dr. Boyun Guo. *Horizontal and Multilateral Wells: Completion and Stimulation*. Houston, Texas, U.S.A.

[20]. Renpu, W. 2011. *Advanced well completion engineering*, third. ed. Amsterdam u.a.: Gulf Professional.

[21]. Middle East Well Evaluation Review: Horizontal Highlights: Middle East & Asia Reservoir Review **1996**. Industry Articles.

[22]. M. Reynolds. 2014. *Horizontal Well Completion Designs for Unconventional Gas Reservoirs*.

[23]. Aadnoy, B. S. and Hareland, G. *Analysis of Inflow Control Devices*. https://doi.org/10.2118/122824-MS.

[24]. Freyer, R. and Huse, A. *Swelling Packer for Zonal Isolation in Open Hole Screen Completions*. https://doi.org/10.2118/78312-MS.

[25]. Coronado, M. P. and Knebel, M. J. 1998. *One-trip external-casing-packer cement-inflation and stage-cementing system*.

[26]. Denney, D. 2010. Analysis of Inflow-Control Devices. *SPE-0510-0052-JPT*. https://doi.org/10.2118/0510-0052-JPT.

[27]. Aakre, H., Halvorsen, B., Werswick, B. et al. *Smart Well With Autonomous Inflow Control Valve Technology*. https://doi.org/10.2118/164348-MS.

[28]. Al-Khelaiwi, F. T., Birchenko, V. M., Konopczynski, M. R. et al. 2010. Advanced Wells: A Comprehensive Approach to the Selection Between Passive and Active Inflow-Control Completions. *SPE-132976-PA*. https://doi.org/10.2118/132976-PA.

[29]. Rahman, J. U., Allen, C., and Bhat, G. *Second Generation Interval Control Valve (ICV) Improves Operational Efficiency and Inflow Performance in Intelligent Completions*. https://doi.org/10.2118/153700-MS.

[30]. Zeng, Q., Wang, Z., and Yang, G. 2013. *Comparative Study on Passive Inflow Control Devices by Numerical Simulation*.

[31]. Ellis, T., Erkal, A., Goh, G. et al. 2009. *Inflow control devices - Raising profiles*.

[32]. Zeng, Q., Wang, Z., Wang, X. et al. 2014. *A Novel Autonomous Inflow Control Device Design: Improvements to Hybrid ICD*. https://doi.org/10.2523/IPTC-17776-MS.

[33]. Halliburton. 2009. EquiFlow(R) Systems: Equiflow Inflow Control Devices and EquiFlow Inject System, https://de.scribd.com/document/175729392/Halliburton-EquiFlow-ICD.

[34]. Lee Crow, S., P. Coronado, M., and Khodadad Mody, R. 2006. *Means for Passive Inflow Control Upon Gas Breakthrough*. https://doi.org/10.2118/102208-MS.

[35]. Freyer, R., Fejerskov, M., and Huse, A. *An Oil Selective Inflow Control System*. https://doi.org/10.2118/78272-MS.

[36]. Sang, G., Jiang, Z., Zhang, Q. et al. *A Novel Autonomous Inflow Control Device Design Based on Water Swelling Rubber*. https://doi.org/10.2118/170506-MS.

[37]. H. Aakre and V. Mathiesen. September 2009. Method For Flow Control and Autonomous Valve or Flow Control Device. Patent Pub. Number: US 2009/0218103 A1,

[38]. Halvorsen, M., Elseth, G., and Naevdal, O. M. Increased oil production at Troll by autonomous inflow control with RCP valves. https://doi.org/10.2118/159634-MS.

[39]. Mathiesen, V., Werswick, B., Aakre, H. et al. *Autonomous Valve, A Game Changer Of Inflow Control In Horizontal Wells*. https://doi.org/10.2118/145737-MS.

[40]. Benn Voll. *Autonomous Inlow Control Technology: Tendeka Presentation*.

[41]. Halvorsen, M., Madsen, M., Vikøren Mo, M. et al. Enhanced Oil Recovery On Troll Field By Implementing Autonomous Inflow Control Device. https://doi.org/10.2118/180037-MS.

[42]. Omar Awad, M., F. Al Ajmi, M., Safar, A. et al. 2015. *Advanced ICD Application Alleviating Well Intervention Challenges*. https://doi.org/10.2118/175204-MS.

[43]. Halliburton. 2015. NETool Data Sheet: NETool Software.

[44]. Halliburton, E. P. 2014. NETool Technical Manual: 5000.0.4.x.

[45]. Halliburton, E. P. 2015. NETool User Guide: 5000.0.4.1.

[46]. Mira Persaud. 2013. *Geomechanics Report 16th-Th: Geomechanical Study of 16th TH*.

[47]. Peter Toth. 2015. *Bockfliess ReDevelopment Project - New Wells: AAR - After Action Review*.

[48]. OMV Exploration & Production GmbH. 2013. *Well Design Criteria (WDC) BO 204: Production Well*.

[49]. Giden, I. 2015. *Behandlungsbesprechung BO 204, BHB-BO 204: Bockfliess 204*.

[50]. Zekiri Fatime. 2013. *Bockfliess 204 - Log Interpretation: Final Loginterpretation*.

[51]. Wischt J. 2013. *Fertigstellungs- und Übergabeakt der Produktionsbohrung Bockfließ 204: BO 204 Übergabeakt_20131120*.

[52]. OMV Exploration & Production GmbH. 2014. *Well Design Criteria (WDC) BO 205: Production Well*.

[53]. Schmidt Dennis. 2015. *Bockfliess 205 - Log Interpretation: Final Loginterpretation*.

[54]. Sieberer. 2014. *Behandlungsbesprechung BO 205, BHB 205: Bockfliess 205*.

[55]. Wischt J. 2014. *Fertigstellungs- und Übergabeakt der Produktionsbohrung Bockfließ 205: BO 205_Fertigstellungs- und Übergabeakt 20140928*.

[56]. Schmidt Dennis. 2016. *Bockfliess 208 - Log Interpretation: Final Loginterpretation*.

[57]. Mörtl M. 2017. *Sondenskizze BO 208*.

[58]. Resch m. 2015. *Fertigstellungs- und Übergabeakt der Produktionsbohrung Bockfließ 208: BO208_Übergabeakt_20150824_signed*.

[59]. Byrom, T. G. 2014. *Casing and liners for drilling and completion: Design and application*, secondnd ed. Waltham, MA: Gulf Professional Pub.